Saccade triggered local field potential modulations in the primate hippocampus

Guillaume Doucet

Department of Physiology
McGill University
Montréal, Québec, Canada

August 2018

A thesis submitted to McGill University in partial fulfillment
of the degree of Doctorate of Philosophy

Copyright © Guillaume Doucet 2018

Table of Contents

Abstract

The hippocampus is a cortical structure highly conserved across mammalian species. It plays an essential role in memory function by encoding context dependent associations between features and organizing them across multiple dimensions (e.g. spatiotemporal). It is believed that hippocampal local field potential oscillations, reflecting the activity of groups of co-active neurons that represent associated parts of an experience, are important to this process. Oscillations within a narrow frequency band are further thought to bear particular importance: ~3 – 12 Hz, henceforth known as hippocampal theta oscillations. Individual theta cycles separate the continuous experience into successive "snapshots" of attended stimuli (e.g. spatial trajectory or viewpoint) and allow for the separation of individual features (e.g. locations or objects) within that snapshot by interacting with high frequency oscillations. Theta phase thus plays a significant role in coordinating neuronal activity and is thought to be "reset" by sensory events, such as stimulus onsets, and active sensing behaviors, such as whisking and saccades. However, conflicting results across stimuli conditions, such as complete darkness versus complex stimuli, and inconsistencies in experimental protocols, such as the interchangeable use of saccade and foveation onsets to measure phase reset, generate uncertainty about the prerequisites (e.g. task and stimuli), nature (e.g. sensory or motor) and information content of sensing triggered phase "resets".

First, I created a virtual reality (VR) testing suite using a video game engine (Unreal Engine 3) and interfaced it with our electrophysiological recording system. This allowed for the creation of a context dependent associative memory task, specifically tailored to highlight hippocampal function. Under experimental conditions, the system achieved a temporal precision of a few milliseconds between VR position, on-screen gaze position and neuronal data.

Second, I analyzed hippocampal local field potentials recorded around stimulus onsets and self-generated eye movements in the aforementioned associative memory task, in addition to two new tasks: an open-field foraging and a cued saccade task. I found that stimulus onsets, as well as saccades and foveation onsets, triggered significant phase resets in the primate hippocampus in a frequency-specific manner. Moreover, saccade triggered local field potentials correlated with saccade parameters (i.e. amplitude and direction) and were stimulus independent. On the other hand, stimulus and foveation triggered potentials occurred within a frequency band correlated with

the presence of visual stimulation. Lastly, the undertaken VR task directly influenced the reliability of saccade triggered phase resets, where the associative memory task engendered a stronger signal.

In summary, theta phase is not simply "reset" to a default state by active sensing but is behaviorally modulated to represent both the motor and sensory aspects of saccadic exploration, in a frequency-specific manner. These results are in accordance with the role of the primate hippocampus in binding together self-motion, spatiotemporal context and stimulus feature into a coherent representation of experience. The relationship between gaze and hippocampal activity further highlights important distinctions between primate and rodent hippocampal function that must be taken into consideration when trying to bridge the rodent and human literature.

Résumé

L'hippocampe est une structure corticale hautement conservée chez les mammifères. Elle joue un rôle essentiel dans la mémoire en formant des associations entre les divers éléments explorés et en les organisant selon les dimensions appropriées au contexte. Il a été proposé que les potentiels de champ locaux de l'hippocampe, qui reflètent l'activité de groups de neurones coactifs, sont importants dans ce processus. Une plage de fréquences d'oscillation a un rôle particulièrement important : les oscillations thêta entre ~3 et 12 Hz. Les cycles individuels de thêta fragmentent l'expérience continue selon les stimuli explorés (par ex. trajectoires spatiales ou points de vue), et permet la séparation des différentes caractéristiques individuelles (par ex. positions) à l'intérieur de ces fragments en interagissant avec des oscillations à haute fréquence. La phase de thêta joue donc un rôle significatif dans la coordination de l'activité neuronale et est « réinitialisée » par des événements de nature sensorielle, tels l'apparition de stimuli ou des comportements d'exploration. Cependant, plusieurs résultats conflictuels à travers les conditions de stimulation, tels la noirceur totale ou la présence de stimuli complexes, et des incohérences dans les protocoles expérimentaux, tels l'utilisation de l'initiation des saccades ou fovéations pour quantifier la « réinitialisation » de phase, ont généré beaucoup d'incertitude quant aux conditions préalables (par ex. la tâche accomplie et les stimuli), à la nature (par ex. motrice ou sensorielle) et à l'information contenue dans les « réinitialisations » de phase.

Premièrement, j'ai créé une suite de réalité virtuelle (RV) basée sur un engin de jeu vidéo et créé son interface avec nos équipements d'enregistrement neurophysiologiques. Ce système a permis la création d'une tâche spécialement désignée pour activer l'hippocampe, par l'utilisation de navigation allocentrique et de formation de mémoires associatives dépendantes du contexte. Sous les conditions expérimentales, une résolution temporelle de quelques millisecondes a été obtenue entre la position dans la RV, la position des yeux sur l'écran et les données neuronales.

Deuxièmement, j'ai analysé les potentiels de champ locaux enregistrés lors de l'apparition de stimuli et de mouvements oculaires volontaires, lors de la tâche de mémoire associative et de deux nouvelles tâches : une tâche de recherche en RV et une tâche de mouvement oculaires dirigés. J'ai trouvé que l'apparition de stimuli, ainsi que l'initiation de saccades et de fixations, engendrent une réinitialisation de la phase en fonction de bandes de fréquences spécifiques. De plus, les

modulations de potentiels de champ locaux engendrées par les saccades corrèlent avec les paramètres de la saccade (par ex. l'amplitude et la direction) et sont indépendantes des stimuli. Alternativement, les réinitialisations de phase causées par les stimuli et fovéations se produisent dans des fréquences qui correspondent à la présence de stimuli visuels. En dernier lieu, la tâche entreprise en RV a une influence directe la robustesse des réinitialisations de potentiels de champ, où la tâche de mémoire associative a une plus forte influence.

En résumé, la phase des oscillations thêta n'est pas simplement « réinitialisée » à une valeur par défaut, mais est modulée par le comportement pour représenter l'activité motrice et sensorielle de l'exploration visuelle, et ce, dans des bandes de fréquences spécifiques. Ces résultats sont en faveur du rôle de l'hippocampe du primate dans la fusion des représentations de mouvements volontaires, du contexte spatiotemporel et des stimuli en une image cohérente de l'expérience. Les relations entre la vision et l'activité de l'hippocampe mettent également en évidence d'importantes distinctions entre l'hippocampe des primates et rongeurs, qui doivent être considérées lors de l'étude de leurs littératures respectives.

Acknowledgements

I would first like to thank my supervisor, Dr. Julio Martinez-Trujillo, for providing great advice and support through all these years, while giving me almost complete freedom to design and construct my vision of this project. I am also extremely grateful for his trust in my abilities, letting me implement the experimental software and VR suites, and for his understanding of the specific requirements and sometimes limited productivity inherent to being both a parent and a graduate student.

I would further like to thank the members my supervisory committee: Drs. Curtis Baker, Maurice Chacron and Erik Cook, for their vital feedback in times of utter confusion, for their challenging yet essential questions and for helping me develop the critical line of thinking required for this work. I acknowledge that this work might be far from your respective areas of expertise, and I am grateful that you made this journey with me, across the many variations of this project, consistently providing support and encouragements.

My most heartfelt thanks go to the past and current members of the Martinez's lab family for their craziness, their brilliance and eagerness to help. I have really enjoyed each moment passed and am really grateful as they made sure no one was ever the proverbial "smartest person in the room". Thank you for your input, challenge and support. Special thanks go to Roberto Gulli for knowing virtually every paper ever published, to Ben Corrigan for his tedious but meticulous work on dissecting eye movements, without which this thesis wouldn't exist, and to Lyndon Duong for his help with the dreaded LFPs and their analysis. Thanks also to Drs. Nour Malek and Theda Backen for making this lab full of life and laughs.

Last but not least, I wish to thank my family for their support and understanding for the countless late nights and work-shortened week-ends. To Genevieve, Annabelle and Albert, thank you for keeping me awake at night and helping me focus on the truly important aspects of life. I dedicate this thesis to you in hopes that you see the rewards of hard work and dedication.

Contributions of authors

Chapter 2 presents a published manuscript: Doucet, G., Gulli, R.A., Martinez-Trujillo, J.C. (2016) Cross-species 3D virtual reality toolbox for visual and cognitive experiments, *Journal of Neuroscience Methods*, 266: 84-93. For this study, I designed, built and tested the architecture of the system, and wrote the manuscript. Mr. Gulli designed the "associative memory" task and its virtual environment and provided feedback for the system's architecture and manuscript. Dr. Martinez-Trujillo offered guidance for the requirements of the system, proper controls and manuscript writing.

Chapter 3 presents a submitted manuscript: Doucet, G., Corrigan, B.W., Gulli, R.A., Duong, L., Martinez-Trujillo, J.C. (2018) Frequency specific phase resetting of local field potential oscillations in primate hippocampus by visual transients and saccades. For this study, I devised the research questions, programmed the behavioral tasks, designed and ran the analyses on the local field potential data, and wrote the manuscript. Mr. Corrigan provided the saccade detection data, Mr. Gulli designed the "associative memory" and "foraging" tasks and their virtual environment and provided significant conceptual counsel, Mr. Duong supplied considerable feedback in the planning and execution of the field potential analyses. Animal training and electrophysiological recordings were performed collaboratively by Mr. Gulli, Mr. Corrigan and myself. Lastly, Dr. Martinez-Trujillo helped on every aspect of the project and conducted the surgeries.

Chapter 1

1. Introduction and Literature Review

1.1 Classical experiments and their limitations

Early sensory electrophysiological research began with the pioneer work of Edgar Adrian, who defined the basic firing properties of somatosensory neurons (Huang, 2016). These specific properties dictate that single sensory neurons fire in an "all-or-none" fashion and the magnitude of the response correlates with stimulus strength (Adrian, 1926b, 1926a, Adrian and Zotterman, 1926a, 1926b). Hubel and Wiesel (1959) then transposed these findings to neurons in the cat's primary visual cortex, and studied their responses when presented with single light spots of varying shape, size and movement. In doing so, they defined neuronal receptive fields (i.e. individual neurons each encode a small portion of the sensory field) and discovered that individual neurons do not simply respond to any stimulus, but preferentially respond to certain features (i.e. tuning), such as size and orientation (Hubel and Wiesel, 1959).

Since then, the vast majority of electrophysiological research has applied the same principles of reverse engineering, namely identifying the single and narrow tuning of individual neurons to infer function (Rigotti et al., 2013; McKenzie et al., 2016), regardless of brain region. Absolute control over sensory stimulation is however required to properly identify neuronal tuning, which has led researchers to use single, highly salient and over-simplified stimuli (e.g. white bars or dots on a black background), without competing sensory or cognitive inputs (Loomis, Blascovich and Beall, 1999; Bohil, Alicea and Biocca, 2011; Parsons, 2015; Frank and Sabatinelli, 2017). Moreover, the stimuli are frequently presented regardless of the subject's behavior (i.e. anesthetised animals or passive presentation) and, if behavioral input is required, it is often highly constrained and un-natural (Dombeck and Reiser, 2012). For example, in order to maintain stable visual receptive field positions, subjects are often head-fixed and tasked with holding their gaze within a very narrow fixation window for an extended period of time (Dombeck and Reiser, 2012; Guo et al., 2014; Parsons, 2015).

Although such experimental procedures have led to paramount discoveries, it has recently been suggested that they can fail to elicit the full range of possible computations within a studied brain region, leading to ceiling effects and to incomplete descriptions of the network's function (Kayser, Körding and König, 2004; Zaki and Ochsner, 2009; McKenzie et al., 2016; Krakauer et al., 2017). For example, the responses of visual neurons have been shown to be modulated by the simultaneous presentation of competing stimuli, even when presented outside of the cells'

receptive field and tuning preference (Krause and Pack, 2014). Furthermore, naturalistic stimuli have been shown to be more efficiently encoded by sensory neurons, when compared to spectrally matched and un-natural controls (Rieke, Bodnar and Bialek, 1995; Kayser, Körding and König, 2004; Movshon and Simoncelli, 2014). In other words, basic sensory processing seems to be more holistic than what was expected from initial studies. This effect is even greater in studies of high-order areas, such as prefrontal cortex or medial temporal lobe, where simplified tasks or stimuli hardly elicit reliable neuronal responses, leading to a considerable proportion of recorded neurons to be described as "untuned", "unclassified" or "unresponsive" (Rigotti et al., 2013; Hardcastle et al., 2017). This failure to properly correlate experimental variables with neuronal responses highlights the inefficacy of classical paradigms in fully characterizing local brain function.

Limited generalizability of simplified tasks and stimuli have also been documented in the field of psychology, despite experimental control being often relinquished in favor of behavioral relevance (Bohil, Alicea and Biocca, 2011; Parsons, 2015). For example, the Wisconsin Card Sorting Test, one of the most used tests in clinical assessments of frontal lobe function, has been described by Burgess et al. (2006) as:

> *"*[…] *so unlike everyday situations, that knowledge of performance in it is of very little help for assessment since it is of uncertain predictive validity (or "generalizability"): We do not really know what situations in everyday life require the abilities that the WCST measures."*

Moreover, in social cognition and attention, the quality and saliency of stimuli vary according to contextual cues and subjective experience, which, when ignored, yield results incompatible with real-life situations (Li et al., 2002; Zaki and Ochsner, 2009; Frank and Sabatinelli, 2017). Indeed, both gaze and neuronal responses have been shown to differ between watching social cues on a computer monitor and real-life stimuli (Reader and Holmes, 2016). Lastly, when trying to correlate impairments with localized brain lesions, the failure of classical experiments has led researchers and clinicians to use tasks directly replicating real-life conditions, such as running errands in a shopping center (Burgess et al., 2006). Although highly informative, these tasks are costly, impractical and sometimes unsafe.

1.2 Virtual reality in neuroscience

A possible solution to theses limitations was found in a natural, instinctive and omnipresent behavior: play. Play behavior is indeed present in most species, from invertebrates to mammals (Miller, 2017), and allows developing individuals to explore and gain a multitude of real-life skills, while being in a highly challenging yet safe environment (Cardoso-Leite and Bavelier, 2014). Although play behavior can vary across species, genders and age groups, it seems to serve the same purpose across all demographics, and addresses the aforementioned drawbacks of classical experiments, namely: high cognitive demands, ecological validity and generalizability (Spinka, Newberry and Bekoff, 2001). However, as animals mostly engage in active play (e.g. wrestling and chasing), these behaviors are hardly applicable in larger animals, especially when trying to record neuronal data in a laboratory setting. Similarly, humans also engage in active play during early age, while a more composed form of play appears alongside aging: board games. It is thus unsurprising that a game, such as chess, could spark a strong interest in cognitive research. This interest has been present since the 1890s and reached a point where it became so ubiquitous as to be labelled the "Drosophia of cognitive science" (Gray, 2017). In the words of Chabris (2017):

> *"Games have been an experimental paradigm in cognitive science since before cognitive science existed as a recognized discipline. […] Games are not just one particular environment for studying human behavior; they are the best environment. They are complex enough to simulate real physical and social systems with great precision. Games are like laboratory experiments in psychology, with decisions constrained enough to be digitized and analyzed, but not so constrained (e.g., down to binary yes/no answers) as to sacrifice much validity."*

Despite this auspicious definition, few games other than chess, have been consistently used in the literature (Chabris, 2017; Gray, 2017).

This trend is rapidly reversing due to the advent of modern computers and to the ubiquity of consumer electronics (e.g. smartphones, gaming consoles), triggering the creation of a new kind of game: video game (VG). Indeed, VG usage now transcends all demographic groups (Washburn and Gulledge, 1995; Chabris, 2017), where average "gamers" are believed to total around 10,000

hours of play time by the age of 21 (McGonigal, 2011). Consequently, total worldwide usage of highly-anticipated games has been found to exceed 65,000 hours within the first month following their release (Bavelier and Davidson, 2013), and surpass 2.33 billion hours within the first year (RockStar Games, 2014). The excessive amount of available data has sparked strong scientific interest in studying the various impacts of VG usage, yielding a similar increase in the number of annual publications mentioning "video game", with as many as 723 publications in a single year (Figure 1-1). Scientific inquiries about VG have been categorized in three groups: gamification, treatment condition and "Game-XP" (Gray, 2017). Firstly, gamification refers to the practice of adding game elements to unrelated tasks to improve user experience (i.e. educational games; Morris et al. 2013). Secondly, treatment condition designates all studies comparing task performance (e.g. cognitive tasks) before and after VG exposure or across VG users and non-users, to quantify variations in intellectual or motor capabilities (Gray, 2017). Lastly, "Game-XP" has been defined as the creation of "game-like" cognitive tasks to measure behavioral or neuronal data (Washburn and Gulledge, 1995; Gray, 2017) and is the main focus of this thesis.

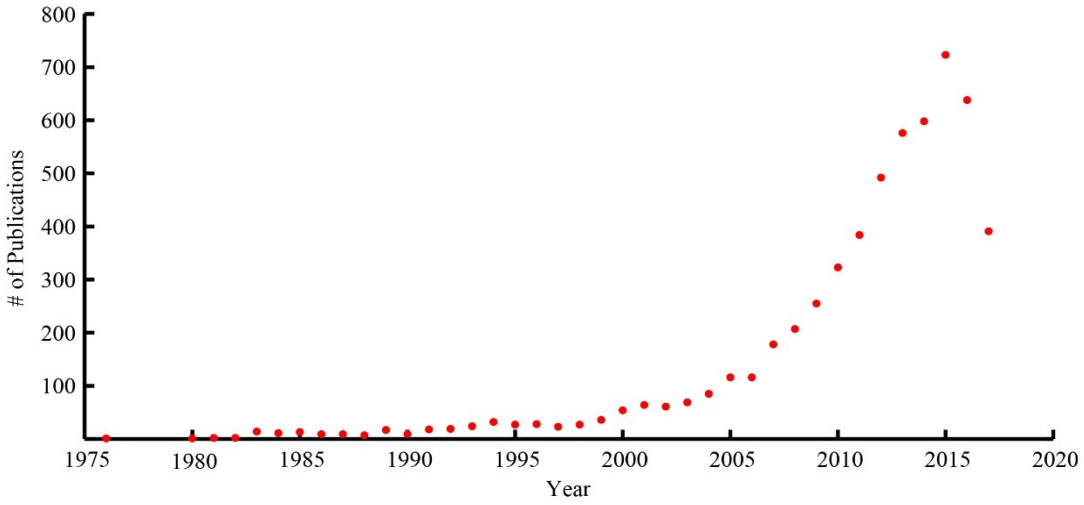

Figure 1-1. Number of annual publications mentioning the words "video game". Data taken from NCBI Pubmed (http://www.ncbi.nlm.nih.gov/pubmed).

VGs as experimental paradigms offer numerous advantages over classical experiments. Firstly, and analogous to real-life play, they present more complex and challenging stimulations,

increasing motivation and fully engaging complex cognitive processes, such as attention, memory, problem solving and planning (Washburn and Gulledge, 1995; Baniqued et al., 2013; Morris et al., 2013; Gray, 2017). Additionally, prolonged exposure to VGs has been shown to improve performance in untrained tasks requiring similar cognitive traits, including: attention and working memory (Green & Bavelier 2003; Anguera et al. 2013; Belchior et al. 2013; Latham et al. 2013; Blacker et al. 2014), executive functions (Nouchi et al., 2013), contrast sensitivity (Li et al., 2009) and face processing in autistic patients (Tanaka et al., 2010), possibly overcoming the limited real-world generalizability of simplified experiments. These results are however heavily debated and their experimental paradigms are frequently described as poorly designed or poorly controlled (Boot et al. 2011; Green et al. 2013; Latham et al. 2013; Latham et al. 2013(1)). Furthermore, the strong overlap between the cognitive processes believed to be involved in VG play and the ones believed to be improved following VG treatment create significant confounds. Indeed, in explaining significant differences in cognitive task performance between VG users and non-users, researchers cannot rule out a selection bias in the expert population, where experts are inherently better in such tasks, hence being more motivated to engage in similar activities (i.e. VGs; Boot et al. 2008). On the other hand, the vast majority of negative results come from VG training regimes, where exposure is greatly limited, typically tens of hours, when compared to the hundreds and thousands of hours experienced by VG users (Boot et al. 2011; Latham et al. 2013). Although some level of consensus about cognitive improvements following VG usage exists, these improvements are often limited to the trained tasks themselves and rarely generalize to untrained ones (Owen et al., 2010; Baniqued et al., 2014; Simons et al., 2016).

The vast inconsistencies across the aforementioned studies, and resulting controversies over VG efficacy for cognitive training, may be explained by the different varieties of games being used. Indeed, some VGs allow the user to directly engage in virtual activities, such as driving a car or walking in an open environment, whereas other games, such as virtual chess or Tetris, do not offer a subjective perspective (Washburn and Gulledge, 1995). The former category corresponds to the definition of virtual reality (VR), which contains all simulations allowing a user to navigate and interact with a virtual environment (Baus and Bouchard, 2014). VR applications, unlike non-subjective ones, are associated with "presence" (i.e. the feeling of actually being in the virtual environment), shown to elicit the same physiological responses as real-life situations and believed

to be essential to real-life skill transfer (Bohil, Alicea and Biocca, 2011). Moreover, they have been found to offer the same advantages as VGs, namely increasing motivation and reducing ceiling effects in task performance (Schultheis, Himelstein and Rizzo, 2002), while keeping subjects static enough to enable clinical testing and electrophysiological recordings (Dombeck and Reiser, 2012; Minderer et al., 2016). Contrary to VGs, these VR applications are built for a specific purpose, allowing them to address most, if not all, classical experiments' drawbacks. Firstly, VR applications can be directly created to train specific skills outside of VR (i.e. real-life generalizability), from fear management to maintenance and repair, with performances analogous to real-life training (Gonçalves et al., 2012; Baus and Bouchard, 2014; Ganier, Hoareau and Tisseau, 2014; Goris, Jalink and ten Cate Hoedemaker, 2014). Accordingly, VR applications can also be used to quantify impairments for clinical purposes (Allain et al., 2014). Secondly, they maximize experimental control while maintaining ecological validity, eliciting instinctive behaviors under strictly controlled and naturalistic stimulation (Schultheis, Himelstein and Rizzo, 2002; Allain et al., 2014; Krakauer et al., 2017). Furthermore, scientists can dissect the influence of individual variables on behavior or neuronal activity, by independently modifying them. For example, since the virtual world is not constrained by the laws of physics, impossible events, such as teleportation (Vass et al., 2016), dissociation between perceived object size and distance (Loomis, Blascovich and Beall, 1999) or instantaneous changes in the environment (Bohil, Alicea and Biocca, 2011; Minderer et al., 2016), can be created to probe the neuronal correlates of location, distance cues or context, respectively. Lastly, VR simulations can be used to bridge the species gap, by allowing similar experiments to be presented to every species, from rodents to humans (Washburn and Gulledge, 1995; Watrous et al., 2013). There is however a major caveat to VR, namely the high implementation cost, as both highly specialized skills and considerable time are required to design such experiments (Loomis, Blascovich and Beall, 1999; Mueller et al., 2012). This results in individual laboratories building their own highly specialized and inflexible experimental paradigms, tailored to their species of interest, therefore impairing comparison and replication across studies (Jangraw et al., 2014).

Despite this drawback, the many advantages of VR applications have led them to become established paradigms is many areas of neuroscience, such as hippocampal research (Bohil, Alicea and Biocca, 2011; Dombeck and Reiser, 2012). The following sections will thus describe how

moving away from oversimplified experiments has allowed for significant findings in hippocampal research. I will further emphasize the important role played by VR paradigms, such as the creation of more cognitively demanding tasks and their adaptation across multiple species, or the precise manipulation of experimental variables otherwise impractical in real-life.

1.3 Anatomy of the hippocampus

The hippocampus (HPC) is a bilateral cortical structure of the medial temporal lobe highly conserved across mammalian species. Although there are species specific differences in relative position within the brain (Figure 1-2b), in the orientation of its longitudinal axis (dorsal to ventral in rodents; posterior to anterior in primates; Figure 1-2a) and in overall cellular architecture (Figure 1-2c), subsequently mentioned sub-regions and their overall connectivity are consistent across most mammalian species (Amaral and Lavenex, 2006; Seress, 2007; Witter, 2007; Strange et al., 2014). Despite extensive anatomical literature, there is no consensus on which anatomical sub-regions constitute the HPC. While the cornu Ammonis (CA) regions numbered from 1 to 3 are common to all definitions, the dentate gyrus (DG) and subiculum (Sb) are inconsistently included (Lisman, 1999; Jutras and Buffalo, 2014; Kitamura et al., 2017) or excluded (Robertson et al., 1998; Malkova and Mishkin, 2003; Seress, 2007; Clark and Squire, 2013). For the purpose of this work, both DG and Sb sub-regions will be included in future HPC references.

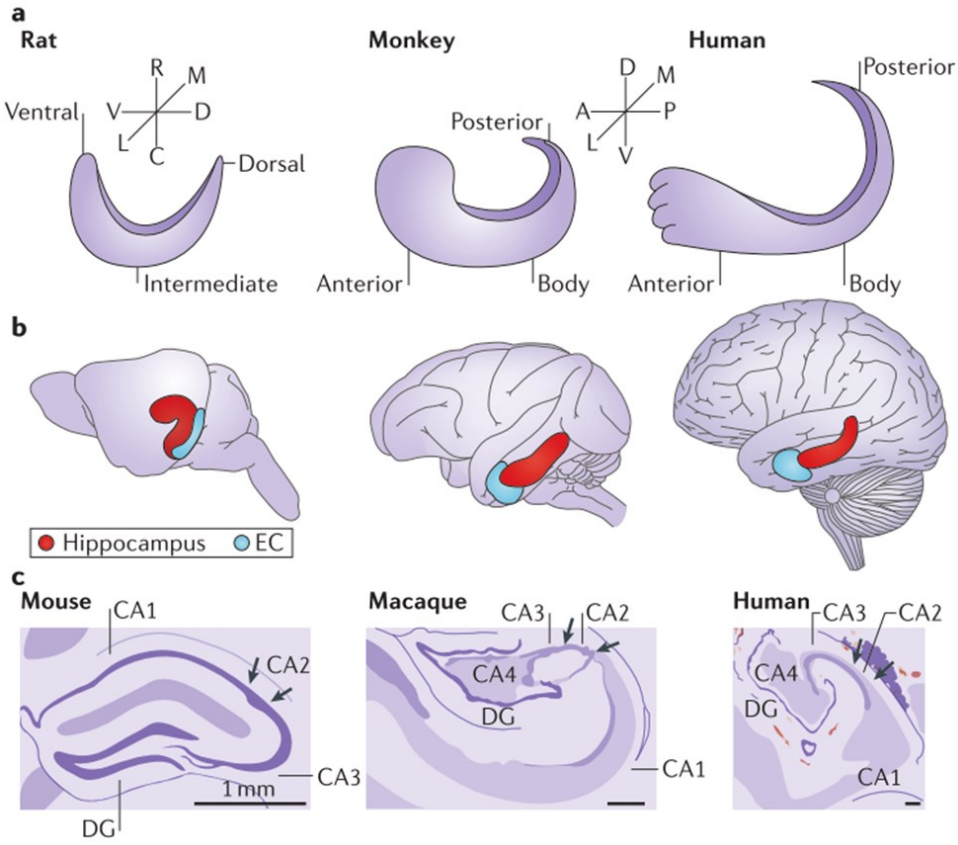

Figure 1-2. Hippocampal anatomy. a) Hippocampal longitudinal axis description in the Rat (rotated 90 degrees), Monkey and Human. b) Relative whole brain position of the hippocampus (red) and entorhinal cortex (blue). c) Graphical representation of hippocampal cross-sections and relative organization of cornu Ammonis (CA) and dentate gyrus (DG). A: anterior; C: caudal; D: dorsal; L: lateral; M: medial; P: posterior; R: rostral; V: ventral. Adapted from Strange et al. (2014).

Functionally, the HPC is connected with a wide variety of cortical and subcortical structures. Although not exclusive, most of its input comes from two white fibre tracts, namely the angular bundle and the fimbria-fornix (Amaral and Lavenex, 2006). Firstly, the angular bundle includes projections from the entorhinal cortex (EC) to all HPC sub-regions, and serves as the main source of cortical input to the HPC (Suzuki and Eichenbaum, 2000; Bauer, 2008). The EC relays highly segregated information (Figure 1-3) about explored objects via the perirhinal cortex and ventral, or "what", visual pathway, as well as spatiocontextual information via the postrhinal/parahippocampal cortex and the dorsal, or "where", visual pathway (Burwell, 2006;

Eichenbaum, Yonelinas and Ranganath, 2007; Murray, Bussey and Saksida, 2007; Komorowski, Manns and Eichenbaum, 2009; Maass et al., 2015). Consistently, the EC is believed to encode both object and spatiotemporal context representations, where the lateral EC (LEC) prioritizes local and sensory centered information and the medial EC (MEC) focuses on global and spatially centered information (Buzsáki and Moser, 2013; Neunuebel et al., 2013; Ritchey, Libby and Ranganath, 2015; Keene et al., 2016). While some MEC neurons have been shown to have robust spatial tuning and encode, for example, a grid-like representation of the environment (Hafting et al., 2005) as well as its edges (Solstad et al., 2008), exact LEC function and tuning have been less extensively characterized (Moser, Kropff and Moser, 2008).

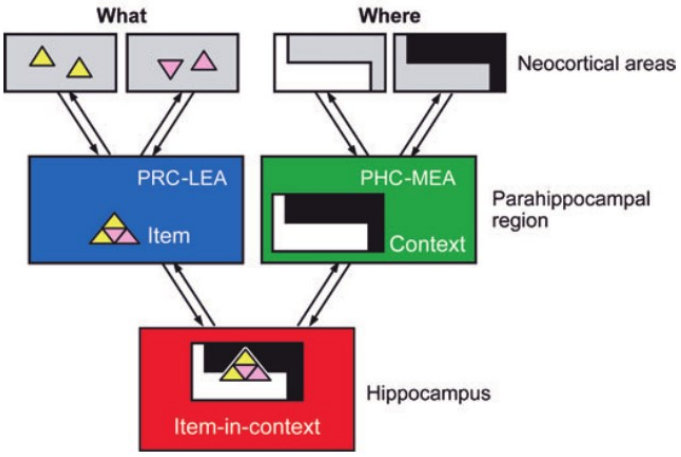

Figure 1-3. Schematics of segregated HPC input from the "what" and "where" visual pathways. PRC: perirhinal cortex; LEA: lateral entorhinal area; PHC: parahippocampal cortex; MEA: medial entorhinal area. Adapted from Eichenbaum et al. (2007).

Secondly, the bulk of subcortical input is believed to reach all parts of the HPC through the fimbria-fornix, which includes projections from the basal forebrain (e.g. medial septum, MS), ventral tegmental area and brain stem (Van Hoesen, 1985; Hartley et al., 2014). Most of these subcortical connections provide the HPC with specific neuromodulators. For example, the MS is responsible for the majority of cholinergic input, the ventral tegmental area for dopamine and the raphe nuclei and locus coeruleus of the brain stem are responsible for serotonin and norepinephrine, respectively (Cassel et al., 1997; Cassel and de Vasconcelos, 2015). For the

purpose of this work, we will focus solely on the cholinergic input from the MS, as it has a direct influence on HPC neuronal responses, as opposed to the broad modulatory effects of other neurotransmitters (Cassel et al., 1997). Indeed, acetylcholine is believed to have a direct functional role in HPC function, by enhancing attentional responses to stimuli, coordinating neuronal firing and enhancing memory encoding, whereas low cholinergic conditions are associated with memory consolidation processes (Cassel et al., 1997; Tsanov, 2015).

It is important to note that the aforementioned connections are not comprehensive. For instance, the HPC receives input from every sensory modality and cortical association areas (Eichenbaum, 2004), and not only the visual one. Moreover, the rodent EC has been shown to receive subcortical projections from the midline thalamus, although these projections are believed to act as a bi-directional relay between the medial prefrontal cortex to underlie goal-directed behavior (Vertes et al., 2007; Cassel and de Vasconcelos, 2015; Ito et al., 2015). Due to the extensive nature of HPC connectivity, I have thus limited the description to connections relevant for this work.

Lastly, the internal connections that process cortical inputs to the HPC (Figure 1-4, from the EC towards the subicular (Sb) output regions, are labeled the trisynaptic pathway. Firstly, the vast majority of EC output targets granule cells in the DG through the perforant path, although monosynaptic projections from the EC to all hippocampal sub-regions have been identified (Insausti et al., 2002; Hartley et al., 2014). Subsequently, axonal projections from the DG, termed the mossy fiber system, almost exclusively target CA3 cells. In turn, CA3 cells present collateral projections to either other CA3 neurons (recurrent collaterals) or to downstream CA1 neurons (Schaffer collaterals). Lastly, CA1 neurons targeting the subiculum are believed to be responsible for the greater part of hippocampal output (Ding, 2013).

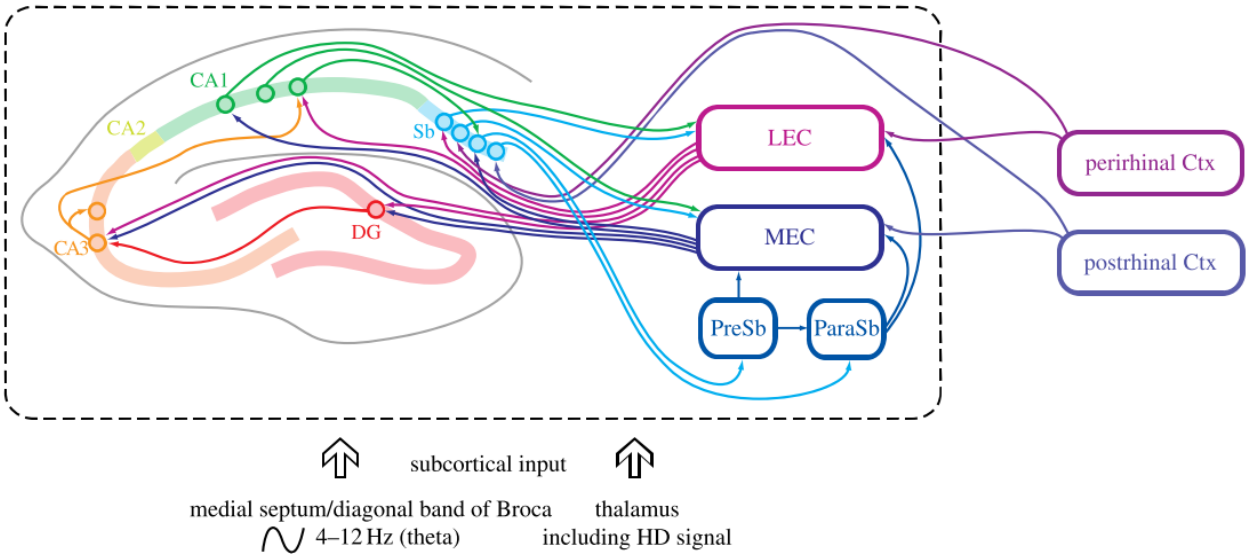

Figure 1-2. Trisynaptic pathway. Cortical input enters the hippocampal formation (dashed box) via connections between the lateral (LEC) and medial (MEC) entorhinal cortex. Information is then relayed to the dentate gyrus (DG) through the perforant path. DG neurons then project to CA3 neurons (mossy fiber system), which further reach CA1 through the Schaffer collaterals. CA1 to subiculum (Sb) form the majority of HF output. Adapted from Hartley et al. (2014).

1.4 Early hippocampal research

Anatomical considerations led researchers to initially label the HPC as an olfactory brain region, an hypothesis challenged by the seminal work of Alf Brodal (1947). However, and despite a thorough description of hippocampal connectivity, a specific function could not be inferred at that time (Brodal, 1947). Significant insight into hippocampal function was gained a decade later, by the study of surgical patients who underwent medial temporal lobe (MTL) resections to treat epilepsy and psychosis, under the care of Drs. Milner, Penfield and Scoville (Milner and Penfield, 1955; Scoville and Milner, 1957; Corkin, 2002; Milner, 2005). Amongst these patients, including the famous patient HM, clear trends in behavioral impairments were apparent. Indeed, patients displayed robust anterograde amnesia and impaired semantic learning, the amplitude of which correlated with the size of resected HPC. Conversely, pre-operative semantic knowledge, procedural learning and cognitive skills remained mostly intact, although some impairments in autobiographical knowledge were described (Augustinack et al., 2014). Earliest conclusions

placed the hippocampus and the hippocampal gyrus at a pivotal position for the retention of current experiences, or "recent memories" (Scoville and Milner, 1957).

The recent memory hypothesis of hippocampal function inspired a vast number of lesion studies in animals aimed at replicating these results (Douglas, 1967). However, as semantic and episodic memory, later described as declarative memory (i.e. the conscious recollection of facts and events; Manns et al. 2007), is not as readily accessible in animals, human tasks were further simplified to be used on animals. This procedure yielded highly conflicting results. For example, rodents' performance in conditioning tasks, then believed to be equivalent to human learning, were inconsistently impaired, with some reports of accelerated learning (Kimble, 1963; Douglas, 1967). Similarly, primate experiments failed to produce reliable impairments in learning and retention (Correll and Scoville, 1965), as well as failed to replicate human findings (Clark and Squire, 2013). Researchers thus began to question the memory hypothesis (Douglas, 1967), in favor of a role in "response inhibition" (Kimble, 1968).

Concurrently, electrophysiological studies in rodents were undertaken, and identified a population of cells that were only active when the animal was in a specific location within the environment (O'Keefe and Dostrovsky, 1971). The spatial tuning of these neurons, termed "place cells", was subsequently found to be dependent on allocentric (i.e. external to the body or world centered) cues, independently of sensory modalities, stable over time and in the dark (Quirk, Muller and Kubie, 1990; Thompson and Best, 1990; O'Mara, 1995). It was therefore argued that the HPC was involved in spatial mapping (Burgess, Recce and O'Keefe, 1994), where previously identified impairments following HPC lesions were due to a failure to construct cognitive maps of the environment, preventing change detection or the identification of reinforcement contingencies (O'Keefe and Dostrovsky, 1971; O'Mara, 1995). Studies examining spatial processing in lesioned animals found that rodents seemed impaired in the formation of a spatial map (i.e. memory for a spatial configuration), but not in simple navigation (Packard and McGaugh, 1996). For example, HPC lesioned rodents were unable to navigate to the position of a hidden platform when the starting position changed (Morris et al., 1982) and repeatedly re-entered the un-baited or previously scavenged arms of a radial maze (Moser and Moser, 1998). Despite apparently conflicting results, similar studies in non-human primates displayed highly impaired performance in open-field foraging tasks, and unreliable impairments in manual or computerized spatial

memory analogues (Murray and Mishkin, 1998; Bachevalier and Nemanic, 2008; Lavenex and Lavenex, 2009).

The vast inconsistencies across experiments allowed for two parallel streams of research to co-exist: namely memory impairments following hippocampal lesions in human patients and the encoding of spatial representations in rodent electrophysiological recordings (Eichenbaum and Cohen, 2014; Buffalo, 2015; Schiller et al., 2015; McKenzie et al., 2016). This divide was further exacerbated by the inability to test both human and rodents under the same experimental conditions, where, for example, recording human hippocampal neurons in an open-field foraging task would not be possible.

1.5 Modern hippocampal research

Despite both research streams being highly successful independently, the most straightforward explanation that the HPC could serve distinct roles, within differently organized memory systems across species, was rejected by most researchers (Lavenex and Lavenex, 2009; Clark and Squire, 2013). This rejection was confirmed when a human patient was tested on the same set of tasks used in animal studies to discredit the memory function hypothesis, and was found similarly unimpaired (Orbach, Milner and Rasmussen, 1960; Gaffan, 1974). Further investigation of possible confounds across lesion and electrophysiological studies verified that inappropriate tasks played a significant role in exaggerating discrepancies found between animals and humans.

Firstly, the study of physiological correlates of animal memory has been dominated by variants of the delayed match to sample task (DMS; Suzuki and Eichenbaum, 2000). In this task, animals are first presented with a sample stimulus (e.g. image, object, spatial location) and, following a variable delay, have to respond to the presentation of a matching or non-matching test stimulus. As this task can be undertaken by different HPC independent memory systems (e.g. visual short-term memory or working memory), HPC dependent versions often include extended delays (Murray and Mishkin, 1998) or indirectly measure memory performance through the innate preference for novel objects exploration across a large number of stimuli (Manns et al., 2007; Jutras and Buffalo, 2014). Despite their extensive use in hippocampal studies, performance

impairments in DMS variants have been highly contradictory across lesion studies (Bachevalier and Nemanic, 2008). As these differences could be attributed to the variations in the extent of damage to the region of interest (i.e. HPC), neighboring regions (e.g. EC) and passing fibre tracts (Bayley, Frascino and Squire, 2005; Jutras and Buffalo, 2014), Murray and Mishkin (1998) selectively lesioned the HPC and found no impairments in delayed non-matching tasks for both objects and locations. Similarly, when tested on DMS tasks, the performance of patient H.M. was comparable to that of control subjects (Augustinack et al., 2014).

Research was then undertaken to isolate the contribution of individual regions within the medial temporal lobe to the completion of DMS tasks. To do so, tasks were broken down into their constituents, namely discrimination of individual stimuli, the maintenance of their representations during the delay period and comparison with the test stimuli, whose neural correlates were identified. It was found that neurons within the perirhinal and entorhinal cortices could differentiate between individual stimuli, maintain their representations during delay periods and have selective responses following their repeated presentations (Buckley and Gaffan, 1998; Aggleton, Kyd and Bilkey, 2004; Wilson, Langston, et al., 2013; Wilson, Watanabe, et al., 2013). However, neuronal representations during task delays in the perirhinal cortex are disrupted by the presentation of intervening stimuli, whereas EC representations remain stable, suggesting a role in stimuli differentiation and recognition, respectively (Suzuki and Eichenbaum, 2000). Accordingly, rats with EC lesions were able to recognize simple items and contexts when no intervening stimuli were used, but were unable to recognize the combination of these two stimuli (Wilson, Langston, et al., 2013; Wilson, Watanabe, et al., 2013).

While hippocampal lesions have been shown to similarly impair “item in context” recognition performance (Bachevalier, Nemanic and Alvarado, 2015) and HPC neurons have also been found to respond to match or non-match stimuli, their responses were not stimulus specific but seemed to encode the outcome of the comparison and the “conjunctive coding” of the comparison objects with other variables, such as their location (Eichenbaum, Yonelinas and Ranganath, 2007; Squire, Wixted and Clark, 2007; Bachevalier and Nemanic, 2008). These results highlighted possible confounding effects of the different strategies that could be used to undertake DMS tasks. For example, it is impossible to distinguish whether a decision was based on familiarity (i.e. indistinct feeling) or recollection (i.e. qualitative description) of the sample

stimulus (Eichenbaum, Yonelinas and Ranganath, 2007; Johnson et al., 2012), where animals tend to use the former, and humans the latter (Bayley, Frascino and Squire, 2005; Milner, 2005). Moreover, many of these tasks can be performed using various HPC independent spatial reference frames (i.e. retinotopic and egocentric; Burgess, Maguire and O'Keefe, 2002; Lavenex and Lavenex, 2009).

Secondly, despite the use of the proper allocentric reference frame, electrophysiological recordings of hippocampal place cells are equally plagued by methodological biases. Indeed, the combination of open-field foraging paradigms, where space is the only relevant variable (Eichenbaum et al., 1999), with the selection of high-firing units (i.e. selecting responsive neurons and discarding low firing ones) has lead researchers to state that the majority (≥ 60%) of cells in the HPC are spatially tuned (Henriksen et al., 2010; Langston et al., 2010; Wills et al., 2010). However, the "selection bias" within these studies leaves a significant proportion (~ 40%) of neurons to be labelled as "untuned" or "unresponsive" and directly leads to a "confirmation bias", defined by Harris et al. (2016) as:

> *"find[ing] an over-abundance of neurons that respond precisely to the stimulus or condition being investigated."*

More complex tasks were then designed, adding experimental variables such as time, context or item associations. The spatial encoding of place cells was found to depend on both task and context, where different cell populations can encode position within identical environments only differentiated by experimental contexts (McKenzie et al., 2014; Ekstrom and Ranganath, 2017). These neurons not only respond to location within a physical space, but can also respond to location within a temporal space (i.e. time cells; Kraus et al., 2013; Eichenbaum, 2014; Ekstrom and Ranganath, 2017) and to sound pitch within a frequency space (Aronov, Nevers and Tank, 2017). Moreover, the encoding of position within a conceptual space has been shown to represent information within the current focus of attention, such as exploration of local versus distal cues (Fenton et al., 2010) or the order in which task dependent variables are processed during target sampling, from location, to identity and value (McKenzie et al., 2014). Multidimensional (i.e. spatiotemporal) representations are also present where the past, current or future trajectories can be encoded by neuronal populations, corresponding to the animal's current goals (Eichenbaum et

al., 1999; Ferbinteanu and Shapiro, 2003; Dragoi and Buzsáki, 2006; Lisman and Redish, 2009; Johnson et al., 2012; Wikenheiser and Redish, 2015).

As the physiological study of self-generated motion within an allocentric space is hard to apply to human and non-human primates (Bohbot et al., 2017), the aforementioned results were almost exclusively limited to rodents. In an attempt to bridge the gap between rodents and primates, VR tasks have been developed and successfully applied to rodents (Harvey et al., 2009; Chen et al., 2013; Ravassard et al., 2013; Aghajan et al., 2014; Aronov and Tank, 2014; Acharya et al., 2016) and primates (Washburn and Astur, 2003; Sato et al., 2004). Initial research found strong analogies between rodents, primates and humans in terms of neuronal firing properties (Skaggs et al., 2007) and activity (Hargreaves et al., 2012). Furthermore, strong allocentric position encoding has been found in monkeys (Hori et al., 2005; Furuya et al., 2014) and humans (Ekstrom et al., 2003; Chadwick, Bonnici and Maguire, 2012; Jacobs et al., 2013), as well as non-spatial reference frames, such as temporal (Naya and Suzuki, 2011; Sakon et al., 2014) and semantic (Jafarpour et al., 2017). Of note, primates primarily use vision to explore their surroundings, unlike rodent's locomotor and whisking behaviors (Meister and Buffalo, 2016). Accordingly, allocentric gaze position within an environment (i.e. where the subject looks) is encoded by hippocampal neurons (Feigenbaum and Rolls, 1991; Rolls and O'Mara, 1995; Rolls, Robertson and Georges-frangois, 1997; Georges-François, Rolls and Robertson, 1999; Rolls, 1999) and can be more informative than the subject's actual position (Rolls and Xiang, 2006; Hsieh et al., 2014; Wirth et al., 2017).

1.6 Unified theory of hippocampal function

The aforementioned results suggest that HPC neurons are not tuned in the classical (i.e. sensory) sense, but are tuned to both spatial and non-spatial features (Moser, Kropff and Moser, 2008), to their association (Eichenbaum, 2004; Komorowski, Manns and Eichenbaum, 2009; Komorowski et al., 2013; McKenzie et al., 2014) and that this tuning can vary across experiences (Wirth et al., 2003). The non-linear combination of inputs driving neuronal responses has been termed "mixed selectivity" and has further been found in many high-order brain areas, such as the prefrontal cortex (Rigotti et al., 2013; Bittner et al., 2015; McKenzie et al., 2016). This feature

allows for relatively simple networks to perform highly complex computations across a large set of dimensions, while having a relatively simple readout (Rigotti et al., 2013). The combination of mixed selectivity and the broad features encoded by the HPC has lead to a few updated hypotheses about its function.

Firstly, building from the conflicting "spatial" and "memory" hypotheses, it was proposed that the HPC was indeed involved in spatial processing and that the same mechanisms could be used to navigate into a memory or mental space (Buzsáki and Moser, 2013; Buffalo, 2015). Conversely, supporters of the memory hypothesis suggested that the HPC enabled spatial navigation through memory mechanisms, allowing the creation of context dependent associations across multiple dimensions (Eichenbaum and Cohen, 2014). Regardless of whether the HPC is spatially tuned to support memory, or memory tuned to support spatial processing, the spatiotemporal dimensions are inherent to experiences and are thus believed to be automatically represented within the HPC (Eichenbaum et al., 1999; Fyhn et al., 2004). Secondly, building from the encoding of temporally separated signals (i.e. past, present and future) and the outcome encoding in the DMS task, it was hypothesized that the HPC acts as a comparator, where expectation signals (e.g. future outcomes) are compared with current stimuli and past experiences, to either update memory traces or draw inferences and generalizations across experiences (Lisman, 1999; Numan, 2015; Palombo, Keane and Verfaellie, 2015). It is important to note that the HPC is not believed to be involved in the generation of expectation or decision signals, but only in comparing their outcomes (Catanese et al., 2012).

From the common threads in the previous hypotheses, a unifying theory of HPC function can be stated: the creation and updating of context-dependent associations between behaviorally relevant features, required for the planning and execution of goal directed behavior, which can be organized across both abstract and physical dimensions (Milivojevic and Doeller, 2013; Eichenbaum and Cohen, 2014; McKenzie et al., 2014, 2016; Collin, Milivojevic and Doeller, 2015; Schiller et al., 2015; Spellman et al., 2015; Eichenbaum, 2017; Ekstrom and Ranganath, 2017; Stachenfeld, Botvinick and Gershman, 2017). The HPC thus automatically encodes attended stimuli and organizes their representations within current behavior. However, the mechanisms involved in such organization are not fully understood, as stated by Kelemen and Fenton (2015):

These studies suggest that multiple mechanisms organize place cell activity into coactive same-function subgroups to signal distinct qualities of location that include position, spatial frame, and behavioral episode. Although the specific mechanisms have not been fully clarified, they seem to involve the dynamic coordination of excitation and inhibition, operating on multiple timescales much shorter than the several minutes of the typical analysis of place fields.

1.7 Hippocampal local field potentials

In order to understand how single neurons are coordinated by their excitatory and inhibitory inputs, such a signal must first be recorded. Local field potentials (LFPs) are low frequency oscillations (≤ 250 Hz) that represent the summation of all electrical activity from afferent pathways and local populations, reflecting information processing and flow across neural networks (Ekstrom et al., 2007; Buzsáki, Anastassiou and Koch, 2012; Herreras, 2016; Rangel et al., 2016). To correlate field activity and behavior, LFP traces are first transformed into an analytic signal and analysed on three dimensions: frequency, power and phase (Figure 1-3). Frequency values represent the number of complete oscillations per second (i.e. Hz) and are classically divided in bands based on the EEG literature: delta (≤ 4Hz), theta (4-8 Hz), alpha (8-12 Hz), low-beta (12-20 Hz), high-beta (20-30 Hz), low-gamma (30-60 Hz), mid-gamma (60-120 Hz) and high-gamma (120-256 Hz; Tremblay et al., 2015). Note that the "classical" definition of theta differs significantly to the one being used in the hippocampal literature. I will therefore use the "classical theta" label to define frequencies between 4 and 8 Hz, in accordance with the EEG literature. Hippocampal frequencies between 3 to 12 Hz will remain labelled theta or hippocampal theta. Power values quantify the amount of energy within a certain frequency range and are defined as the squared amplitude of the filtered oscillations. Phase values point to "when" within the oscillation an event occurs (e.g. peak, trough, ascending or descending portion) and are defined in degrees (0 - 360).

Considering that LFPs represent the sum of all electrical currents (i.e. ionic flow) within the vicinity of the recording electrode, a wide variety of biophysical processes can influence the recorded signal. Theses processes are however well know and have been extensively reviewed by

Buzsáki and colleagues (2012). First of all, the network architecture can have a profound impact on the recorded field potentials, where variations in cellular density, cortical layer or recurrent projections could potentially modulate the power, polarity and rhythmicity of the LFPs, respectively. Moreover, the diverse properties of neuronal subtypes, such as morphology, intrinsic current and membrane channels/receptors, directly modulate their activity patterns, and thus their influence on field potentials. For example, membrane receptors, such as GABA, AMPA and NDMA, operate at different speeds, where longer activation times increase the probability of having multiple coactivated neurons, summing to larger amplitudes at a lower frequency. Although fast bursting neurons are appropriately associated with lower amplitudes and higher frequencies, their robust activation can lead to afterhyperpolarizations lasting for up to two seconds, which also yields oscillations at a low frequency (Buzsáki, Anastassiou and Koch, 2012). The previous examples are directly involved in the major problem of LFP oscillations: identical LFP traces can be obtained from any combination of the aforementioned biophysical mechanisms. It is therefore almost impossible to identify the exact origin of LFP oscillations from single electrode recordings (Kajikawa and Schroeder, 2011; Herreras, 2016). It is however possible to correlate behavior with changes in LFP properties (i.e. frequency, power and phase) within a well-defined brain region, to infer putative changes in cognitive states, active neuronal populations or inputs (Colgin, 2013, 2016; Herreras, Makarova and Makarov, 2015). Indeed, frequency-specific changes in LFP activity within a network are believed to represent individual cognitive processes or interactions, where multiple frequency bands (i.e. multiple processes) can be active at once (Siegel, Donner and Engel, 2012). The following sections will thus present the fundamental frequency bands identified within the HPC, their behavioral correlates and interactions.

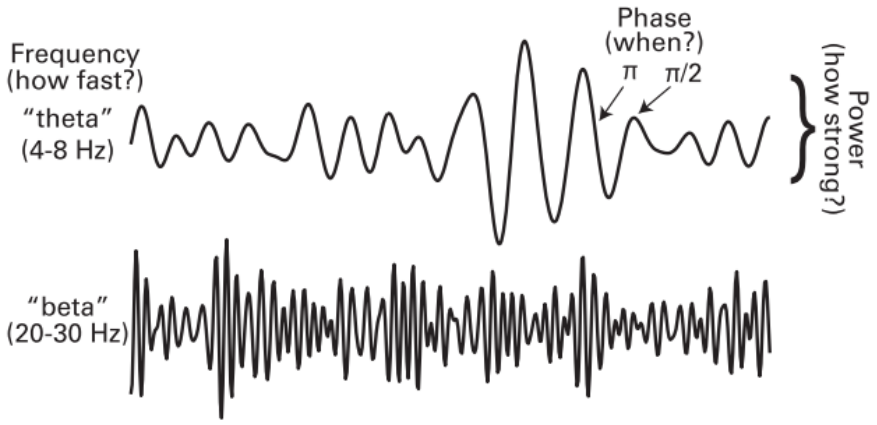

Figure 1-3. Example LFP traces and the different dimensions used for their analysis. Adapted from Cohen (2014).

Firstly, the theta rhythm has been labelled as the most salient and most studied rhythm of the rodent HPC (Berg, Whitmer and Kleinfeld, 2006; Colgin, 2016). It is found in every HPC sub-region, across all mammalian species, during hippocampal "active" states (Buzsáki, 2002; Colgin, 2016). Additionally, two different sub-types of theta oscillations have been identified: type 1, or atropine resistant, operates at higher frequencies (~6 – 12 Hz), is task independent and has been associated with motor activity during open field exploration; and type 2 (~4 – 9 Hz), or atropine sensitive, occurs during immobility, is modulated by the MS and is related to task dependent sensory processing (Sainsbury, Harris and Rowland, 1987; Bland and Oddie, 2001; Buzsáki, 2002; Colgin, 2013; Ekstrom and Watrous, 2014; Gangadharan et al., 2016). It is important to note, as locomotor behaviors typically require the processing of sensory information from the environment, that type 2 theta can exist in isolation during immobility, but is always present during type 1 behaviors (Bland and Oddie, 2001). This has led to the two sub-types being seldomly distinguished in the literature and to significant inconsistencies regarding theta definitions, where virtually every frequency within the 3 to 12 Hz range has been labelled as such (Skaggs et al., 2007; Killian, Jutras and Buffalo, 2012; Ekstrom and Watrous, 2014; Jacobs, 2014; Colgin, 2016). Furthermore, "primate" theta has been associated with lower frequencies (~3 - 4 Hz; Stewart and Fox, 1991; Clemens et al., 2013; Watrous et al., 2013; Jacobs, 2014; but see Bohbot et al., 2017) while higher frequencies within the 8 to 12 Hz range are typically referred to as alpha. Despite the

incoherence of the theta label, it will be used as it is defined in the literature (i.e. 3 - 12 Hz) and a proper band separation will be addressed in the discussion (Section 4.2.1).

Although the power of these oscillations has been correlated with virtually every overt and covert behavior (Buzsáki, 2005), most observations are in agreement with either a role in motor or sensory processing. Accordingly, theta power has been shown to directly correlate with running speed and with the magnitude of ballistic displacements (e.g. jumps or teleportation; type1: Bland and Oddie, 2001; Ekstrom et al., 2005; McNaughton et al., 2006; Watrous, Fried and Ekstrom, 2011; Hartley et al., 2014; Vass et al., 2016). On the other hand, it is also correlated with memory performance and task context and is modulated by MS activation/inhibition which does not influence place field formation or locomotor behaviors (type 2: Ekstrom et al., 2007; Brandon et al., 2014; Hasselmo and Stern, 2014; Vandecasteele et al., 2014; Wang et al., 2014). Furthermore, the evaluation of the relationships between HPC place cell spiking and LFP oscillations (i.e. spike-field coherence) has revealed a strong correlation with theta phase, where the preferred phase of spiking shifts as the animals move through a neuron's place field, a process termed phase-precession (O'Keefe and Recce, 1993). Indeed, as presented in Figure 1-4, the place cells fire at successively earlier theta phases as the animal progresses through a place field, with stronger activation at the trough of the theta rhythm, corresponding to the center of the place field (Skaggs et al., 1996; Jeewajee et al., 2013). The same mechanism has been found during the encoding of past and future trajectories (Itskov et al., 2008; Lisman and Buzsáki, 2008; Lisman and Redish, 2009), where individual theta cycles contain information related to a single attended representation or path (Jezek et al., 2011; Colgin, 2013). Theta driven neuronal firing has also been found in non-spatial cells, such as interneurons (Rangel et al., 2016), and is believed to play a role in memory formation, as both synaptic potentiation/depression (Huerta and Lisman, 1995; Hyman et al., 2003; Buzsáki, 2005) and memory encoding/retrieval (Manns et al., 2007; Siegle and Wilson, 2014) have been linked to different preferred theta phases. Of note, similar phase preferences were found in humans (Jacobs et al., 2007) and the reliability of spike-field coherence is thought to be predictive of memory strength (Rutishauser et al., 2010). While the separation of distinct representations within an area is essential for processing, it is also necessary when exchanging information between brain regions. Theta band synchrony between the HPC and the prefrontal cortex (PFC) has been repeatedly found (Hyman et al., 2005; Jones and Wilson, 2005; Gluth et al., 2015; Gruber

et al., 2017), and the direction of information correlates with undertaken behaviors, such as contextual exploration (Place et al., 2016) and learning (Brincat and Miller, 2015).

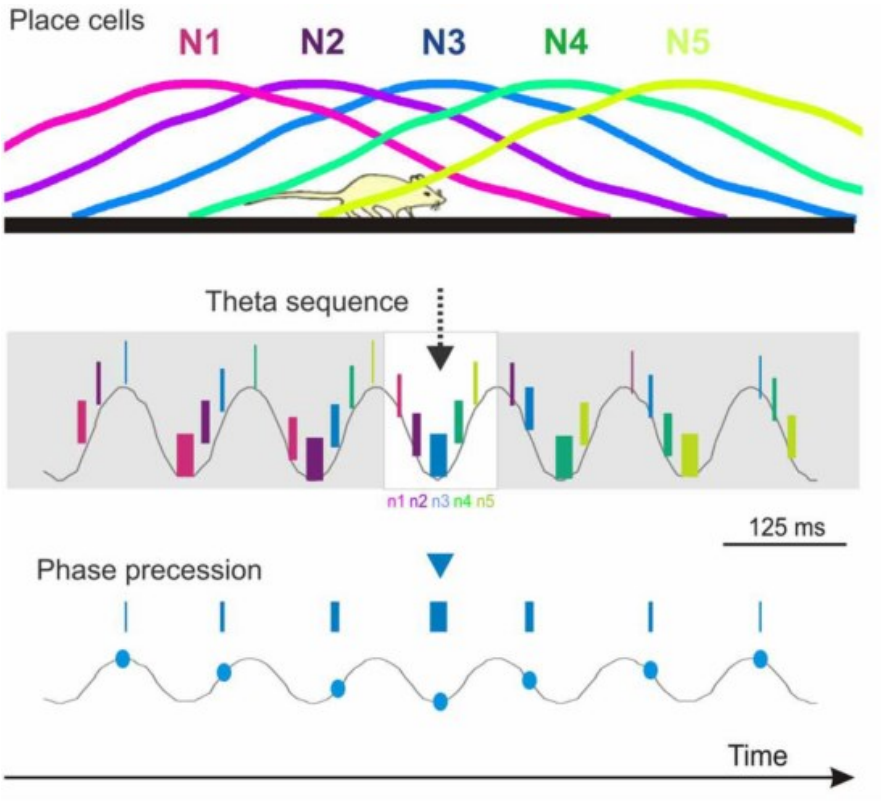

Figure 1-4. Phase precession example for 5 place cells (N1-5). As the animal move through successive place fields, individual neurons fire at successively earlier theta phases, peaking at the trough. Adapted from Dragoi (2013).

Secondly, while sequential theta oscillations can serve to differentiate behaviorally distinct representations, such as different trajectories (Lisman and Jensen, 2013), and phase preferences within a single oscillation can differentiate cognitive processes, such as prospective or retrospective coding (Hasselmo, 2005), individual items must be segregated and organized within these sequences. This is achieved through cross-frequency coupling (CFC), where neuronal spiking is modulated by the interactions of the theta phase with a higher frequency band, namely the gamma band (Aru et al., 2014). According to this model, termed theta-gamma phase code, the

firing of cells encoding individual items occurs at the consecutive peaks of the gamma oscillation, nested within a single theta cycle (Figure 1-5), thus sequentially segregating distinct location or object representations (Jensen and Lisman, 2005; Lisman, 2005; Dragoi and Buzsáki, 2006; Lisman and Redish, 2009; Wikenheiser and Redish, 2015). The gamma band is further divided, where the low-gamma band (slow gamma; ~30 - 60 Hz) is hypothesized to represent memory related information flow from CA3 to CA1, whereas the mid-gamma band (~60 - 120 Hz; fast gamma) is believed to represent cortical and sensory information coming from the EC (Rey, Fried and Quian Quiroga, 2014; Colgin, 2016; Rangel et al., 2016; Fernández-Ruiz et al., 2017). Their interactions in CA1 could thus serve to bind, retrieve or compare expectations with current spatiotemporal context and attended sensory information (Huxter, Burgess and O'Keefe, 2003; Staudigl and Hanslmayr, 2013). Consequently, fast gamma power increases during early target sampling and during retrospective (i.e. short-term memory buffer) coding, whereas slow gamma power increases during late sampling and prospective coding (Bieri, Bobbitt and Colgin, 2014; Takahashi et al., 2014). Moreover, during prospective path encoding, longer paths yield longer theta cycles with an increased number of embedded gamma cycles (Gupta et al., 2012). The reliability of theta and low-gamma CFC also increases across learning during the context exploration phase of a context-dependent associative memory task, suggesting a role in memory recall (Tort et al., 2008, 2009).

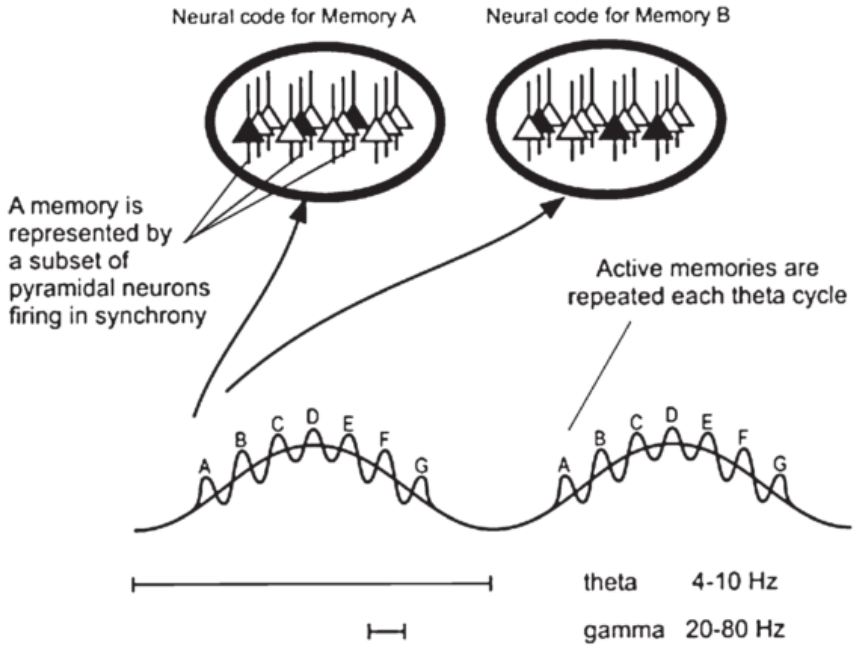

Figure 1-5. Nested gamma cycles within successive theta cycles segregate individual representations (A – G), such as memories or objects. Adapted from Lisman and Buzsàki (2008).

Lastly, another type of phase coupling is present in the HPC during non-exploratory states (e.g. sleep or quiet wakefulness): the sharp wave-ripple complex (SPWR). This complex is composed of a large amplitude and low frequency field potential (i.e. sharp wave) on which a short duration and high frequency (i.e. high-gamma; ripple) burst of activity is superimposed (Figure 1-6b). Its presence has been closely linked to the neuronal replay of experienced events to sustain memory consolidation and trajectory planning (Girardeau et al., 2009; Girardeau and Zugaro, 2011; Jutras and Buffalo, 2014; Leonard et al., 2015; Leonard and Hoffman, 2016). Accordingly, high cholinergic input to the HPC from MS stimulation, associated with memory encoding (Cassel et al., 1997; Tsanov, 2015), has been found to inhibit ripple production (Vandecasteele et al., 2014). Ripple inhibition has been further shown to impair spatial learning (Girardeau et al., 2009; Roux et al., 2017), whereas neuronal representations during single ripple events have been shown to encode either past or future trajectories (Colgin, 2016). However, considering the high correlation with spiking activity and its leakage into high frequency LFPs (Zanos, Mineault and Pack, 2011), hippocampal ripple events are believed to mostly represent local spiking activity (Buzsáki, Anastassiou and Koch, 2012; Dvorak and Fenton, 2014).

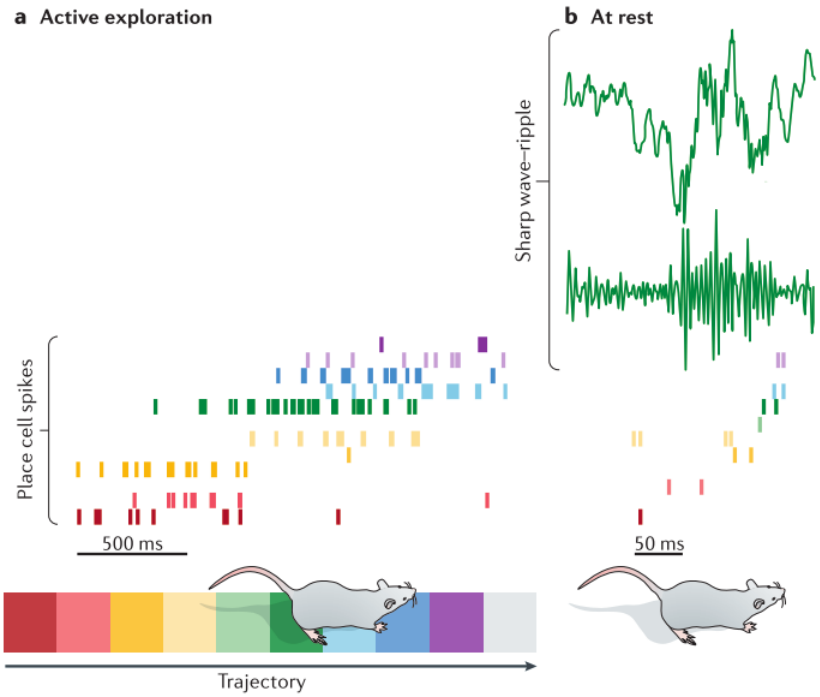

Figure 1-6. a) Hippocampal place cell activity during active exploration. b) SPWR complex (top) and the ripple band filtered signal (bottom) atop the place cell replay of the previous experience during a). Adapted from Colgin (2016).

1.8 Local field potentials phase and behavior

Hippocampal low frequency oscillations undoubtedly play a significant role in coordinating high frequency oscillations and neuronal spiking to support hippocampal function. As previously stated, they can be controlled by either the MS or the EC (Williams and Givens, 2003), although little is known about their behavioral correlates. In both rodents and humans, significant phase resetting was found within the first 200 ms following the onset of behaviorally relevant stimuli, over a broad range of frequencies including the theta band (Tesche and Karhu, 2000; Mormann et al., 2005). This stimulus driven phase reset seems modulated by task requirements (i.e. behavioral relevance; Givens, 1996) but not by sensory modality (Williams and Givens, 2003) or task performance (Mormann et al., 2005). They are thus believed to place the HPC into an optimized state to process incoming sensory information (Williams and Givens, 2003; Mormann et al., 2005; Jutras and Buffalo, 2014). Highly salient "pop-out" events are thought to

drive “bottom-up” visual attention to enhance processing. As visual attention can also be volitionally shifted (i.e. top-down; Buschman and Miller, 2007), the continuous sensing of one’s environment is not a “passive” process, but requires energy expenditure to control motor behavior (i.e. eye movements and sniffing/whisking) and attentional resources (Schroeder et al., 2010). Accordingly, top-down attentional shifts during both ballistic eye movements (i.e. saccades) and whisking have been correlated with HPC theta phase resets (Jutras and Buffalo, 2014).

In rodents, significant phase coherence with whisking behavior has been found during task related object sampling and approach, but not while the animals were simply moving about in an open environment (Macrides, Eichenbaum and Forbes, 1982; Berg, Whitmer and Kleinfeld, 2006; Grion et al., 2016). Similarly, in human and non-human primates, saccadic eye movements correlate with hippocampal phase resets and neuronal activation, which are either absent or reduced without visual stimulation (Sobotka and Ringo, 1997; Sobotka, Nowicka and Ringo, 1997; Hoffman et al., 2013; Jutras, Fries and Buffalo, 2013). While saccade and whisking triggered phase resets can serve as an attentional gating mechanism to modulate sensory processing (Fenton et al., 2010; Aly and Turk-Browne, 2016), saccades in primates also play a role in spatial exploration. Indeed, whisking exploratory behavior is limited to proximal objects, whereas saccades are extensively used by primates to explore and structure the external (i.e. allocentric) world, without requiring locomotion (Ekstrom, 2015; Meister and Buffalo, 2016; Wirth et al., 2017).

1.9 Research aims

Summarizing the aforementioned findings, I believe that the HPC is involved in the creation and maintenance of context dependent associations between relevant features on an experience, required for goal directed behavior (Eichenbaum, 2017). These associations are reflected in the complex conjunctive coding of HPC neurons, binding stimuli features within an allocentric spatiotemporal reference frame (McKenzie et al., 2016). Moreover, the firing of these neurons is controlled by the interplay between two LFP frequency bands, namely theta and gamma, forming a robust phase code. While individual theta cycles segregate distinct representations or events, such as trajectories or contexts, the multiple embedded gamma cycles serve to organize and isolate individual features, such as places or objects (Lisman and Jensen, 2013). Within this

framework, the theta band acts as the main coordinator: it provides the start and end reference points of holistic representations and allows the reliable transmission of these "messages" to other brain regions. Behaviorally, the theta phase seems to be controlled by sensory events, such as stimulus onsets and active sensing (i.e. whisking and saccades; Meister and Buffalo, 2016), although our knowledge of this phenomenon is incomplete.

This is especially true for primate species, where inconsistencies across experiments raise doubt on the exact nature of sensing triggered phase resets. For example, HPC response to saccades and gaze positions have been shown to be either present, albeit reduced (Sobotka and Ringo, 1997; Sobotka, Nowicka and Ringo, 1997; Rolls, 1999; Rolls and Xiang, 2006), or fully absent (Hoffman et al., 2013; Jutras, Fries and Buffalo, 2013), during darkness and non-exploratory states. Two competing hypotheses have thus emerged from these conflicting results. It has first been proposed that the saccadic signal within the HPC is "extra-retinal" in origin and most likely reflects motor and spatial processing (Sobotka and Ringo, 1997). Conversely, recent reports suggest that saccades are used to place the HPC in an "optimal state" to receive sensory stimuli and promote memory formation (Jutras, Fries and Buffalo, 2013; Meister and Buffalo, 2016). As these two hypotheses are highly analogous to the "spatial vs. memory" debate of HPC function, I believe that this confusion is due to oversimplified tasks and the oversight of many confounding variables. For example, variations in saccadic behaviors, such as rate, amplitude or direction, are seldomly monitored across the dark/light, high/low memory and stimuli onset conditions. It is however well established that the qualities of saccades are correlated with memory function, where higher rates and amplitudes are associated with better encoding (Kafkas and Montaldi, 2011; Molitor et al., 2014; Meister and Buffalo, 2016), and are modulated by the complexity of the visual stimulation, where impoverished or absent stimuli lead to slower and less frequent saccades (Sobotka and Ringo, 1997; Andrews and Coppola, 1999). Moreover, using saccade onsets to quantify phase resetting across "optimal states" could be biasing the results, as saccade durations can vary greatly, hence jittering the phase alignment and incoming sensory inputs.

The aims of this thesis are thus two-fold. First, to create a VR suite and complex experiments that properly test HPC function, precisely aligning navigational, saccadic and neuronal data. Secondly, I aim to record hippocampal LFPs in the macaque monkey following sensory exploration of said tasks, while closely monitoring all aforementioned confounders and

saccadic behavior, to investigate: whether the motor or sensory components of saccades are driving HPC phase resets, how are the resets modulated by task requirements and whether theta phase is reset to an "optimal state" or whether it represents spatial processing. It is important to mention that non-human primates offer numerous advantages over rodents as a model of human hippocampal function: their anatomical pathways are highly similar, they primarily use vision to explore their environment, they present comparable performance in many attentional and memory tasks, and they allow for invasive electrophysiological recordings (Jutras and Buffalo, 2014).

Firstly, we designed a VR toolbox that interfaces with our electrophysiological recording equipment and minimizes timing errors between the two systems. This toolbox allowed for the creation of an associative memory (AM) task, within a fully navigable 3D virtual environment. This task was specifically designed to highlight HPC processing via: allocentric navigation and context dependent learning. Both system and task are presented in Chapter 2. Using this system, we achieved a temporal resolution of a few milliseconds (~3 ms) between position within the VR environment, eye position on the screen and neural data.

Secondly, we set to investigate open questions regarding sensing triggered theta phase resets in the primate HPC. To do so, we added two separate tasks to our testing suite: an open-field foraging (FOR) task, set in the same environment as the AM task, replicating classical place cell experiments, and a classical cued saccade task (CS), using unnatural and simple stimuli. Our first objective was to parse out the relative contributions of stimulus onsets and subsequent sensing on HPC phase resets. Indeed, when measuring stimulus triggered phase resets, previous studies did not monitor saccades (Tesche and Karhu, 2000; Mormann et al., 2005), which could have a strong confounding effect on the resulting signal. Furthermore, considering the influence of visual stimulation on the reliability of phase resets, we investigated whether the onset (i.e. motor; Sobotka and Ringo, 1997; Jutras, Fries and Buffalo, 2013; Staudigl et al., 2017) or the offset (i.e. visual; Hoffman et al., 2013) of the saccade correlates more strongly with theta phase. Accordingly, we asked the question whether it is the visual nature or the behavioral relevance of the object being saccaded to that engenders the phase resets. Lastly, considering the dual role (i.e. spatial and object exploration) of gaze in primates, we investigated the information content of saccade triggered phase resets. Results are presented in Chapter 3. We found that both saccades onsets and offsets reset HPC phase in a frequency specific manner, where saccade triggered resets correlate with the

saccade parameters (i.e. amplitude and direction) and where fixation triggered resets correlate with visual input.

Chapter 2

2. Cross-species 3D virtual reality toolbox for visual and cognitive experiments

Classical experiments using oversimplified tasks and stimuli (e.g. dots or gratings) have been found inefficient at properly activating brain regions involved in high-order cognitive operations, yielding conflicting results across studies. For example, hippocampal research has been plagued by studies using ambiguous reference frames and a limited number of behaviorally relevant stimuli or dimensions. The objective of the presented study was thus to create a virtual reality testing suite, to enable the creation of complex cognitive tasks using allocentric navigation in macaque monkeys, while undertaking electrophysiological recordings. The system was designed to obtain milliseconds temporal precision across the multiple systems used in monitoring behavior, such as the virtual reality engine, eye tracker and neurophysiological recording equipment. This chapter has been adapted from: Doucet G, Gulli RA and Martinez-Trujillo JC. 2016. Cross-Species 3D Virtual Reality Toolbox for Visual and Cognitive Experiments. *J. Neurosci. Methods*. 266. Elsevier B.V.:84–93.

2.1 Abstract

Although simplified visual stimuli, such as dots or gratings presented on homogeneous backgrounds, provide strict control over the stimulus parameters during visual experiments, they fail to approximate visual stimulation in natural conditions. Adoption of virtual reality (VR) in neuroscience research has been proposed to circumvent this problem, by combining strict control of experimental variables and behavioral monitoring within complex and realistic environments.

We have created a virtual reality toolbox that maximizes experimental flexibility while minimizing implementation costs. A free VR engine (Unreal 3) has been customized to interface with any control software via text commands, allowing seamless introduction into pre-existing laboratory data acquisition frameworks. Furthermore, control functions are provided for the two most common programming languages used in visual neuroscience: Matlab and Python.

The toolbox offers milliseconds time resolution necessary for electrophysiological recordings and is flexible enough to support cross-species usage across a wide range of paradigms.

Unlike previously proposed VR solutions whose implementation is complex and time-consuming, our toolbox requires minimal customization or technical expertise to interface with pre-existing data acquisition frameworks as it relies on already familiar programming environments. Moreover, as it is compatible with a variety of display and input devices, identical VR testing paradigms can be used across species, from rodents to humans.

This toolbox facilitates the addition of VR capabilities to any lab without perturbing pre-existing data acquisition frameworks, or requiring any major hardware changes.

2.2 Introduction

In visual neuroscience, researchers have long faced the challenge of conducting ecologically valid measurements of experimental variables while maintaining strict experimental control over visual displays. For example, most visual experiments in both human and non-human primates (e.g. bars, dots or gratings) have used simplified stimuli on homogeneous backgrounds, raising the question of whether their results could be directly extrapolated to more naturalistic viewing conditions (Bohil, Alicea and Biocca, 2011; Nishimoto and Gallant, 2011). Indeed, under

normal viewing conditions the retina is bombarded by a multitude of background signals and visual receptive fields seldom contain a single stationary stimulus. Although challenging, some studies have shown that it is possible to decipher basic neuronal properties (e.g. receptive field and tuning) from more naturalistic stimuli, using sophisticated analysis methods (Nishimoto and Gallant, 2011). However, ecological validity might still be undermined by the nature of the visual stimuli, often limited to passive viewing of static pictures or movies, whose relevance to the subject's natural behavior is unclear. Thus, recording and interpreting physiological signals in naturalistic environments remains a challenge for visual neuroscientists.

Modern virtual reality (VR) technology may provide a solution to this problem. It allows researchers to design and therefore strictly control dynamic, realistic and immersive environments, while closely monitoring behavioral and physiological responses during testing (Loomis, Blascovich and Beall, 1999; Bohil, Alicea and Biocca, 2011). VR technology has indeed been preferred over real stimuli to generate intuitive sensorimotor responses across multiple species, from insects to humans, as its advantages range far beyond precise experimental control (Bohil, Alicea and Biocca, 2011). Firstly, subjects are kept sufficiently static during VR navigation to enable electrophysiological or imaging experiments. Secondly, VR environments can be created, scaled and manipulated by researchers in a manner that is almost impossible in physically constrained real-world testing environments. Thirdly, VR experiments are more engaging for subjects, compared to passive viewing, as they require complex and ecologically valid behavioral responses to multisensory stimulation (e.g., approaching a virtual food source or escaping from a virtual predator). Finally, VR environments circumvent many ethical limitations by preventing injuries in "hazardous" tasks (Tarr and Warren, 2002; Slater et al., 2006; Mueller et al., 2012).

Although most drawbacks of early VR solutions (i.e. poor image quality and low level of details) have been addressed through technological advances, the resulting increase in systems' complexity and in the expertise required for their implementation have forced most laboratories to design inflexible and singularly purposed systems (Loomis, Blascovich and Beall, 1999; Bohil, Alicea and Biocca, 2011; Mueller et al., 2012; Jangraw et al., 2014). For example, laboratories interested only in monitoring behavioral responses during navigation or foraging often lack the temporal precision and/or resolution required for electrophysiological experiments (Caplan et al., 2003; Astur et al., 2004; Newman et al., 2007; Weidemann, Mollison and Kahana, 2009; Doeller,

Barry and Burgess, 2010). Additionally, previous systems have been designed in a species-specific manner by either using fixed input/output devices (e.g. gamepad or trackball) or written cues (Hölscher et al., 2005; Harvey et al., 2009; Aronov and Tank, 2014; Slobounov et al., 2014). Although many existing VR platforms are customizable to fit one's desired paradigm, they often require a two-tier architecture (i.e. one computer for the VR engine and a second computer running experimental control software). This entails learning each tier's specific script library, sometimes under multiple programming languages (Mueller et al., 2012; Jangraw et al., 2014), which greatly increases implementation cost in both time and resources. While many commercial applications have been proposed to overcome these issues (e.g. Vizard, WorldViz, USA; Eon Reality, USA), their high cost may hinder their widespread use. Furthermore, as is often the case with third-party solutions, most of commercial applications use proprietary control software and require specific input/output computer peripheral devices, which could render their implementation in an pre-existing experimental pipeline problematic (Mueller et al., 2012; Jangraw et al., 2014).

Here we aimed to create a freely available VR solution that combines professional grade graphics, high flexibility and cross-species support, which could be implemented in any existing laboratory's data acquisition framework. To achieve this, we applied the architecture proposed by Adobbati et al. (2001) and Carpin et al.(2007): remotely controlling a VR engine via simple text commands sent over a dedicated network connection. Since most programming environments implement the transmission control protocol (TCP) for network data transfer, virtually any programming language can be used to control the VE. Furthermore, as experimenters are most likely to select control software with which they are already acquainted, they are only required to familiarize themselves with the VR engine, greatly reducing implementation costs. As examples, we provide fully functional control script libraries based on the two most common platforms in neuroscience research: Matlab (Psychophysics Toolbox: Brainard 1997; MonkeyLogic: Asaad et al. 2012) and Python (PsychoPy: Peirce 2007; Vision egg: Straw 2008). These libraries were designed to interact with the freely available Unreal Engine 3 development kit (UDK, May 2012 release; Epic Games, USA). Although UDK was specifically designed for commercial video game creation, it has been used in countless virtual applications, from static architectural design to dynamic physics simulation (e.g. driving, fire propagation). This broad range of possible

applications showcases its high flexibility and ease of use, two required characteristics in any VR engines.

2.3 Materials and Methods

2.3.1 General Architecture

The proposed VR system completely segregates the experimenter and subject during the experimental procedures via a two-tier architecture (Figure 2-1). Indeed, as information is bi-directionally exchanged between the UDK computer and the control computer, both subject and experimenter interact with their own distinct interface. The separate interfaces allow the experimenter to instantaneously modify the task parameters, while preventing input devices conflicts (e.g. multiple computer mice) and preserving the subject's experience. Moreover, the available computational resources on the control computer can allow experimenters to monitor the subject's behavior by displaying position, gaze or current state information in real-time. Although it is possible to run VR experiments on a single computer, we strongly recommend to avoid non-VR operations execution on the UDK computer in order to optimize display quality, to prevent frame loss and maximize temporal precision. This is especially important for electrophysiological experiments where the control computer must integrate inputs (e.g. eye tracker and VR engine) and synchronize output signals (e.g. electrophysiological recording equipment and reward system) to properly guide task flow. While these procedures might not be sufficiently computationally demanding to affect display quality in purely behavioral studies, the high computing power required to render high-quality 3D environments at higher refresh rates (i.e. > 100 Hz) might alter the proper timing of data recording and output signals. Lastly, as this toolbox is aimed at facilitating the addition of VR capabilities to any pre-existing visual neuroscience data acquisition framework, the simple introduction of the VR computer, while preserving the current experimental computer and its pre-existing interface with external hardware (e.g. eye tracker, electrophysiological recording system and reward system) greatly reduces implementation costs. The UDK computer and the TCP control scripts thus replace the display adapter of the previous system.

The experimental cascade begins with the subject interfacing with the UDK computer (Figure 2-1, gold rectangle; 8 core 3.4 GHz Windows 7 PC with 16GB of RAM and 2 GB of dedicated video memory) through its appropriate input device. As this framework was developed to be species independent, subjects could be rodent, monkey, or human. To accommodate physiological differences between species, we have created two distinct user classes: humans and animals. While humans are restricted to either a gamepad or mouse and keyboard, animals can interact with the VE through a wide variety of input devices, with the only restriction that it must be configured to operate as a computer mouse. This configuration has been widely used in the rodent VR literature, e.g., trackballs (Hölscher et al., 2005; Harvey et al., 2009; Aronov and Tank, 2014). On the other hand, many primate species have been shown to properly manipulate joysticks in virtual tasks, from capuchins (Leighty and Fragaszy, 2003) to macaques (Washburn and Astur, 2003; Sato et al., 2004; Hori et al., 2005). Although some studies have used human gaming controllers on animals (Kraft KC3 joystick : Leighty and Fragaszy 2003; Washburn and Astur 2003), we recommend the use of more recent industrial strength "plug and play" USB controllers (e.g. CTI electronics, Connecticut, USA or NSI, Belgium). However, the separation between monkeys and humans is not absolute as any joystick input can be converted to gamepad input using freely available software (i.e. x360ce, www.x360ce.com). Indeed, the following experiments, for both humans and monkeys, were undertaken using the aforementioned software and a modified model 215 joystick (PQ Controls, Connecticut, USA). Lastly, despite the fact that we narrowed the range of possible user input to devices keeping subjects still enough for electrophysiological recordings, this range could easily be expanded to haptic or position tracking devices in purely behavioral experiments, either through vendors' drivers or device servers (e.g. VRPN; Taylor et al., 2001).

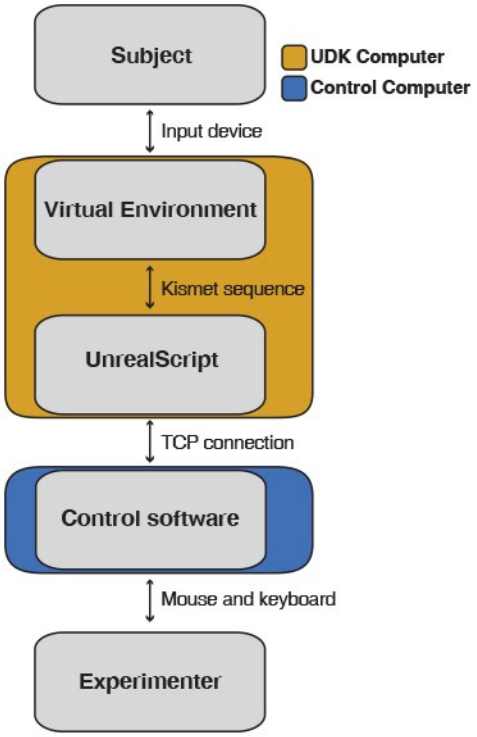

Figure 2-1. Detailed system architecture. Subject actions in the virtual environments first trigger UnrealScript execution through Kismet sequences. Experimental data is then exchanged between the UDK computer (blue box) and the control computer (gold box) via a network connection. On the other hand, the experimenter can trigger changes in the virtual environment by modifying task settings in the control software.

Following proper device configuration, the UDK computer translates user input into appropriate movement in the virtual environment (VE). To do so, it updates the subject's previous position with the incoming input, logs the new coordinates and computes the visual scene accordingly. This is undertaken on a frame-by-frame basis. The course of the virtual simulation is in turn directed by Kismet (see section 2.2.3; Figure 2-2A), a visual scripting language proprietary to UDK, which acts as a two-way translator between virtual interactions and core script functions. Both Kismet nodes and core functions are written in UnrealScript, a C++ and Java inspired object-oriented programming language controlling the inner workings of the virtual engine. Kismet sequences are triggered by *Events* (Figure 2-2A, red hexagon), either internally by actions in the environment or externally by commands sent by the control computer (Figure 2-1, blue rectangle;

2 × quad-core 3.2 GHz Mac Pro with 8 GB of RAM and 512 MB of dedicated video memory). They can, for example, modify the variables read by the control computer when the user reaches a delimited location or, inversely, translate an experimenter's command into a visual change in the environment. Subject data from UDK and experimenter's commands are exchanged between the two computers through a dedicated TCP connection.

2.3.2 **Temporal synchronization**

As the TCP connection is the cornerstone of the system, it is important to note that its communication speed might not be instantaneous in some programming environments. This is the case for the Matlab software, which was not designed for real-time network implementation. Yet, achieving millisecond temporal precision is of upmost importance when combining VR with behavioral or electrophysiological monitoring. According to Asaad and Eskandar (2008), true millisecond precision can only be obtained by overcoming three hurdles: synchronization of display and subject's behavior, adequately reading hardware acquisition buffers, and controlling for supra-millisecond execution speed of high order programming languages. We achieved this by first synchronizing the UDK engine to the monitor's refresh rate, allowing each displayed frame to be precisely time stamped. The UDK engine thus computes the subject's position and state for each frame and stores it in an internal buffer. Subsequently, data is read from the buffer and sent to the control computer through the network connection. However, time-stamping of subject's data on the UDK computer uses a different clock than the control computer, impairing temporal alignment. To circumvent these drawbacks, the two computers' internal clocks were synchronized with a Network Time Protocol (NTP) algorithm (Automachron freeware, http://automachron.software.informer.com/). In a small network and in optimal conditions the NTP algorithm is believed to reach sub-millisecond precision (Pitimon and Nintanavongsa, 2014). The control computer's clock is thus set as a master and the UDK computer is programmed to synchronize to it at fixed time intervals (16 seconds) and to log any recorded time differences.

2.3.3 Unreal Engine

The Unreal Engine running on the UDK computer is a highly customizable and dynamic software. Researchers and developers can interact with the engine through two open and customizable modules provided in the development kit. First, the UnrealScript programming environment, which controls the engine itself (i.e. controllers and classes). Second, the Level Editor is used to create the visual environments with their associated Kismet sequences and user interaction points (e.g. start positions, goals).

While the description of UnrealScript is beyond the scope of this paper, it is necessary to define object-oriented programming (OOP) terminology and explore a few key scripts to properly understand the engine's internal architecture. Firstly, OOP applications are modularly designed, where each module, or class, is uniquely responsible for a specific aspect of the application. An object is simply defined as a single instance of a specific class. For example, the multiple enemy objects displayed on the screen in a video game are merely individual instances of the same "enemy" class. This implies that, while they all have the same default properties upon creation, they can behave and be modified independently once instantiated. The same principles hold true for the Unreal engine, which, upon initialization, loads a default environment, or map, and instantiates a *GameInfo* object from its class definition (Figure 2-2B). The latter contains the list of specific sub-classes to use for the selected task (i.e. *PlayerController*, *Pawn* and *Server*). A single instance of the *PlayerController* class is created for each individual user inserted in the VE. Much like the strings in a puppet/puppeteer relationship the *PlayerController* acts as the intermediary between user commands and the virtual avatar: the *Pawn* class. A *Pawn* object is defined as the transient physical representation of the user in the VE. In simpler terms, it manages collisions and locomotion. Thus, if a user "dies" in a VE, the *PlayerController* object would persist and retain all static information (e.g. user identity and input type). Conversely, a novel *Pawn* object would need to be instantiated to re-initialize its transient properties (i.e. health). The same architecture holds true for the *Server* instance, which responds to connection requests by instantiating *Connection* objects. As is the case for transient *Pawns*, if a connection is lost a new and independent *Connection* object would be created upon reception of a request by the lasting *Server* object. It is through the *Connection* objects that control queries are received, parsed and executed.

Secondly, the engine needs a way for UnrealScript to directly interact with the virtual environment. This occurs through Kismet, a visual scripting language that uses linearly activated nodes to control the world's behavior (Figure 2-2A). Cascades begin with *Events* ("touched" red hexagon) that are triggered by user input in the VE (e.g. *Pawn* collisions) or control queries in UnrealScript. Subsequently, either *Actions* (purple rectangles) or *Conditions* (blue rectangles), are sequentially executed until the cascade reaches an end. While *Conditions* are used to compare or evaluate *Variables* (colored circles), *Actions* directly affect the actors of the virtual scene by modifying their properties (e.g. color, state and visibility).

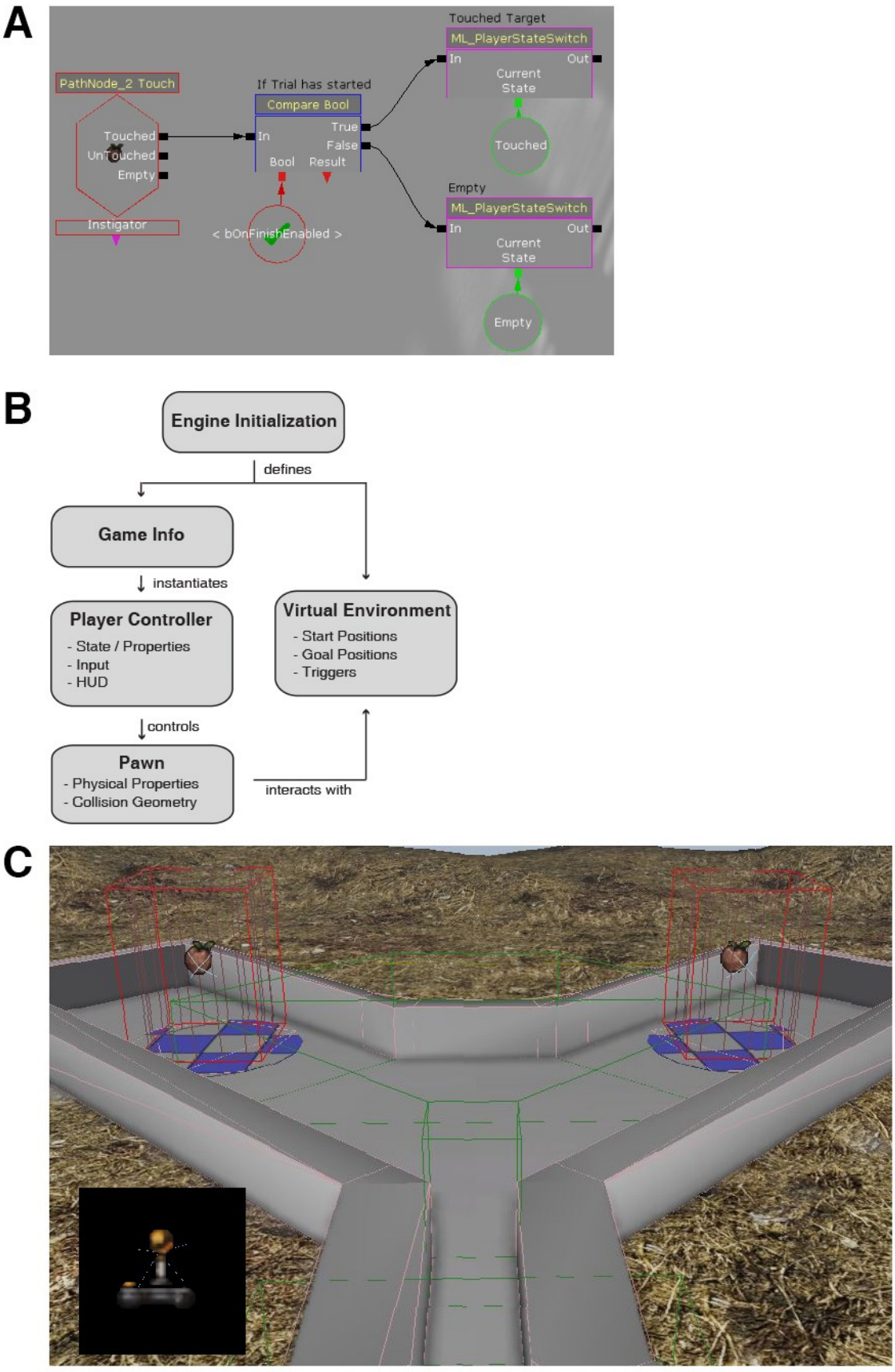
A
Touched Target
ML_PlayerStateSwitch
In
Out
Current State
Touched
PathNode_2 Touch
Touched
UnTouched
Empty
Instigator
If Trial has started
Compare Bool
In
True
False
Bool
Result
< bOnFinishEnabled >
Empty
ML_PlayerStateSwitch
In
Out
Current State
Empty
B
Engine Initialization
defines
Game Info
instantiates
Player Controller
- State / Properties
- Input
- HUD
Virtual Environment
- Start Positions
- Goal Positions
- Triggers
controls
Pawn
- Physical Properties
- Collision Geometry
interacts with
C

Figure 2-2. Unreal Engine general architecture. A. Kismet script cascade example executed when a specific PathNode is touched by the subject. It then changes the current player state if the trial has started. B. Engine initialization cascade. The Game Info class defines the subclasses to use for any specific task while the virtual environment contains all the geometry and usable objects. C. Functional elements as seen in the level editor. PathNodes are represented by apples and their collision volume by a red wireframe mesh. *Trigger* volumes are displayed as a green wireframe mesh, *PlayerStart* as a joystick (inset) and *InterpActors* as the checkered disks.

Lastly, functional elements need to be inserted in the environment to properly register *Pawn* behavior and initiate Kismet sequences, namely *PlayerStart*, *Triggers*, *PathNodes* and *InterpActors*. As its name implies, the *PlayerStart* (Figure 2-2C, inset) indicates where the user initially appears in the environment. In our case, it is placed in a pitch-black room to display a blank screen during inter-trial intervals. *Triggers* (green wireframe box) are invisible volumes that register when the user's Pawn enters or exits them (i.e. collisions). For example, they could be used to precisely control when or where certain cues are displayed, by triggering separate Kismet sequences upon *Pawn* entry or withdrawal. Although *PathNodes* were initially created to guide artificial intelligence navigation across the environment, they can be configured to have a collision volume and behave like T*riggers* (apples and red wireframe volume; Figure 2-2C). In our case, they mark the possible start and goal positions and, through their collision volume, indicate when the user reaches them by modifying the *PlayerController*'s state. Lastly, the engine is designed to optimize computational resources usage by pre-rendering many visual features, for instance: textures, shadows and lighting. However, in many situations, dynamic objects are required and incompatible with pre-calculated graphics. For example, if an external cue needs to be removed in one trial its shadow must be updated accordingly. *InterpActors* (Figure 2-2C, checkered disks) are such objects, as they tell the engine to dynamically compute their visual properties to allow for naturalistic behavior. Since their appearance can be controlled in real-time, they are mainly used as either allocentric or contextual cues.

2.3.4 **Control scripts**

While the Unreal Engine (Kismet and Level Editor) contains information about the VE itself, it does not contain any information about trial specific objectives and conditions. Information thus needs to be exchanged between the UDK and control computers to properly execute tasks. This occurs through queries sent from the experimental control computer, to which the UDK computer replies by either modifying the environment or by sending back user data. A typical flow chart of information transmission and function execution for a single trial can be seen in Figure 2-3.

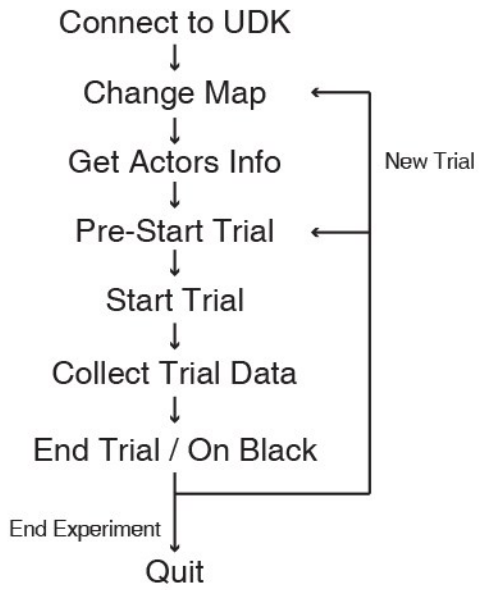

Figure 2-3. Typical trial script execution cascade. Upon initialization, the control software establishes a connection with the Unreal Engine and proceeds to load the appropriate map for the selected task. It then retrieves information about the functional elements contained in the map ("Get Actors Info"). Following trial parameter selection, the control computer sends the information to the engine in the "Pre-Start Trial" phase. Data collection is initiated by trial onset, and continues until the end of trial criterion is met. Subsequent trials can either continue in the same (back to "Pre-Start Trial") or in a different (back to "Change Map") environment.

Connect to UDK:

Following engine initialization, the control computer establishes a TCP connection with the UDK *Server*.

Change Map:

As an environment needs to be specified to initialize the Unreal Engine, we have programmed it to begin in a default blank environment. The control computer thus needs to send a query to load the proper map for the selected task.

Get Actors Info:

When a new environment is opened, the control computer must primarily gather information about its possible targets (i.e. *PathNodes*) and cues (i.e. *InterpActors*) in order to prepare trials. This script gathers the name and position of all usable actors in the VE. The experimental software can now be programmed to either manually or randomly select the trial's start and goals positions, as well as contextual cues information.

Pre-Start Trial / Start Trial:

This function then sends back to UDK the selected start, goals and cues, as well as their respective properties, to implement the required changes in the VE. Although the "Start Trial" script can be used to transport the subject to the selected start position and force trial onset, this procedure can also be included in the "Pre-Start Trial" Kismet sequence, leaving user initiated movement as the trial start trigger. In this scenario, the trial start would be time-stamped by UDK through a change in the *PlayerController*'s state, later read by the control software.

Collect Trial Data:

While most data collection occurs during the active trial phase, it can also be used to monitor the subject's behavior during inter-trial intervals. It could thus prevent a new trial from starting while keyboard keys or joystick are engaged, enforcing the release of input devices between trials. Regardless of trial epoch, the data received from UDK contains, for each displayed frame since the last query, the time-stamped player positions, rotations and states (i.e. last touched *Trigger* / *PathNode* or trial initialization time).

End Trial / On Black:

By analyzing the acquired list, the control software can compare either user position or state values with the previously selected goals and evaluate if a trial termination criterion has been met. Subsequently, an "End Trial" command could be issued to reset Kismet variables and inactivate *PathNodes* collisions in preparation of the next trial. Alternatively, an "On Black" command could be sent to transport the user back to the *PlayerStart* position to have a blank inter-trial interval screen. Though these two functions could be used interchangeably and seem

redundant, their combination permits the introduction of a "free roam" period, in which the subject can freely explore the environment for a limited time at the end of each trial.

In summary, following complete engine initialization (Figure 2-2B), the execution of the "Connect to UDK" control function (Figure 2-3A) results in the instantiation of a new *Connection* object by the UnrealScript *Server*. Queries (e.g. Change Map or Get Actors Info) can then be received and parsed to execute the appropriate UnrealScript functions. These functions are either activating Kismet sequences (e.g. Pre-Start Trial or On Black) to change the VE or reading *Pawn* collision data (i.e. states) stored in the *PlayerController*'s buffer. These data are then parsed into a single string and sent back to the control computer for analysis.

2.4 Results

2.4.1 **Clock Synchronization**

As previously stated, the NTP algorithm is believed to allow for sub-millisecond temporal precision in an optimal setting. However, these values might vary greatly under normal operating conditions. We thus aimed to quantify the efficiency of the synchronizing algorithm by evaluating the reported time differences between the two computers' clocks. The Automachron software (http://automachron.software.informer.com/) is programmed to synchronize clocks once every 16 seconds and to log the resulting time difference. By analyzing the logged values for a period of over 5 months, we found an averaged difference value of 0 ± 3 ms (mean ± standard deviation; Figure 2-4A). Since most of the recorded values occurred while the computers were unused, the relatively high standard deviation and the presence of extreme values (≤-5ms and ≥ 5ms) could be explained by impaired synchronization during experiments' high network load. To test this hypothesis, we recorded an hour-long session of a subject undertaking the contextual learning task, described in section 2.4.2. Figure 2-4B shows that synchronization is only slightly affected by experimental procedures as the mean delay value barely changed (1.1 ± 0.7 ms; N.S. two-sample t-test). Considering the rare occurrence (< 1%) of extreme delays and the robustness of the algorithm during heavy load, we thus estimated the temporal jitter of the synchronizing algorithm under any load to be ± 3ms.

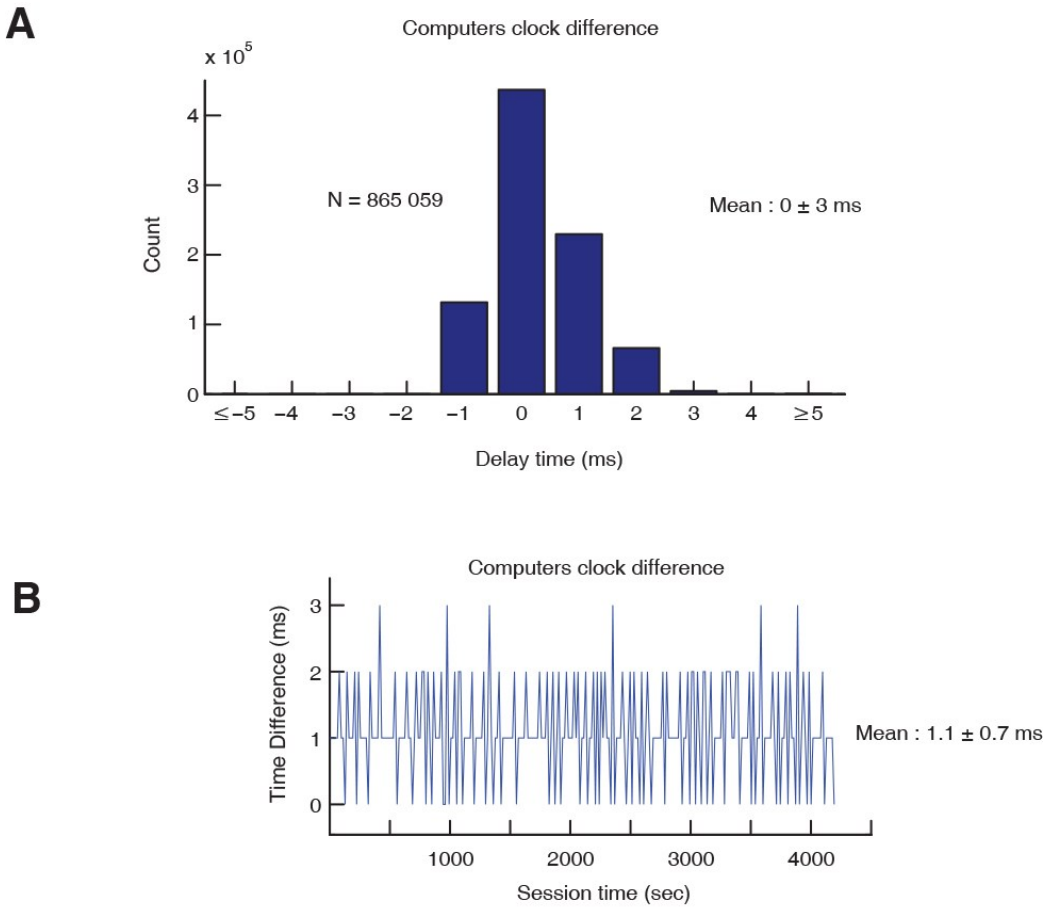

Figure 2-4. Performance of the clock synchronization algorithm. **A.** Distribution of time differences between the Unreal and control computers as recorded by the algorithm over a 5 months period. **B.** Recorded time differences between computers during a ~1 hour recording session, under normal experimental conditions and heavy network load. Values indicated are mean ± standard deviation.

It is of note to mention that the clock synchronization algorithm is only necessary for non-real-time network implemented programming environments. Having developed the control script library in real-time and non-real-time enabled languages, Python and Matlab respectively, further enabled us to validate the synchronizing algorithm's precision and to quantify Matlab's performance in TCP data transfer. To do so, we sent a total of 4000 "Collect Trial Data" queries, on two separate sessions and under normal experimental conditions, while precisely time-stamping every step of the process. As the first row of Table 2-1 shows, Python's real-time capabilities were confirmed considering that the total time for data collection fell below 1 ms. Furthermore, when

we compared the timing values between Python and UDK ("Receiving query in UDK" column), the resulting difference of 2 ± 1 ms (mean ± standard deviation) concurred with our previously measured synchronization jitter. On the other hand, Matlab's performance was far from optimal with a total time of 24 ± 11 milliseconds. Although the synchronization algorithm prevents issues with temporal alignment of data acquired from Matlab, it greatly impedes the rate at which it can be sampled. Indeed, control software written in Matlab would fail to sample subject data at more than 25 to 30 Hz and would introduce a small, albeit barely noticeable, ~25 ms delay between environmental events and control software response.

Table 2-1.

Sending Query in Python	Receiving Query in UDK	Executing Query in UDK	Receiving Data in Python	
< 1 ms	2 ± 1 ms	< 1 ms	< 1 ms	N = 4000

Sending Query in Matlab	Receiving Query in UDK	Executing Query in UDK	Receiving Data in Matlab	
< 1 ms	4 ± 4 ms	< 1 ms	24 ± 11 ms	N = 4000

2.4.2 **Example tasks**

Morris water maze analogue and radial arm maze

As basic examples, we provide complete implementation of two frequently used cognitive tasks, namely the Morris water maze (Morris, 1984) and the radial arm maze (Olton and Samuelson, 1976). Since these tasks, or analogous derivatives, have been widely used across species, in both virtual and real-world situations (D'Hooge and Deyn, 2001; Washburn and Astur, 2003; Astur et al., 2004; Hori et al., 2005; Bohil, Alicea and Biocca, 2011), they are the best example to showcase our system's simplicity.

General layout of the environment for both tasks is illustrated on the left of Figures 2-5A and B, while example screen captures are shown on the right. Initial *PlayerStart* (joystick image) is located in the small square left of the environment (i.e. pitch black room). Since is it located below the main arena, it is invisible to the subject as depicted by the screen captures. In both tasks, *PathNodes* can be interchangeably used as start or goal location and could either be constant or randomized across trials. Of note, *PathNodes* being invisible in the VE, goal locations must then be identified by using colored (white) disks in the Radial Arm paradigm (Figure 2-5A right). *InterpActors* (purple circles, left; red and yellow spheres, right) are used as external cues. While we have used spheres for simplicity, all displayed items can be entirely customized in both color and form.

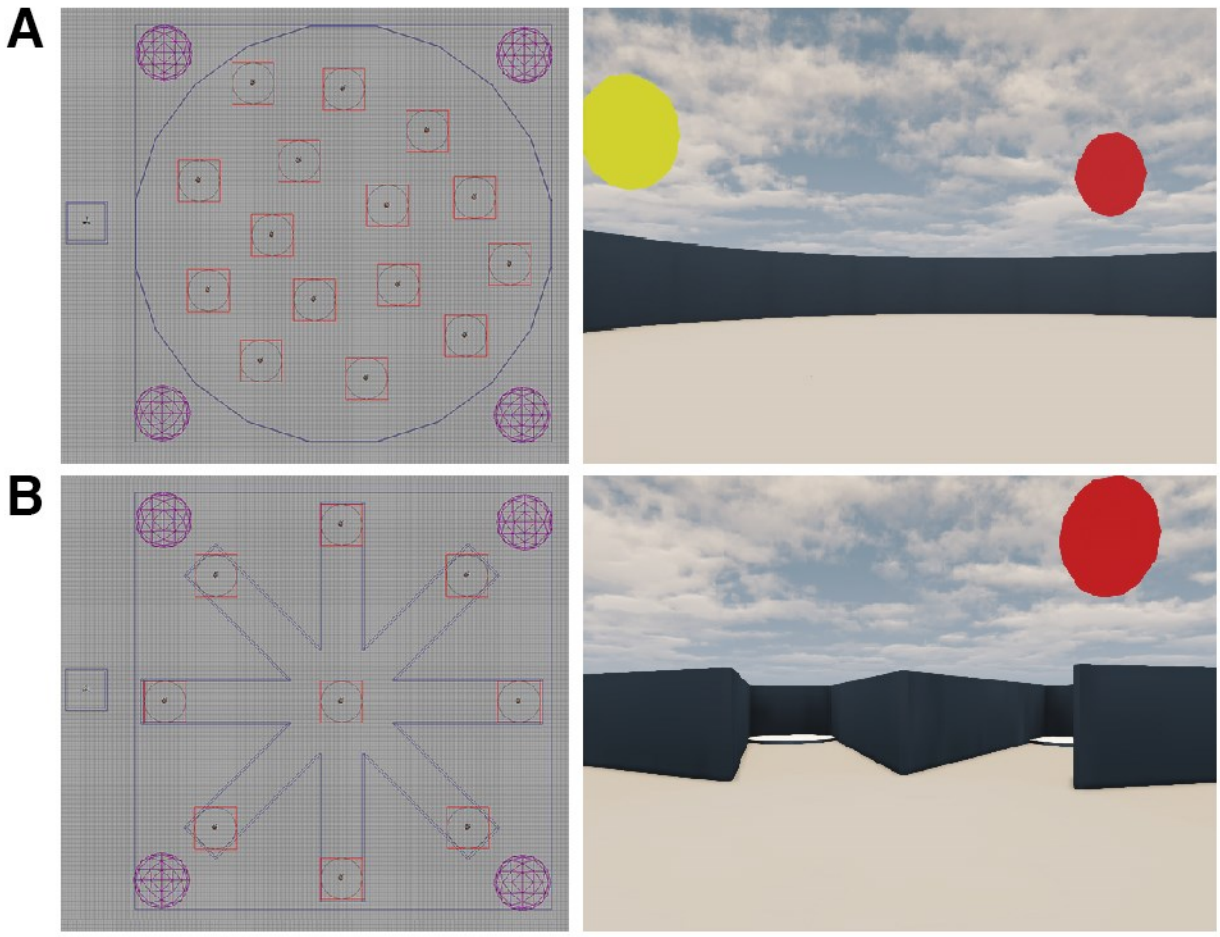

Figure 2-5. Overhead views and screenshots for the Morris water maze analogue (**A.)** and the radial arm maze (**B.)**. LEFT: general layout of the virtual environment. The *PlayerStart* is located on the left (joystick in square), walls are illustrated as blue lines, *PathNodes* as apples inside the circle contained in the red squares and allocentric cues (*InterpActors*) as purple circles. RIGHT: Examples views of the virtual environment as would be seen by subject.

Contextual learning task

At the other end of the spectrum, we have developed a more complex contextual learning task using the proposed architecture, by simply modifying a few scripts and Kismet nodes.

Furthermore, this task utilizes the continuous navigation option, which means that completed trials are presented in an uninterrupted fashion, with no inter-trial intervals. The only exception occurs if a subject fails to reach his target in the allocated time. Considering that the next trial could start with the user in an inappropriate position, the subject is sent back to the *PlayerStart* (i.e. blank screen) for a short period as "penalty" for not completing the trial properly, before being sent back in the arena at the predetermined start position.

The arena has been created as a double-ended Y maze, in which the subject navigates back and forth along the north-south axis to complete trials (Figure 2-6A). This task uses two contexts that define the symmetry of a three-level color-defined reward hierarchy (Figure 2-6B). The largest rewarded color in one context is thus the least rewarded one in the other, and vice-versa. While the two possible contexts are constant across sessions, the rewarded color hierarchies must be re-learned each session through trial and error. Figures 2-6 C and D illustrates trajectory examples from two trials (C) and overall learning performance (D) of a macaque monkey performing the task. A typical trial would begin exactly where the previous one ended, with current goals and contextual information hidden (beginning of solid black arrow, Figure 2-6C). The subject must then turn around and navigate to the central corridor (section between lines A and B). Upon entrance, contextual information is revealed on the inside walls of the arena. Similarly to the central corridor, entry in the decision area triggers the simultaneous appearance of both goals (line B for trial 1 and A for trial 2). The subject must then gather information about the presented colors and their associated context, and navigate to the disk that maximizes reward (white arrow, Figure 2-6B bottom). Subsequently, the areas' organization is flipped along the north-south axis, transforming the decision area into the start area of the next trial.

Understandably, to accommodate the current task requirements, few basic scripts needed modifications in UnrealScript. However, from the list presented in Figure 2-3A, only the "Pre-Start Trial" script was altered to include information about the trial direction (north or south), the selected context, and their associated goals (color and position). The remaining differences from the simpler task presented above came from the addition of *Triggers* and custom Kismet nodes to control context and goals appearance. Surprisingly, the largest amount of work was required on the control computer side to properly select the trial/goals combination, to validate selected target and reward the subject accordingly.

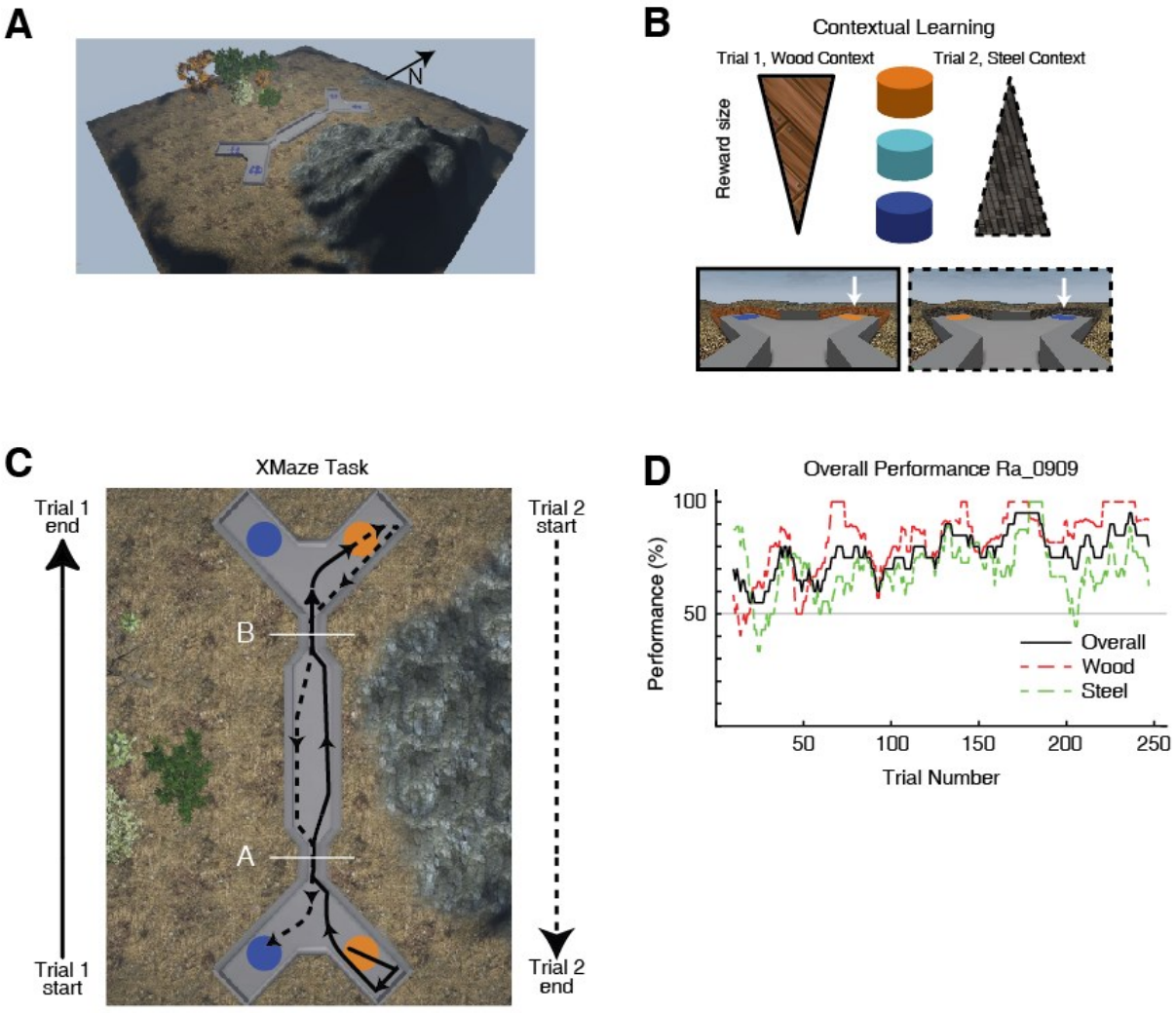
A
N
B
Contextual Learning
Trial 1, Wood Context
Trial 2, Steel Context
Reward size
C
XMaze Task
Trial 1 end
Trial 2 start
B
A
Trial 1 start
Trial 2 end
D
Overall Performance Ra_0909
100
50
Performance (%)
Overall
Wood
Steel
50
100
150
200
250
Trial Number

Figure 2-6. Overview of the contextual learning paradigm. **A.** Overview of the virtual environment. The "north" end of the maze is identified by the black arrow. **B.** Reward hierarchy is dependent on contextual information where the highest reward in one context (e.g. orange color in Wood context) equates to a null reward in the second context (e.g. Steel context). Color hierarchies were randomly generated on a daily basis. **C.** Trajectory examples for two trials (solid and dashed lines) undertaken by a macaque monkey during task training. Any trials begin where the previous trial ended. Contextual information then becomes available upon entry in the central corridor (A for trial 1 and B for trial 2). Continuing navigation into the decision area then reveals the trial specific goals (B for trial 1 and A for trial 2), to which the subject navigates, thus ending the trial. **D.** Single session training performance in a 20 trial sliding window from monkey Ra. Individual performances in each context are illustrated by the colored dashed lines. Although the monkey gets a small amount of juice reward for selecting the middle color (cyan), trials are considered "hits" only when the monkey selects the presented color associated with the highest reward.

2.5 Discussion

In summary, the proposed toolbox was designed to facilitate the introduction of VR capabilities to pre-existing visual neuroscience data acquisition systems. To do so, it responds to simple texts commands received over a TCP connection, which can be sent by virtually any programming language. Implementation costs are thus minimized by preserving the prior system's architecture, not requiring any hardware change to interface with external devices (e.g. eye tracker or reward system), and by allowing experimenters to utilize programming environments with which they already are familiar. Furthermore, it provides experimenters with key functional elements (e.g. Kismet nodes) to create a broad range of cognitive paradigms with minimal, if any, programming requirements. Lastly, it addresses many drawbacks from previously proposed VR solutions, namely: single species support, insufficient temporal resolution for electrophysiological experiments, the requirement for multiple external libraries and having to learn multiple programming languages to operate.

2.5.1 **Cross-species support**

Although this toolbox was developed and tested only on human and non-human primates, the presented VR engine is flexible enough to be used with any species capable of VE navigation.

Indeed, it can be configured to address several potentials shortcomings of using the toolbox with non-primate species, namely, physiological differences in size, perception and cognitive abilities.

Firstly, while flat computer monitors are sufficient for animals with frontally positioned eyes and stereovision (i.e. primates), they are not usable for species with laterally positioned eyes (e.g. birds or rodents). To circumvent this problem, the VR engine's displayed field of view is configurable to accommodate cylindrical or large format displays. It can further be configured to output a stereoscopic signal either through *RealD* 3D side-by-side display (RealD Technologies, CA, USA), NVidia's 3D Vision (NVidia Corporation, CA, USA) or AMD's HD3D (Advanced Micro Devices, Inc., CA, USA), without external plug-ins or additional drivers, unlike most competing engines (Jangraw et al., 2014).

Secondly, since visual aptitudes such as colored vision and contrast sensitivity can vary greatly across species, experimenters can rapidly change the appearance of a visual scene through simple texture manipulation or "post-process" effects (e.g. color desaturation or visual distortion).

Lastly, physical restrictions must be addressed when selecting proper subject interface device and when defining its avatar in the VE. Indeed, small rodents and larger primates differently experience the same environment due to variations in height and walking speed. Both of which can be modified in the *Pawn* properties. Furthermore, the movement speed of the avatar is directly linked to the type of input device used. While any input device configured as a mouse (i.e. joystick, trackball, treadmill) can be used with this toolbox, each one would need to be specifically calibrated with the *Pawn*'s speed property. This process is easily undertaken as 1 unit of length in the VE is typically equivalent to 2 cm in the real world.

2.5.2 **Clock synchronization and temporal precision**

While the toolbox was designed to study high-order cognitive processes, it could also be used for lower-level studies. Unfortunately, the temporal precision achieved by the NTP algorithm, correcting poor TCP performance in non-real-time environments, might not be sufficient for such low latency studies. Many alternatives, to improve synchronization performance and limit jitter, are now available to researchers.

Firstly, a more efficient standard for time protocol algorithms, believed to reach sub-microsecond precision, has been recently developed (Precision Time Protocol, IEEE Standard 1588-2008). Although most implementations of this algorithm on the Windows platform are only available as commercial products (Domain Time II, Greyware Automation Products Inc, Texas, USA; Real-Time Systems GmbH, Real-Time-Systems, Germany), their low cost and provided customer support renders them easily accessible. On the other hand, open-source alternatives are available on the Linux and Apple platforms (Precision Time Protocol Deamon, http://ptpd.sourceforge.net).

Secondly, most programming environments can benefit from using lower-level languages libraries. For example, Matlab can interface with C/C++ or FORTRAN languages through the "mex" functions. It is then possible to use these languages real-time TCP capabilities to avoid any TCP communication delays. This will be undertaken in further versions of this toolbox.

Thirdly, we emphasised temporal precision and encouraged using two separate computers to maximize the frame rate of the UDK computer, in order to ultimately reduce display latency. This phenomenon, defined as the delay between user action and change on the visual display, is a major issue in immersive VR technology as it can generate motion sickness, especially in head-mounted displays, but is frequently disregarded in visual neuroscience. This latency can come from three separate sources: input devices, VR software and display devices. A total latency of less than 20 ms is typically recommended to avoid motion sickness (Zheng et al., 2014). As modern input devices latency is often negligible and as the engine's refresh rate is synchronized with the display device, we strongly recommend caution in its choice. Indeed, LCD monitors are generally slower than older CRT monitors as they pre-process the image before displaying it and their input latency has been shown to range from 1 ms to 150 ms for older monitors (Garaizar et al., 2014). Display latencies less than 20 ms can thus be achieved using monitors with > 100 Hz refresh rates and low-input latencies.

2.5.3 **Current and newer versions of Unreal Engine**

While there are many other video game engines available (Quake 2: Harvey et al. 2009; Unreal Engine 2: Doeller et al. 2010; Vision Engine: Mueller et al. 2012; Ogre3D: Ravassard et

al. 2013; Unity3D: Jangraw et al. 2014), we have found UDK (May 2012 release) to provide the best combination of power, flexibility and intuitive use. Unlike its nearest competitors (i.e. Unity and Panda3D), it does not require external libraries to present multisensory stimuli or to interface with stereoscopic displays (Jangraw et al., 2014). Furthermore, it contains a broad library of scripts, 3D models, textures, particles and sound effects, reducing the need for content creation. Lastly, since it has been released over 10 years ago and used in more than 100 professional video games, it has a remarkable level of developer support through thousands of lines of codes readily available to implement drastic engine changes (UDK Gems, https://udn.epicgames.com/Three/DevelopmentKitGems.html), and extensive documentation, libraries and bug reports from the Epic Game's user forums (https://forums.epicgames.com/forums/366-UDK). Moreover, unlike Unity, in which users need to filter the documentation across three different programming languages, UDK's single programming language renders all available tutorials relevant.

While undertaking these experiments, a newer and more powerful version of the Unreal Engine (version 4), was freely released to universities (September 4th 2014) and to the public (March 2nd 2015). Due to a major reconstruction of the engine's internal architecture, the present work could not be transferred to this environment prior to publication. This is unfortunately a recurring event, since most neuroscience laboratories developing VR applications are faced with very limited resources. Indeed, it is not uncommon that at the time of publication of a study, a newer version of the proposed video game engine is already available. For example, Harvey et al., (2009) published results using the Quake II engine four years after the release of the Quake III engine. The same holds true for Doeller et al., (2010) using the Unreal Engine 2, 6 years following the availability of Unreal Engine 3.

Understandably, small laboratories cannot keep up with multi-national private companies and delays between novel technology development and its application in a research setting are expected. As video game companies only have to deal with technological considerations, laboratories must go through a complex iterative process of task design, implementation and preliminary data collection before undertaking finalized experiments. However, this delay can be significantly shortened by facilitating implementation to replicate and expand experiments. For this reason, the entire libraries of Matlab, Python and UnrealScript scripts, as well as

documentation, will be made available for download at http://www.robarts.ca/martinez/default.htm, while work is carried out to transfer this environment onto a new generation engine.

2.5.4 **Matlab and Python architectures**

Matlab has been widely used in neuroscience research for the past decades. Through its extensive toolbox selection, ranging from robotics and computer vision to machine learning and statistical analyses, it can undertake any data processing task. Furthermore, it benefits from a wide variety of third-party toolboxes that tackle every step of an experiment, from stimulus presentation and data collection (Psychophysics Toolbox: Brainard 1997; MonkeyLogic: Asaad et al. 2012) to the analysis of any possible signals (electrophysiology: Chronux toolbox, Bokil et al. 2010; functional imaging: TDT, Hebart et al. 2015; microscopy: Patel et al. 2015). Lastly, as it has been used for many years, thus, textbooks (Wallisch et al., 2009) and online courses have been developed around it.

On the other hand, recently emerging from the modelling field, Python is now increasingly used across all neuroscience fields. Although its current research usable form was only developed in the late 1990s/early 2000s, this open-source software is rapidly evolving. Indeed, the list of available toolboxes (described in Muller et al. 2015), although not as extensive as Matlab's, now covers most experimental steps from stimuli generation to complex systems' analysis. Additionally, a novel programming interface, IPython notebooks, is reinventing the way scripts are executed and shared (Shen, 2014). In this environment, descriptive texts, scripts and results are intertwined in a single user-friendly interface in order to facilitate communication and reproducibility (Topalidou et al., 2015).

Since both languages are widely used and offer comparable processing power, we did not select one over the other for this study. While Matlab presents poor TCP performance, it compensates with a unified architecture, massive help documentation and customer service. On the other hand, Python might benefit from open-source development, improved sharing capabilities through IPython notebooks and high flexibility (Perkel, 2015); it greatly suffers from the slow transition between two incompatible versions (2.7 and 3.4). Furthermore, by selecting

only one of the two proposed programming languages, we would have greatly reduced the usability of this toolbox. Indeed, even if Python presents better performance in this context, the temporal cost of switching an already established Matlab based experimental pipeline to a Python one would greatly surpass any obtained benefits. We have thus developed and will continue to support both programming languages.

2.6 Acknowledgements

This work was supported by Canadian Institutes of Health Research, Natural Sciences and Engineering Research Council, and Canada Research Chair program grants to J.M.-T. R.G. was supported by a Natural Sciences and Engineering Research Council Post-Graduate Scholarship and a McGill University David G. Guthrie Fellowship in Medicine. We thank Mr. Walter Kucharski and Mr. Stephen Nuara, for technical support; and members of the J.M.-T. Laboratory for providing writing assistance and proof-reading this manuscript.

Chapter 3

3. Frequency specific phase resetting of local field potential oscillations in primate hippocampus by visual transients and saccades

3. Frequency specific phase resetting of local field potential oscillations in primate hippocampus by visual transients and saccades

Using the virtual reality engine developed in the previous study, we investigated the saccade triggered phase resets in the primate hippocampus. The first objective was to create a series of tasks that replicated classic saccade tasks using simplified stimuli (i.e. white dots on a black background; cued saccade task), that replicated classical open-field foraging experiments used to highlight place cell activity (foraging task) and that combined allocentric spatial navigation with context dependent and hippocampal mediated associative learning (associative memory task). The second objective was to record hippocampal local field potentials during the execution of these three tasks and determine the relative contributions of stimulus, saccade and foveation onsets on the measured phase resets. Methods for the analysis of local field potential data, and their transformation into an analytic signal using wavelet convolution, were developed and tested in a prior publication: Tremblay S, Doucet G, Pieper F, Sachs A and Martinez-Trujillo J. 2015. Single-Trial Decoding of Visual Attention from Local Field Potentials in the Primate Lateral Prefrontal Cortex Is Frequency-Dependent. J. Neurosci. 35 (24):9038–49. The current results suggest that saccades in primates modulate hippocampal activity in a comparable manner as locomotion and whisking in rodents. Moreover, these events trigger local field potential variations in a frequency specific manner, confirming the multidimensional tuning and associative function of the hippocampus. This chapter has been adapted from a submitted manuscript: Doucet G, Corrigan BW, Gulli RA, Duong L and Martinez-Trujillo JC. 2018. Frequency specific phase resetting of local field potential oscillations in primate hippocampus by visual transients and saccades.

3.1 Abstract

The phase of local field potential (LFP) oscillations in the hippocampus coordinates neuronal firing patterns encoding the features of an experience, facilitating synaptic plasticity and memory formation. Several studies have found that sensory and motor events can reset hippocampal LFP phase, potentially gating inputs into the area. This phenomenon has been extensively documented in rodents, however, the primate literature is more restricted. Here we measured hippocampal LFP power and phase, aligned to visual transients and saccades, in two macaques performing different tasks: saccade, virtual foraging and associative memory. We found that LFP phase in the alpha/beta (8 – 16 Hz) band preferentially clustered following visual transients (i.e. stimulus and foveation onsets). On the other hand, delta (≤ 4 Hz), theta (4 – 8 Hz) and mid-gamma (~60 – 120 Hz) phase clustered following saccade onsets. Theta power modulated with saccade amplitude and delta phase modulated with saccade direction. Our results show that visual transients and saccades cluster the phase of hippocampal LFPs in different frequencies, allowing segregation of sensory and motor signals. Moreover, the modulation of LFP power and phase with saccade parameters suggests that saccade related signals could be a source of LFP phase resetting in primate hippocampus.

3.2 Introduction

The hippocampus (HPC) is thought to bind incoming sensory signals within the spatiotemporal context of an experience to sustain memory function (Eichenbaum, 2004; Eichenbaum and Cohen, 2014; Watrous and Ekstrom, 2014; Buffalo, 2015; Schiller et al., 2015). In rodents, performance in memory tasks has classically been correlated with the robustness (i.e. power) of local field potential (LFP) oscillations in the theta frequency range, most prominent during active behaviors (Bland and Oddie, 2001; Buzsáki, 2002, 2005; Hasselmo, 2005; Buzsáki and Moser, 2013; Colgin, 2013, 2016; Ekstrom and Watrous, 2014). Although identified in human and non-human primates (Ekstrom et al. 2005; Jutras et al. 2013; Leonard et al. 2015), theta oscillations are considerably weaker and shorter than those in rodents (Stewart and Fox, 1991;

Skaggs et al., 2007; Jacobs, 2014; Brincat and Miller, 2015). Currently, the role of theta power in primate memory remains unclear (Rutishauser et al. 2010; Jutras et al. 2013).

Alternatively, rodents' theta cycles have been shown to strongly modulate the firing patterns of HPC place cells, both within and across place fields (O'Keefe and Recce, 1993; Skaggs et al., 1996) (but see (Brandon et al., 2014)), reflecting the currently attended dimension (Fenton et al., 2010). Indeed, alternating spatial representations between distinct environments, following "teleportation" (Jezek et al., 2011), or representations of future paths inside a single environment (Gupta et al., 2012) are fully segregated within sequential theta cycles. Similarly, neuronal firing patterns coding non-spatial features and behavioral states have been found to be modulated by theta LFPs (Lisman 1999; Tort et al. 2009; Staudigl and Hanslmayr 2013; Rangel et al. 2016; Fernández-Ruiz et al. 2017). These results strongly advocate for a role of theta LFPs in coordinating task-dependent neuronal representations to induce synaptic plasticity and promote memory function (Lisman and Jensen, 2013; Colgin, 2016).

The phase (i.e. position within a cycle) of the theta oscillations have been shown to reset in animals engaged in active sensing (Schroeder et al., 2010) of their environment (e.g. exploratory whisking and saccades (Macrides, Eichenbaum and Forbes, 1982; Hoffman et al., 2013; Jutras, Fries and Buffalo, 2013)) and following relevant stimulus onset (Givens, 1996; Tesche and Karhu, 2000; Williams and Givens, 2003; Mormann et al., 2005). Such phase resets could serve as a synchronizing mechanism for neuronal ensembles encoding features of associative memories (Meister and Buffalo, 2016). Despite general consensus about the influence of active sensing on hippocampal LFPs, knowledge about the behavioral modulation of such events is incomplete. For example, studies have highlighted both the absence (Berg, Whitmer and Kleinfeld, 2006; Hoffman et al., 2013) and presence (Sobotka and Ringo, 1997) of sensing triggered phase resets in animals deprived of sensory stimulation. Moreover, phase resets have been shown to be weakened or missing during hippocampal independent tasks (Givens, 1996) and conditions, such as visually guided saccades (Jutras, Fries and Buffalo, 2013). Lastly, significant LFP modulations have been found around the onset (Sobotka and Ringo, 1997; Jutras, Fries and Buffalo, 2013; Staudigl et al., 2017) and offset (Hoffman et al., 2013) of saccades. Thus, it remains unclear whether saccade induced LFP phase resets in the primate hippocampus are analogous to the saccadic suppression

and fixation enhancement seen in the visual cortex (Schroeder et al., 2010; Ito et al., 2011; Meister and Buffalo, 2016), whether they only occur during certain behavioral or stimulus conditions and whether they play a role in stimulus triggered phase clustering.

To address these issues, we monitored eye movements and recorded LFP signals from the right hippocampus of two rhesus macaques performing three different tasks: a classic Cued Saccade task (CS; Figure 3-1 A), and two virtual navigation tasks: Foraging, requiring the animal to navigate through a virtual maze (FOR; Figure 3-1 B), and Associative Memory, requiring the animal to navigate through a maze and memorize context/color associations at a particular maze location (AM; Figure 3-1 C). We found significant phase resets of hippocampal LFPs (measured as phase clustering or PC) around saccades, regardless of task or stimulation condition. Moreover, both saccade onsets (delta, theta and gamma) and offsets (alpha/beta) elicited PC across different frequency bands, where the phase of delta LFPs correlated with saccade direction and the power of the theta and gamma bands correlated with saccade amplitude. These results provide a strong parallel with the rodent literature, where active exploratory behaviors modulate both the power and phase of hippocampal low frequency oscillations.

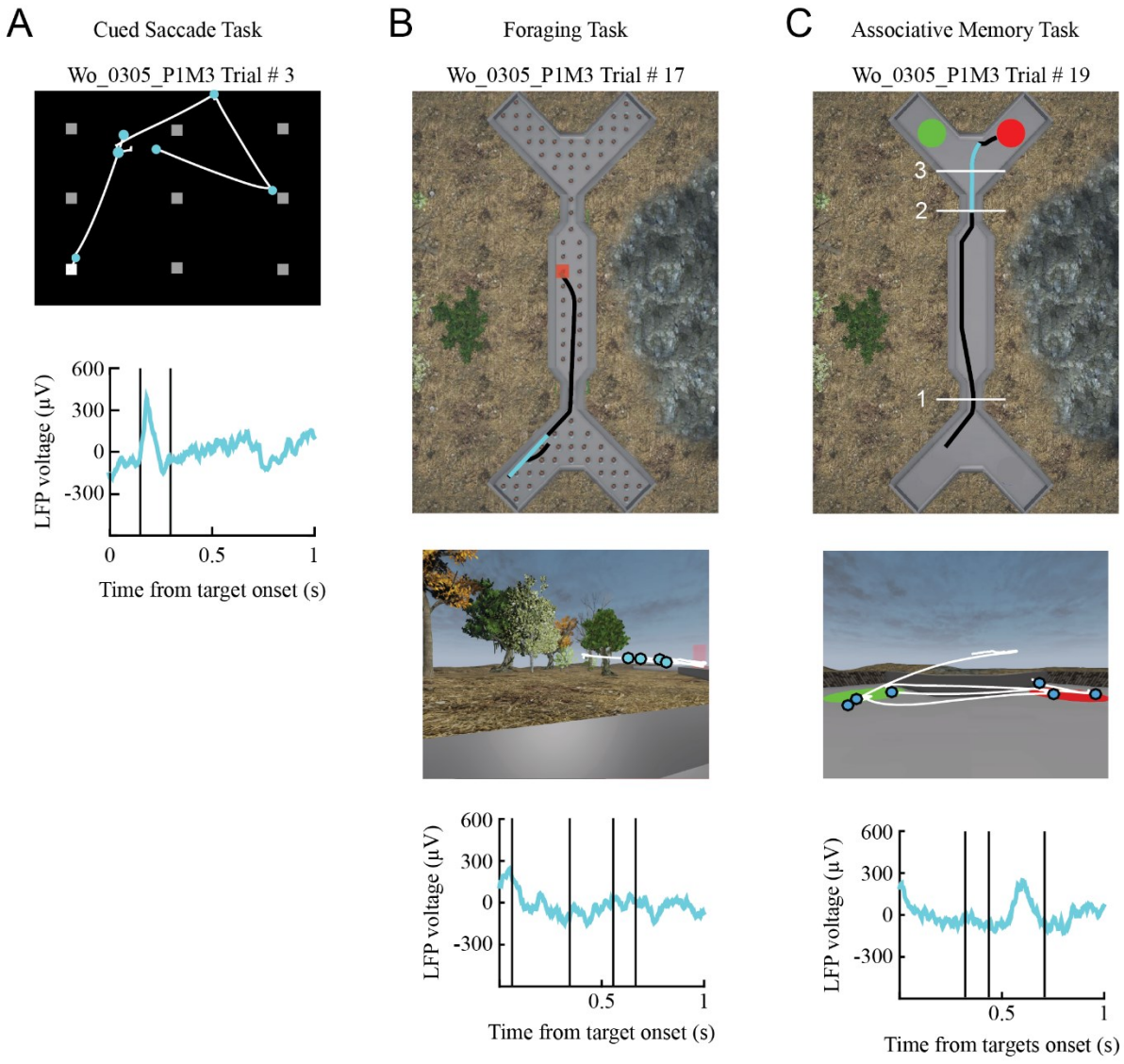

Figure 3-1. Tasks description. (A) Cued Saccade task. Monkeys were presented with a uniform grey background and freely looked until a white target appeared at one of nine possible locations (top). Target fixation was then required to obtain a juice reward. (B) Foraging task. Animals were required to navigate inside a double ended Y-maze towards a red target appearing randomly at one of 84 possible locations (top; brown dots). (C) Associative Memory task. Animals navigated back and forth along the north-south axes of the double ended Y-maze (top). Upon entering the central corridor (1) contextual information was displayed on the maze walls, (2) colored targets were displayed in both arms at the end of the corridor. The animal navigated to the target with highest reward value. Center plots show screen examples with overlaid eye traces (white) and saccade onsets (colored circles). Bottom plots display raw LFP traces associated with the current trials; saccade onsets are marked with black bars.

3.3 Results

We first examined whether LFP power and phase were modulated around stimulus onset and computed the averaged LFP traces aligned to target onset across all tasks (Figures 3-2 A-C, middle row, black trace), as well as the instantaneous power (Figures 3-2 A-C, middle row colored background) and inter-trial phase clustering (PC) (Figures 3-2 A-C, bottom row colored background). Comparisons of pre- and post-onset values, within a 500 ms window before and after target onset, revealed a significant increase in low- to mid-gamma band power (~30 - 120 Hz) across all conditions (Figure 3-2 D, left; paired t-test, $p < 0.05$ Bonferroni corrected), with a task dependent power effect on frequencies below 32 Hz. Indeed, target onset during the CS task elicited a robust power increase across all frequencies below 12 Hz and, similarly to the FOR task, a power decrease for frequencies in the beta band (~12 – 30 Hz). Power in the AM task was significantly decreased across most low frequencies (4 – 20 Hz).

Irrespective of power fluctuations, the inter-trial PC following stimulus onset was significantly greater than baseline (i.e. pre-onset) across all tasks for frequencies below 12 Hz (Figure 3-2 D, right; paired t-test, $p < 0.05$ Bonferroni corrected). Of note, the frequency of peak PC differences varied across tasks, from < 4 Hz in the AM task, to ~7 Hz in the CS task and to ~9 Hz in the FOR task. Moreover, the magnitude of PC differences seemed to correlate with the size of peak saccade probabilities (Figures 3-2 A-C, top row), where: CS > AM > FOR. Thus, phase clustering around target onsets seemed to be influenced by saccade probability.

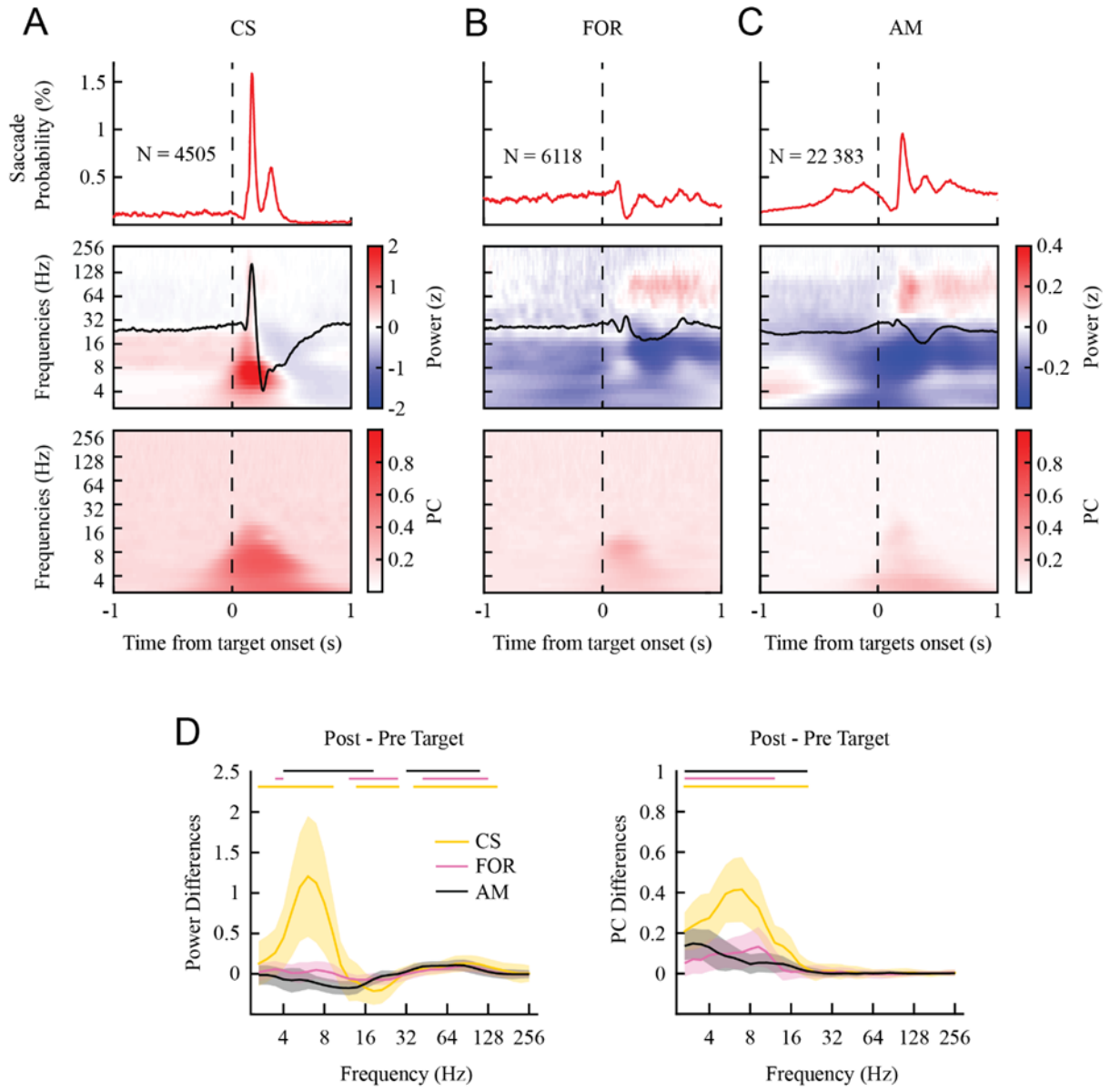

Figure 3-2. Trial averaged behavioral and LFP data. Averaged saccade probability (top), z-scored LFP (black line; middle), z-scored LFP power (middle) and inter-trial phase clustering (bottom), around target onset, for the Cued Saccade (CS; A), Foraging (FOR; B) and Associative Memory (AM; C) tasks. N indicates the total number of trials averaged across all electrodes (CS: 86; Foraging: 82; AM: 91 electrodes). (D) Average power (left) and inter-trial phase clustering (bottom) differences between the first 500 ms post-target and the last 500 ms pre-target, for each of the 34 wavelet center frequencies. Shaded areas indicate standard deviation. Solid lines above the plot indicate statistical significance (paired t-test, Bonferroni corrected, $p < 0.05 / 34$ frequencies).

3.3.1 Saccadic and stimulus triggered phase clustering across tasks

During most trials and irrespective of task, animals responded to a target stimulus onset by re-orienting their gaze towards it. To explore the effects of stimulus onset and saccadic activity on phase clustering, we computed the PC values centered on stimulus onset as well as the first subsequent saccade onset and offset (i.e. foveation onset; Figure 3-3 A). Saccade and foveation onsets were treated as separate conditions as both were interchangeably used in previous studies (Hoffman et al., 2013; Jutras, Fries and Buffalo, 2013). For this analysis, only trials where gaze position was on the screen at the time of stimulus onset and where a saccade was initiated within 500 ms of stimulus onset were included. The PC metric used here may be sensitive to sample size (Cohen, 2014), thus, as we have a different number of saccades in the different tasks, only within-task comparisons are valid (i.e. Figure 3-3 A, within rows). As a proxy for comparison across tasks, we used the proportion of significant electrodes (CS: N = 86; FOR: N = 82; AM: N = 91 electrodes; expected chance level from binomial distribution at $p < 0.05$ are CS: 4%; FOR: 5%; AM: 4%) at each time-frequency point (Figure 3-3 A, black outlines: thin > 5%; middle > 50%; thick: > 75% of all electrodes showed significance). Statistical significance was computed using non-parametric permutation test with pixel-based correction for multiple comparisons ($p < 0.01$, see 3.5 - Materials and Methods).

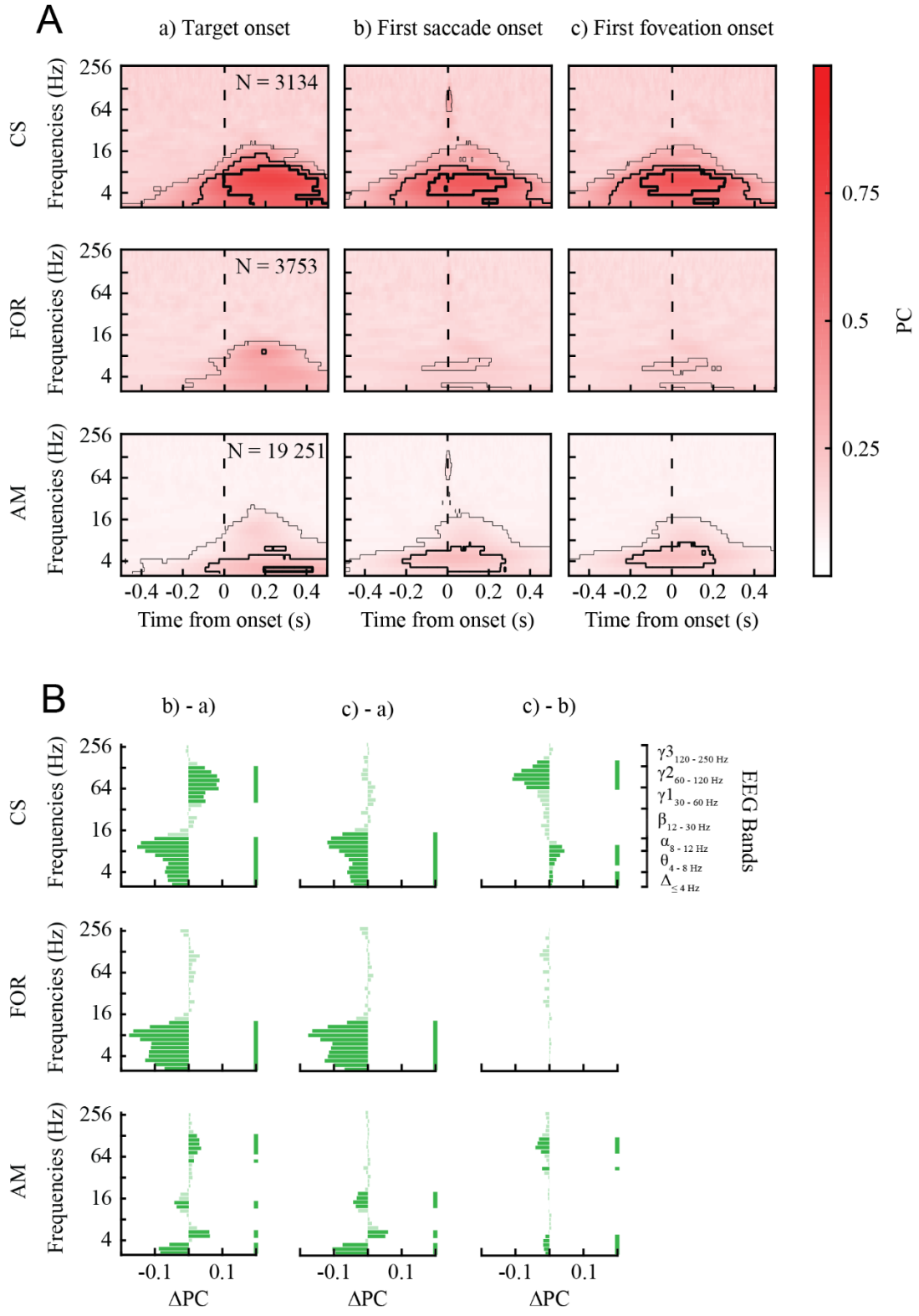
A
a) Target onset
b) First saccade onset
c) First foveation onset
CS
FOR
AM
Frequencies (Hz)
256
64
16
4
N = 3134
N = 3753
N = 19 251
-0.4 -0.2 0 0.2 0.4
Time from onset (s)
0.75
0.5
0.25
PC
B
b) - a)
c) - a)
c) - b)
γ3 120 - 250 Hz
γ2 60 - 120 Hz
γ1 30 - 60 Hz
β 12 - 30 Hz
α 8 - 12 Hz
θ 4 - 8 Hz
Δ ≤ 4 Hz
EEG Bands
-0.1 0.1
ΔPC

Figure 3-3. Target, saccade and foveation triggered phase clustering. (A) Event triggered phase clustering centered on: a) target onset, b) onset of the first subsequent saccade and c) offset of the saccade (i.e. foveation onset), for all three tasks (rows). Black outlines illustrate the proportion of significant electrodes, where thin: > 5%, middle: > 50% and thick: > 75%, computed from non-parametric permutation testing within electrode ($p < 0.01$, pixel-based correction for multiple comparisons). (B) Phase clustering differences between conditions, obtained by subtracting peak PC values within the first 200 ms post-event of each condition, within each electrode. Dark bars and vertical line indicate statistical significance of a paired t-test ($p < 0.05$ Bonferroni corrected).

PC following target onset was significantly greater than chance on more than 50% of electrodes for frequencies below 20 Hz, regardless of task (Figure 3-3 A, a)). Moreover, frequency bands showing maximal significance probability corresponded with inter-trial PC difference peaks previously identified (Figure 3-2), where most of channels showed significance ≤ 4 Hz in the AM task (78%), around 6 Hz in the CS (88%) task and 9 Hz in the FOR task (52%). Interestingly, saccade and foveation onset aligned data (Figures 3-3 A, b) and c)) displayed highly similar significance patterns, even when compared with target onset, with two exceptions. Firstly, mid-gamma band (~60 – 120 Hz) PC was significantly increased at the time of saccade onset for both the CS and AM tasks, but not in the FOR task. Secondly, PC around saccade and foveation onsets in the FOR task was greatly reduced, where only 12% of channels were significant for a very narrow frequency band between 4 and 8 Hz, less than 10% for frequencies below 4 Hz and less than 5 % being significant for the peak frequency at target onset (i.e. 9 Hz).

To quantify the PC differences between different events (i.e. target, saccade and foveation onsets) we compared the distributions of peak PC values for each frequency within the first 200 ms post-event onset (Figure 3-3 B, paired t-test, dark green: $p < 0.05$ Bonferroni corrected; see 3.5 - Materials and Methods). PC triggered by target onset was significantly greater than saccade or foveation onsets for frequencies lower than 16 Hz in both the CS and FOR tasks (Figure 3-3 B, b) – a) and c) – a)). Similarly, target onset triggered PC was greater for frequencies < 4Hz and between ~12 – 14 Hz during the AM task, while being smaller for frequencies between ~4 – 6 Hz (Figure 3-3 B, b) – a) and c) – a)). Mid-gamma band (60 – 120 Hz) phase showed greater alignment to saccade onset (Figure 3-3 B, b) – a) and c) – b)), regardless of task. Although this effect was not significant for FOR, a clear trend was observed. Lastly, we parsed out the relative contributions

of saccade and foveation onsets to measured PC (Figure 3-3 B, c) – b)). While no significant differences were found for the FOR task, PC was significantly greater when aligned to foveation onset during the CS task for frequencies ≤ 8 Hz and significantly greater when aligned to saccade onset during the AM task for frequencies ≤ 4 Hz.

These results suggest that target onset, saccade onset, and foveation onset all are associated with phase clustering of low frequency oscillations. While visual onsets seemed to robustly produce more PC than saccade onsets/offsets for frequencies < 4 Hz and ~12 – 14 Hz across all tasks, no trends were visible for low frequencies showing preferred clustering around saccadic activity. Indeed, PC between ~4 – 6 Hz was greater for saccadic activity only during the AM task. Conversely, a clear trend showing that gamma band PC was preferentially increased following saccade onsets was visible.

3.3.2 Saccade onset and offset evoked changes in LFP power and phase clustering across tasks

The previous analysis suggests that saccades onsets produce stronger phase clustering in the gamma band than saccade offsets, mainly in the CS and AM task. However, the analyzed data was limited to the first saccade following target onset, which led to a small number of saccades relative to the total number made by the animals in the different tasks. Thus, we computed the saccade triggered LFPs (Figure 3-4 A) and power (Figure 3-4 B), as well as PC for both saccade and foveation onsets, including all saccades within each task (Figure 3-4 C).

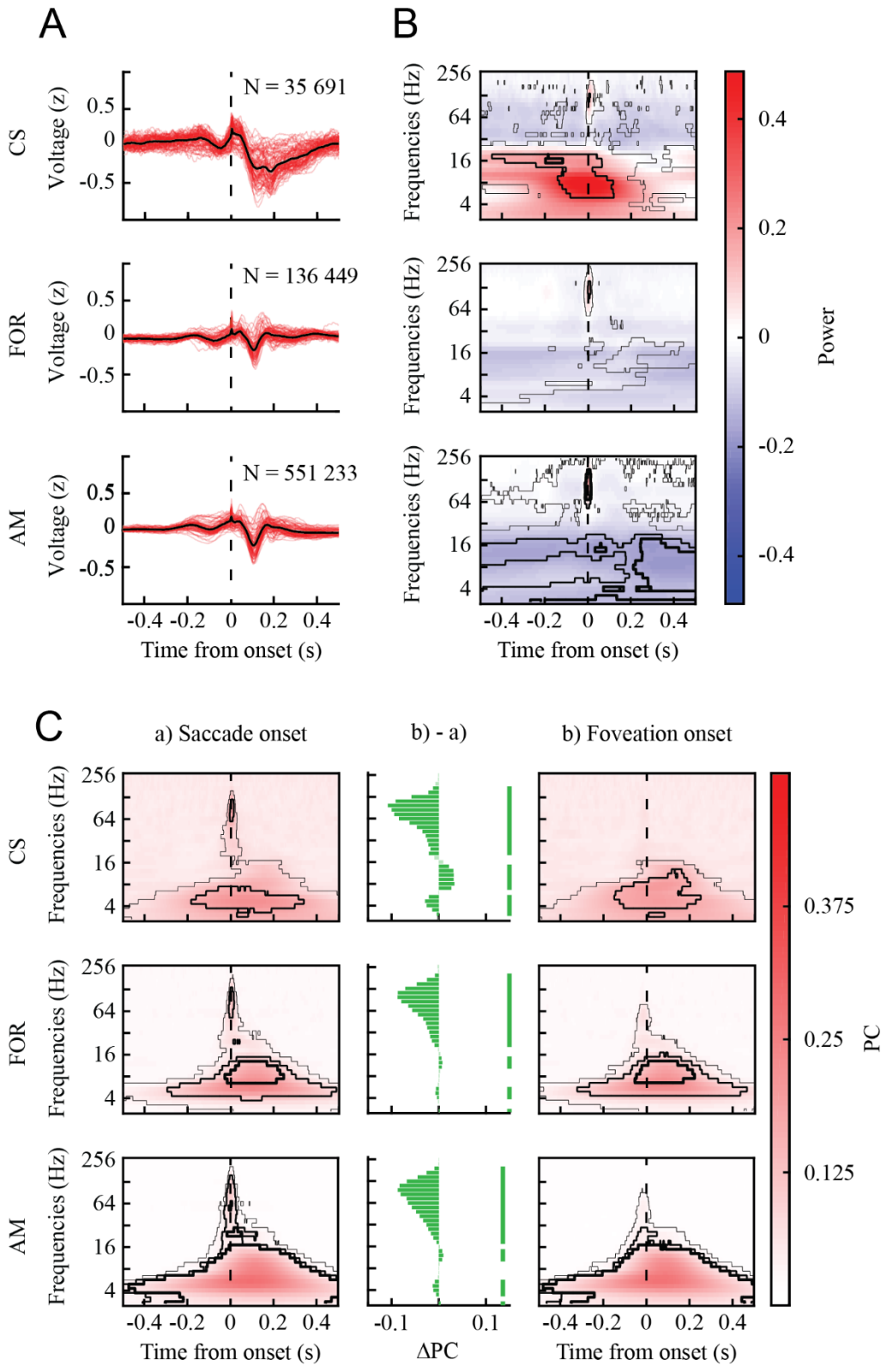
A
B
C
CS
FOR
AM
Voltage (z)
N = 35 691
N = 136 449
N = 551 233
Frequencies (Hz)
Time from onset (s)
Power
PC
a) Saccade onset
b) - a)
b) Foveation onset
ΔPC

Figure 3-4. Saccade triggered LFPs. (A) Averaged saccade onset triggered z-scored LFP traces within each electrode (red traces) and cross-electrode grand average (black traces). (B) Saccade onset triggered z-scored LFP power. (C) Saccade onset (left) and foveation onset (right) triggered phase clustering and their peak differences (center). Black outlines illustrate the proportion of significant electrodes, where thin: > 5%, middle: > 50% and thick: > 75%, computed from non-parametric permutation testing within electrode ($p < 0.01$, pixel-based correction for multiple comparisons). Dark green bars and vertical line indicate statistical significance of a paired t-test ($p < 0.05$ Bonferroni corrected).

Prior to investigating power and PC modulations, the saccade triggered LFP traces were computed to validate our previous results and compare them with the existing literature (Figure 3-4 A). As anticipated, phase clustering was apparent on most electrodes (Figure 3-4 A, red trace: single electrode average; black trace: grand average across electrodes) and mostly contained within 200 ms of saccade onset (Sobotka and Ringo, 1997; Hoffman et al., 2013; Jutras, Fries and Buffalo, 2013).

Investigation of saccade triggered LFP power confirmed a gamma band power increase at the time of saccade onset. This increase was significant for 52%, 74% and 96% of all electrodes during the CS, FOR and AM tasks respectively (Figure 3-4 B, black outlines: thin > 5%; middle > 50%; thick: > 75% of all electrodes showed significance). Conversely, low frequency power displayed a heterogeneous pattern across tasks. Despite having a substantial proportion of all channels (> 45%) showing significant power values around saccade times for frequencies below 20 Hz, the direction (i.e. positive or negative) of the modulation was not consistent across tasks (Figure 3-4 B).

We contrasted the significance patterns of saccade onset triggered PC for the first saccade following stimulus onset (Figure 3-3) with the ones for all saccades within each task (Figure 3-4 C). Results from the CS task were highly similar, despite a 20% decrease ($p < 0.05$, chi-square test) in significance probability, where most of the significant points clustered within the theta and gamma bands. On the other hand, FOR task PC was greatly increased when all saccades were used for its computation. While PC values were barely significant for the first saccade following stimulus onset (≤ 12%), the probability of significance across electrodes increased to 83% ($p < 0.05$, chi-square test) for all saccades, peaking between 10-12 Hz. Similarly, PC significance probability was also increased for the AM task, from 71% to 100% ($p < 0.05$, chi-square test)

between 4 – 12 Hz. Interestingly, the task differences in significance patterns observed in Figure 3-3 were largely diminished; over 50% of channels were significant for frequencies between 4 – 16 Hz regardless of task. Of note, the significance probability of saccade onset triggered PC in the CS task decreased to 50% for frequencies between 8 – 16 Hz, a trend that was absent in the FOR and AM tasks.

Lastly, while a clear effect of saccade onset was visible for the gamma band PC (more than 60 % of all electrodes were significant regardless of task), low frequency PC patterns were highly similar across saccade and foveation onsets (Figure 3-4C). We quantified these differences with the same method as in Figure 3-3B. Again, gamma band PC was significantly greater for saccade onset vs. foveation onset, regardless of task (Figure 3-4C, b) – a)). Contrary to Figure 3-3B, saccade vs. foveation preferences were highly similar across tasks, frequencies in the alpha/beta range of 8 – 16 Hz were significantly more clustered around foveation onsets, whereas frequencies around 4 Hz (~3 – 5 Hz) were significantly more clustered around saccade onsets.

Taken together, these results indicate that the reduced PC following saccades/foveations in the FOR task (Figure 3-3 B b) and c)) and the inconsistencies in saccade versus foveation onset triggered PC (Figure 3-3 B c) – b)) were not due to task differences. Indeed, both saccade and foveation triggered PC patterns were highly similar across tasks (Figure 3-4 C), with the exception of a decreased significance in the alpha/beta range of the CS task. However, these frequencies were found to be more strongly modulated by foveation onset, which, when used to compute PC, increased the significance probability by up to 30% (Figure 3-4 C, CS b)). One possibility is that the observed effect in the alpha/beta frequencies is due to the features of the CS task in which a single target is presented against a dark background. On the other hand, during the VR tasks, animals are constantly presented with different stimuli across the entire visual field.

3.3.3 Contributions of stimulus onsets and saccade signals to LFP power and phase clustering

During visually guided saccades, the contributions of the visual stimulus and saccade command to the neural response are difficult to dissociate because saccades occur right after the visual stimulus onset. However, during the CS task, the animals made two types of saccades: a)

self-generated saccades to a uniform background, when no stimuli were on screen, and b) saccades to appearing visual targets. Thus, by analyzing the electrical activity in both conditions it would be possible to isolate the contribution of saccades (a) and the added contribution of saccades and visual stimulus onset (b).

We first computed the distributions of saccade amplitudes, direction, duration and inter-saccade intervals (ISI) for saccades to the background (N = 24 031) and to the fixation point (N = 7 462; Figure S3-1 A). Despite targets being positioned near the edges of the screen (see 3.5 - Materials and Methods), a large proportion of target saccades were of small amplitude (median amplitude background: 9.33 degrees; target: 3.08 degrees). This could be explained by the animals rapidly making large amplitude saccades to the appearing targets, followed by small corrective saccades to place gaze within our small fixation window. Saccades to the blank background were slower (median duration background: 38 ms; target 24 ms, $p < 0.001$ ranksum test) and less frequent (i.e. longer fixations; median ISI background: 626 ms, target: 204 ms; $p < 0.001$ ranksum test) than visually guided saccades to the fixation target.

Gamma power at saccade onset was increased across a considerable proportion of electrodes (Figure 3-5 B) for saccades to the background (21%) and to the target (45%). Conversely, less than 5% of electrodes showed significant low frequency power fluctuations within 200 ms of saccades to the background (Figure 3-5 B, a)), while 78% showed fluctuations for saccades to targets (Figure 3-5 B, b)). Consistently, LFP power was modulated on a larger proportion of electrodes during saccades to the target than during saccades to the background (Figures 3-5 B, b) - a), chi-square test for equality of proportions, see 3.5 - Materials and Methods).

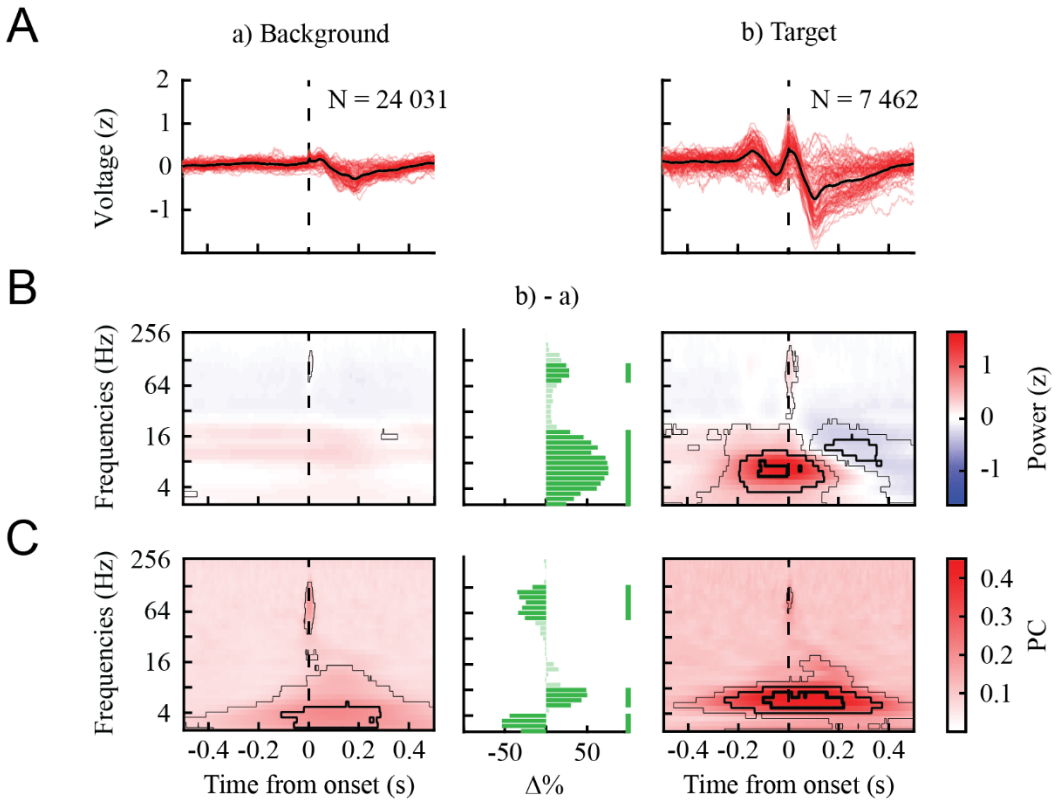

Figure 3-5. Influence of visual stimulation in the Cued Saccade task. (A) Averaged z-scored LFP traces within each electrode (red traces) and cross-electrode grand average (black trace), (B) z-scored LFP power and (C) PC for all saccades landing on a uniform grey screen (background) or on a fixation target (target) during the Cued Saccade task. N values indicate the total number of saccades. Black outlines illustrate the proportion of significant electrodes, where thin: > 5%, middle: > 50% and thick: > 75%, computed from non-parametric permutation testing within electrode ($p < 0.01$, pixel-based correction for multiple comparisons). Proportions of significant electrodes were compared (b) – a)) for power (B) and PC (C) values via a chi-square test for equality of proportions and are labelled as proportion differences (Δ%). Dark green bars highlight significant differences, $p < 0.05$ Bonferroni corrected.

Gamma band PC was significantly greater than chance for both saccades to a target (15% of significant electrodes) and saccades to the background (45% of electrodes). In the low frequencies background saccades showed significant PC values around 4 Hz (70% of electrodes) while saccades to targets showed their significant PC values almost exclusively between 4 and 8 Hz (81% of electrodes), with less than 20% of electrodes showing significance for frequencies below 4 Hz. Contrary to power modulations, PC in the gamma band and for frequencies ≤ 4 Hz

was significant on a greater proportion of electrodes for the background condition, while frequencies between 5 – 8 Hz were significant on more electrodes for the target condition.

These results indicate that saccades to the background, in the absence of a visual stimulus, are sufficient to elicit PC in the HPC. Moreover, saccades to a target seemed to trigger PC in a higher frequency band than saccades to a uniform background. The latter may be due to the contribution of the visual onset to clustering of LPF phase.

3.3.4 Effect of stimulus reward on phase clustering

One possible explanation for the previous results is that the behavioral relevance of the visual stimulus, rather than the stimulus per se, influenced the measured PC. For example, saccades and subsequent fixations to the visual target were rewarded, while saccades to the background were not rewarded. To examine this issue, we divided saccades based on whether they landed on a rewarded target or on non-rewarded features of the environment.

We concentrated on the virtual environment tasks for this analysis because animals made saccades to visual targets that were associated with reward (e.g., the targets they reached to obtain a reward) and to elements of the environment that were not associated with reward (e.g., trees or mountain). In the FOR task, saccades to the rewarded target (N = 46 969) were slightly shorter than saccades to the environment (N = 89 480; Figure S3-1 B; median amplitude environment: 4.98 degrees; target: 4.43 degrees; $p < 0.001$ ranksum test) and of similar duration (median duration environment: 24 ms; target: 22 ms; $p < 0.001$ ranksum test). Both conditions displayed a clear horizontal bias with over 45% of all saccades within 10 degrees of the horizontal meridian (i.e. 0 and 180 degrees). Lastly, saccade rates across both conditions were highly similar, with a small but significant increase for the target condition (median ISI environment: 208 ms; target: 236 ms; $p < 0.001$ ranksum test).

LFP power (Figure 3-6 A) in the mid- to high-gamma range (~110 – 200 Hz) was increased on a larger proportion of electrodes for saccades to unrewarded elements of the environment (73%) compared to saccades to the rewarded target (35%; Figure 3-6 B, b) – a)). Similarly, a larger proportion of electrodes showed significantly modulated low frequency power for saccades to

unrewarded elements (≤ 5 Hz: 65%) compared to rewarded ones (< 25% for all frequencies below 16 Hz). On the other hand, inter-saccade PC significance in the gamma range (environment: 62%; target: 48%) and low frequencies (> 4 Hz: environment: 96%; target 94%) were virtually identical across the two conditions (Figure 3-6C, b) – a)). Similar to the target condition of the CS task, PC below 4 Hz was markedly decreased for both conditions, where only 28% and 24% of all electrodes were significant for the environment and target conditions respectively ($p < 0.001$, chi-square test against probabilities > 4 Hz).

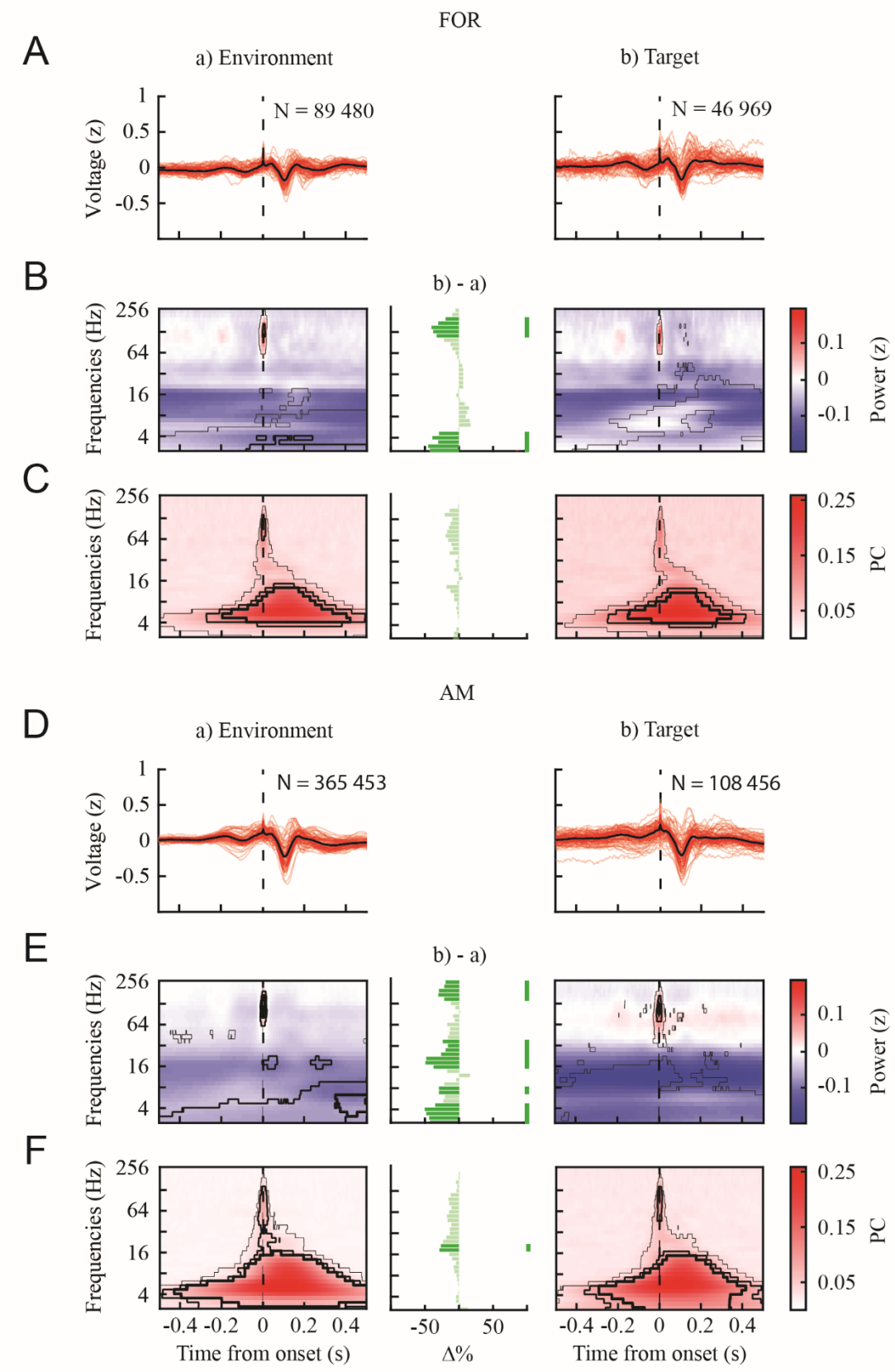
FOR
A
a) Environment
b) Target
N = 89 480
N = 46 969
Voltage (z)
1
0.5
0
-0.5
B
b) - a)
Frequencies (Hz)
256
64
16
4
0.1
0
-0.1
Power (z)
C
0.25
0.15
0.05
PC
AM
D
N = 365 453
N = 108 456
E
F
-0.4 -0.2 0 0.2 0.4
Time from onset (s)
-50 50
Δ%

Figure 3-6. Influence of stimulus relevance in the virtual navigation tasks. LFP traces (right; red: single electrode average; black: cross-electrode average), power and PC values for all saccades landing on the virtual environment or a rewarded target, during the Foraging (respectively: (A), (B) and (C)) and Associative Memory (respectively: (D), (E) and (F)) tasks. Black outlines illustrate the proportion of significant electrodes, where thin: > 5%, middle: > 50% and thick: > 75%, computed from non-parametric permutation testing within electrode ($p < 0.01$, pixel-based correction for multiple comparisons). Proportions of significant electrodes were compared (b) – a)) for power, (B) and (E), and PC, (C) and (F), values via a chi-square test for equality of proportions and are labelled as proportion differences (Δ%). Dark green bars highlight significant differences, $p < 0.05$ Bonferroni corrected.

Similar to the FOR task, AM task saccades to unrewarded elements of the environment (N = 365 453) were of comparable amplitude to target saccades (N = 97 317; Figure S3-1 C; median amplitude environment: 8.57 degrees; target: 7.86 degrees, $p > 0.1$ ranksum test), and presented an horizontal bias in the distribution of directions (> 30% of all saccades within 10 degrees of horizontal meridian). Additionally, saccades were of similar duration (median duration both: 26 ms, $p < 0.001$ ranksum test). Unlike the FOR task, saccades rates were slightly increased for target saccades versus environment ones (median ISI environment: 242 ms; target: 218 ms, $p< 0.001$ ranksum test).

Mid- to high-gamma power in the AM conditions was significantly increased at saccade onset on a large proportion of electrodes (environment: 87%; targets: 84%), although both conditions only differed in the high-gamma band (Figure 3-6 E, b) - a), ≥ 147 Hz). Moreover, low frequency power was significantly modulated on a larger proportion of electrodes for the environment condition than for the rewarded targets, across a broad range of frequencies (Figure 3-6 E, b) – a), ≤ 32 Hz). Despite power being more strongly modulated in the environment condition, gamma band PC was equally modulated across both conditions (Figure 3-6 C, b) - a)). Low frequency PC patterns were also identical across conditions, where virtually all electrodes showed significant PC values for frequencies between 4 and 16 Hz (environment and targets: 100%), as well as comparable behavior for frequencies below 4 Hz (environment: 92%; targets: 89%).

By combining results from all tasks, we can see a dissociation between low frequency power and phase, where power varied across tasks and stimulus conditions, while PC patterns

remained comparable. Moreover, as robust PC was identified without visual stimulation, and no reliable PC preferences could be identified between virtual environment and rewarded targets, we conclude that saccades modulate hippocampal PC regardless of their target. The later suggests a possible role of saccadic motor commands in generating PC in the primate HPC.

3.3.5 Saccade amplitude correlation

To explore the possible relationship between saccadic eye movements and PC we divided saccades according to their amplitude. We pooled saccades from all tasks, binned saccade amplitudes in 14 non-overlapping bins (0 to 28 degrees of visual angle, steps of 2 degrees), and computed the averaged saccade triggered LFP trace for each bin (Figure 3-7 A). Interestingly, both the high frequency peak at saccade onset (Figures 3-7 A-B; vertical dashed line) and the negative deflection around 100 ms post-saccade (Figure 3-7 A: solid black line and Figure 3-7 C) scaled with saccade amplitude ($p < 10^{-20}$, one-way ANOVA against amplitude bins).

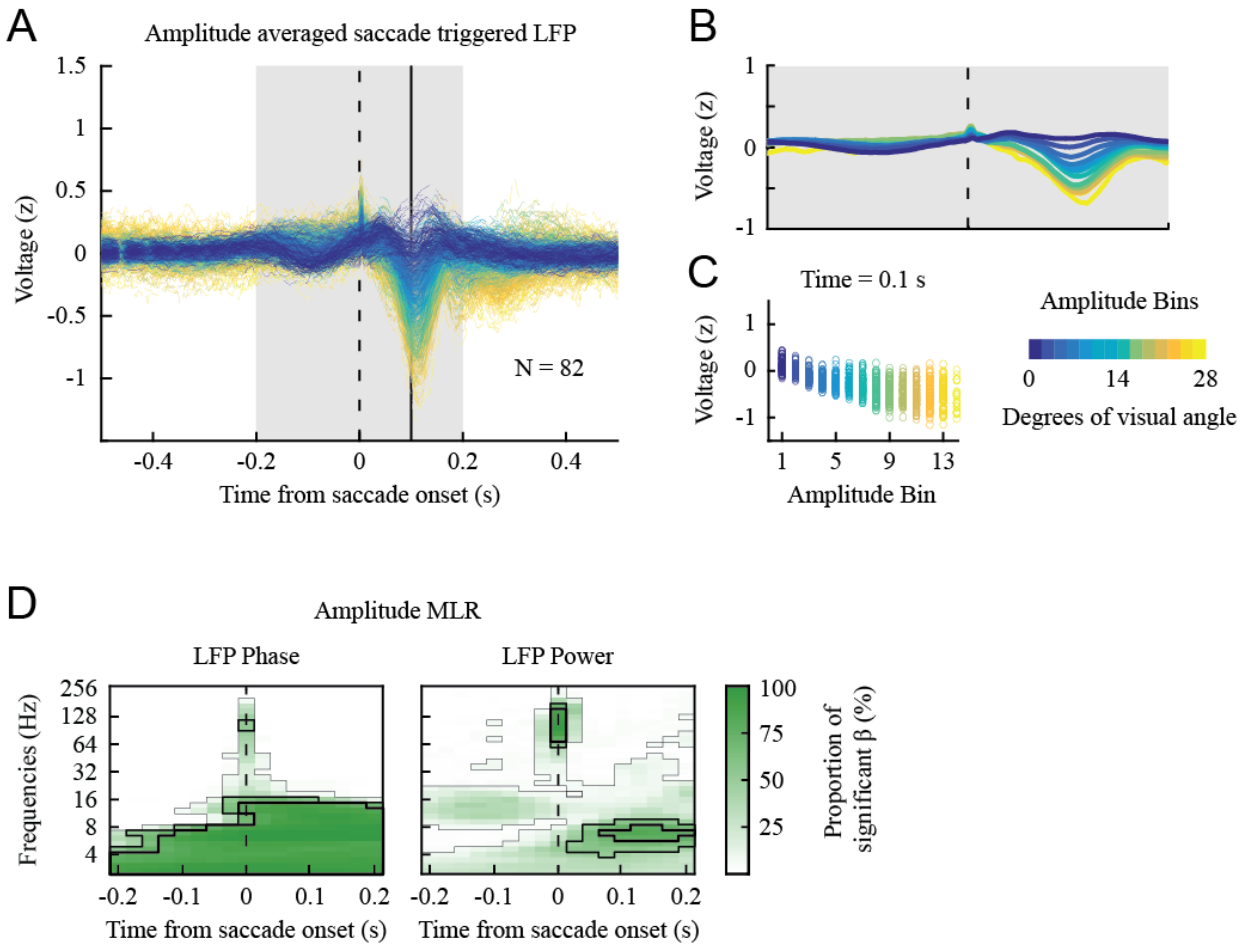

Figure 3-7. Saccade amplitude correlation with LFP power. (A) Within electrode (N=82) averaged LFP traces for each amplitude bin (N=14) around saccade onset (vertical dashed line). (B) Grand average across all electrodes by amplitude bin within a 400 ms window (panel A grey rectangle) centered on saccade onset. (C) Individual electrode values at 100 ms post saccade onset for each amplitude bin (panel A solid black line). D) Proportion of significant regression parameters for the MLR regression between saccade amplitude bins, LFP phase (left) and LFP power (right).

As variations in the scale of averaged LFP deflections could be due to either changes in power or in the reliability of PC, we further characterized the relationship between saccade amplitude and LFP signal parameters (i.e. power and phase) via regression analysis (multinomial logistic regression: MLR; see 3.5 - Materials and Methods). Regression coefficients were computed for the 400 ms around saccade initiation (± 200 ms), in non-overlapping steps of 25 ms. The proportion of electrodes showing significant regression coefficients for LFP power and phase

are illustrated in Figure 3-7 D. The power of the mid-gamma peak at saccade onset significantly correlated with saccade amplitude on 98% of all electrodes, while power in the 4 to 8 Hz range at 100 ms post-saccade correlated with amplitude on 84% of all electrodes ($p < 0.001$, binomial test).

LFP phase was found to be significantly correlated with saccade amplitude in the gamma range (52%) and for virtually every frequency below 16 Hz (> 80%) over the entire 200 ms post-onset epoch ($p < 0.001$, binomial test). However, when controlling for the possible effect of signal power on estimates of phase, we found this effect not to be significant (see 3.7 - Supporting Information). Thus, the power but not the phase of the LFPs was correlated with saccade amplitude.

3.3.6 Saccade direction correlation

We further examined whether saccade direction had a systematic relationship on the power and phase of hippocampal LFPs. We binned saccades into 16 consecutive bins of 22.5 degrees each. Bin-averaged LFP traces from individual electrodes are displayed in Figure 3-8 A, while grand averages across electrodes are presented in Figure 3-8 B. A striking difference in z-scored voltage values over all bins was visible at 0.1 s post-saccade onset (black solid line in Figure 3-8 C; $p < 10^{-20}$, one-way ANOVA against direction bins), peaking between downward saccades (blue) and upward saccades (red). Quantification of saccade direction and LFP phase correlation via MLR validated these findings, where 89% ($p < 0.001$, binomial test) of all electrodes presented a significant regression coefficient for oscillations lower than or equal to 4 Hz (Figure 3-8 D). Furthermore, less than 10% ($p > 0.05$, binomial test) of our electrodes showed significant regression parameters between power and saccade direction, regardless of time and frequency.

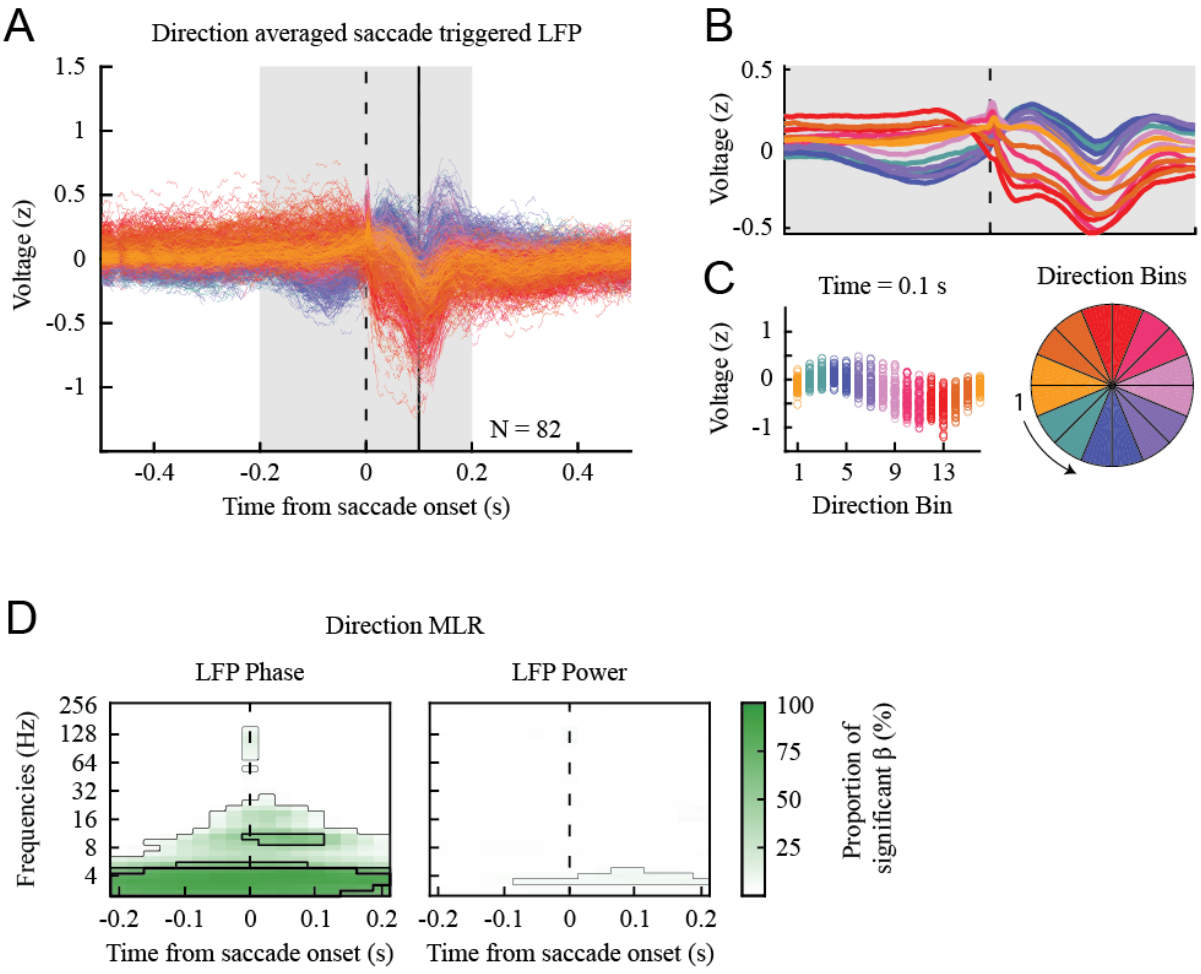

Figure 3-8. Saccade direction correlation with LFP phase. (A) Within electrode (N=82) averaged LFP traces for each saccade direction bin (N=16) around saccade onset (vertical dashed line). (B) Grand average across all electrodes binned by direction within a 400 ms window (panel A grey rectangle) centered on saccade onset (dashed line). (C) Individual electrode averaged values at 100 ms post saccade onset (panel A solid black line). (D) Proportion of significant regression parameters for the MLR regression between saccade direction bins, LFP phase (left) and LFP power (right).

Considering the uneven distribution of saccade amplitudes across direction bins (Figure S3-2 B), and the regression results between saccade amplitudes and low frequency LFP phase (Figure S3-2 D), we replicated the MLR analysis on saccade directions within single amplitude bins. To avoid the confounding effects of saccade amplitude on phase, we selected only amplitude bins within the range of highest PC significance (bin numbers 4-9; Figure S3-2 A right). Single

amplitude bins were then independently selected for each electrode to maximize the number of saccades within each direction bin. The distribution of selected amplitude bins is presented in Figure S3-3 B. Regression results (Figure S3-3 A) confirmed the confounding effect of saccade amplitude on MLR phase regression, showing virtually no relationship between saccade direction and gamma phase (< 3% of electrodes over all time-frequency points, $p > 0.05$, binomial test), and a strong decrease in significance probability for frequencies above 5 Hz (< 20%, $p < 0.001$, binomial test). On the other hand, 55% of all electrodes remained significant for frequencies lower or equal to 4 Hz ($p < 0.001$, binomial test). Of note, the significant regression coefficients were centered on saccade onset and confined within the last and first 100 ms surrounding saccade initiation. These results suggest that the apparent non-specificity of the low-frequency effect in figure 3-8, where virtually all points show significant correlations with saccade direction, could be due to the wide temporal resolution of low-frequency wavelets (> 200 ms). Similarly, peak significance probabilities were found within the same temporal window for all frequencies lower and equal to 4 Hz (Figure 3-8 D).

These results suggest that saccade direction is reliably correlated with the phase, and not power, of very low frequency LFPs (≤ 4 Hz).

3.3.7 Saccade parameters matching

We next set to evaluate whether the task differences identified in Fig 6 were due to different distributions of saccade amplitudes and directions (Figure S3-1). We did not pursue this analysis using CS task saccades (Figure 3-5) because of the confounding effects of stimulus onsets and the absence of visual stimulation for the background condition. Moreover, the low number of target saccades during the CS task (N = 7 462) would impair the number of matches we could obtain across all tasks. We thus matched saccades to both environment and targets in the VR tasks by minimizing amplitude differences across saccades (see 3.5 - Materials and Methods).

A total of 17 586 saccades were matched across the four conditions (Figure S3-3; FOR environment, FOR target, AM environment and AM target). Saccade amplitudes (medians FOR environment: 4.23 degrees; FOR Target: 4.29 degrees; AM environment: 4.30 degrees; AM

Target: 4.30 degrees, p-value = 0.82 kruskal-wallis test), directions (medians FOR environment: -11.66 degrees; FOR Target: -13.40 degrees; AM environment: -11.59 degrees; AM Target: -11.60 degrees) and durations (medians FOR environment: 24 ms; FOR Target: 22 ms; AM environment: 22 ms; AM Target: 22 ms, p-value < 0.001 kruskal-wallis test) were highly similar across conditions. Although the distributions of inter-saccade intervals were statistically significant (medians FOR environment: 230 ms; FOR Target: 200 ms; AM environment: 208 ms; AM Target: 234 ms, p-value < 0.001 kruskal-wallis test), the median values for the onset of the subsequent saccade were at least equal to the furthest edge of our 200 ms window of interest.

Averaged LFP traces (top), power (middle) and PC (bottom) values for matched saccades are presented in Figure 3-9 A. LFP power was more strongly modulated by saccades to the target in the AM task, than other conditions for frequencies below 12 Hz (Figure S3-5: AM Target), with a clear trend in the low-gamma range (30 – 60 Hz). Moreover, saccades to targets tended to yield more robust power modulations for frequencies below 4 Hz (FOR environment: 11%; FOR target: 32%; AM environment: 20%; AM target: 50%) and in the mid-gamma range (FOR environment: 20%; FOR target: 28%; AM environment: 20%; AM target: 26%). Irrespective of power modulations, PC was significantly higher for both AM conditions (Figure 3-9 B) within two bands: below 5 Hz and between 8 to 12 Hz. PC for target saccades during the AM task also tended to be higher than all other conditions for all frequencies between 16 and 128 Hz.

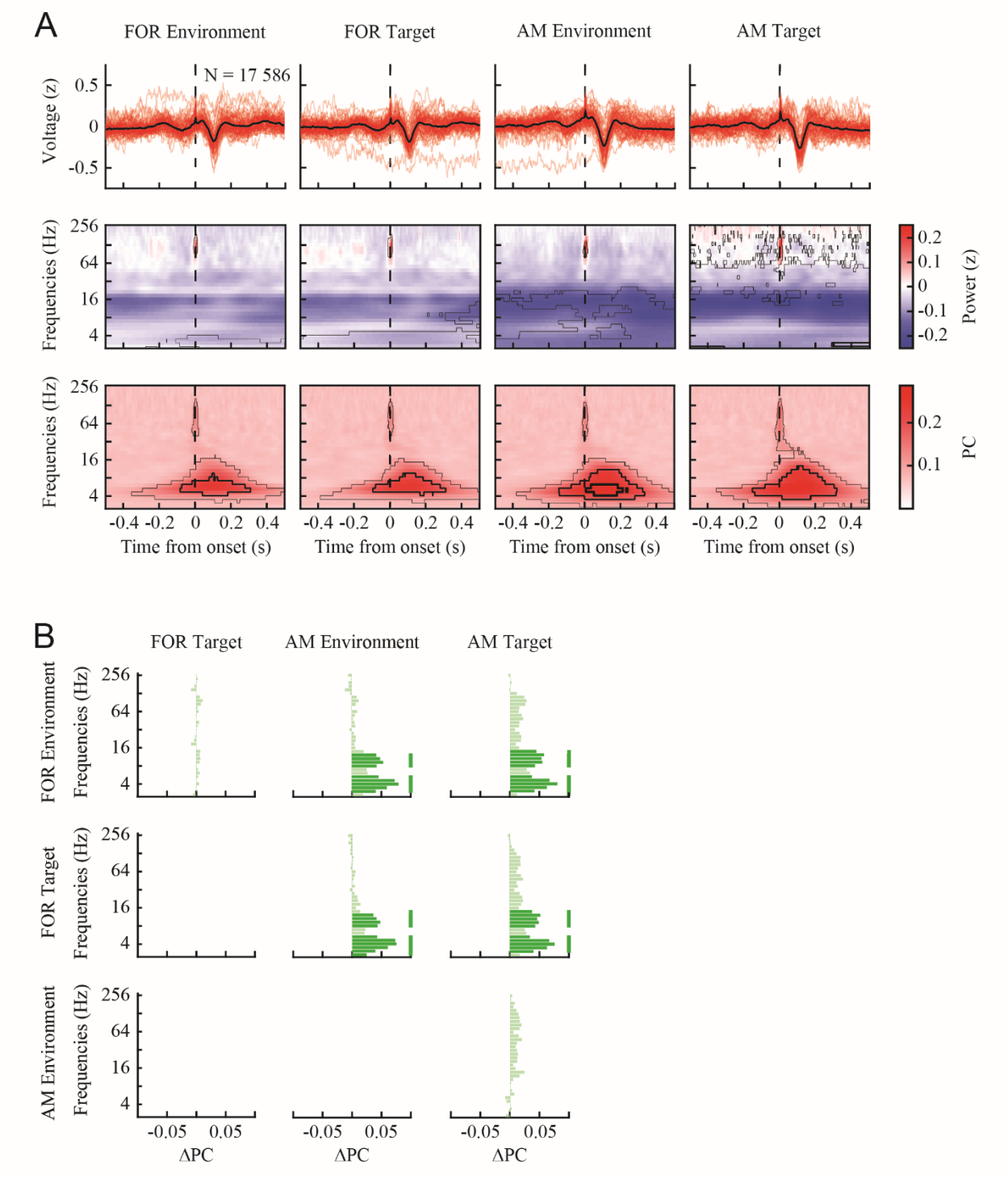
A
FOR Environment
FOR Target
AM Environment
AM Target
N = 17 586
Voltage (z)
0.5
0
-0.5
Frequencies (Hz)
256
64
16
4
0.2
0.1
0
-0.1
-0.2
Power (z)
PC
-0.4 -0.2 0 0.2 0.4
Time from onset (s)
B
FOR Target
AM Environment
AM Target
FOR Environment
AM Environment
-0.05 0.05
ΔPC

Figure 3-9. Task modulation of saccade triggered LFP. (A) Saccade triggered LFP (top), power (middle) and PC (bottom) for amplitude and direction matched saccades across the two VR tasks. Black outlines illustrate the proportion of significant electrodes, where thin: > 5%, middle: > 50% and thick: > 75%, computed from non-parametric permutation testing within electrode ($p < 0.01$, pixel-based correction for multiple comparisons). B) Differences in peak PC value within the first 200 ms post-saccade across condition pairs (column – row). Dark green bars indicate statistical significance using a chi-square test for equality of proportions ($p < 0.05$ Bonferroni corrected).

These results suggest that saccades during an associative learning task might generate a more robust hippocampal activation than other non-learning tasks (i.e. FOR task). This effect was further increased for saccades to the rewarded task elements (i.e. target).

3.4 Discussion

We found that both visual onsets and saccades modulated LFP power and phase in the macaque monkey HPC across three different tasks. Firstly, visual target onset produced reliable PC for frequencies ≤ 4 Hz and between 8 – 16 Hz, despite task-dependent power changes. Moreover, LFP phase within the same 8 – 16 Hz band was found to be preferentially clustered following foveation onset (i.e. saccade offset). On the other hand, saccade onset clustered the phase of the delta (≤ 4 Hz), theta (4 – 8 Hz) and low- to mid-gamma bands (~30 - 120 Hz). The power of both theta and gamma saccade triggered oscillations reliably correlated with saccade amplitudes, and the phase of delta band (≤ 4 Hz) oscillations correlated with saccade direction.

3.4.1 Phase resetting of LFP oscillations in primate HPC

Classically, changes in the power of HPC oscillations have been associated with a broad range of cognitive operations such as learning, movement and decision making (Hasselmo, 2005; Watrous, Fried and Ekstrom, 2011; Belchior et al., 2014), while changes in phase (e.g. phase resetting) are seen as temporal coordinators of neuronal activity associated to memory formation (Lisman and Jensen, 2013; Colgin, 2016). Our results show distinct frequency-specific power

profiles depending on task, visual condition and saccadic target, while presenting power invariant phase clustering (Figures 3-2 to 3-6). These results agree with previous reports of dissociations between the power and phase of LFPs in the hippocampus (Givens, 1996; Hoffman et al., 2013; Jutras and Buffalo, 2014).

Previous studies have proposed that hippocampal activity is modulated by task and contextually relevant information (McKenzie et al., 2016; Ekstrom and Ranganath, 2017; Loonis et al., 2017; Wirth et al., 2017). Accordingly, sensing or stimulus related PC were shown to be absent during hippocampal independent conditions, such as visually guided saccades (Givens, 1996; Jutras, Fries and Buffalo, 2013), and in the absence of stimuli (Berg, Whitmer and Kleinfeld, 2006; Hoffman et al., 2013). Here, we have found significant PC following saccades, regardless of stimulus conditions and during tasks, such as CS, that do not require memory (Figures 3-4 to 3-6). Power and PC modulations were more robust when animals made saccades during an associative learning (AM) task than during a non-learning foraging (FOR) task, within frequency bands previously associated with explicit learning (i.e. delta/theta and alpha/beta; Figures 3-9 and S3-5; Brincat and Miller 2015; Loonis et al. 2017). These results corroborate the hypothesis that explicit learning differentially engage the HPC when compared to HPC independent tasks (Loonis et al., 2017).

The fact that we found significant PC in HPC independent conditions, and despite the absence of visual stimulation, could be explained by different factors. Firstly, self-generated saccades in the dark have been found to be of smaller amplitude (Andrews and Coppola, 1999) and of slower speed (Helmchen, Straube and Büttner, 1994; Sobotka and Ringo, 1997) when compared to complex scene viewing. This trend is also present in our data, where over 30% of all saccades to the background during the CS task are less than 3 degrees **(**Figure S3-1**).** Combined with our finding of less reliable PC following small amplitude saccades (Figure S3-2), this could lead to an impaired detection of significant PC. Moreover, the magnitudes of both microsaccades and ocular drift increase in darkness (Martinez-Conde, Macknik and Hubel, 2004) possibly interfering with fixation detection in dispersion-based algorithms (Salvucci and Goldberg, 2000; Hoffman et al., 2013), rather than saccade detection with amplitude or velocity thresholds (Sobotka and Ringo, 1997; Corrigan et al., 2017). Secondly, the lack of significant PC following visually

guided saccades in (Jutras, Fries and Buffalo, 2013) could be explained by the authors discarding the last 100 milliseconds before the saccade and the first 400 milliseconds after it; we focused our analyses on the first 500 milliseconds following saccade onset, when a signal corresponding to the saccade command could reach cortical and subcortical areas. Although the authors argue that this rejection was made to prevent possible interference from visually evoked potentials driven by fixation point onset, many inconsistencies in their methods impair proper discussion. Indeed, by discarding the last 100 ms before saccade initiation, the onset of the stimuli will inevitably have a confounding effect during the pre-saccade period, unless the animals' reaction times were below 100 ms. We believe that this is highly improbable as our data show a median reaction time of 151 ms. Moreover, during the eye calibration task, monkeys were required to saccade to an appearing grey square, and maintain fixation for 500 to 1100 ms, until a color change occurred, cueing them to release a bar. Importantly, this highly relevant, yet randomized, color change could occur during the post-saccade period of interest (i.e. 400 to 1000 ms), modulating theta phase and destroying coherence. Conversely, no such changes occurred following fixation on the pre-trial cross of the visual preferential looking task. Lastly, the "buffer" period did not seem to be implemented for saccades during the visual preferential looking task, even for the first saccade following stimulus onset.

Similar to us, other studies have identified a PC window following saccades of 200 to 300 milliseconds (Sobotka and Ringo, 1997; Hoffman et al., 2013). Lastly, while our strongest PC was almost exclusively contained within the "classical theta" band (4 – 8 Hz; Figure 3-5, target), the authors in (Jutras, Fries and Buffalo, 2013) band-passed filtered the LFPs between 6 – 12 Hz. Our results also corroborate a series of studies (Ringo et al., 1994; Sobotka and Ringo, 1997; Sobotka, Nowicka and Ringo, 1997) that identified strong neuronal activation following saccadic activity in the primate medial temporal lobe, during hippocampal independent tasks, visually guided saccades and saccades in complete darkness.

Importantly, saccades have been shown to modulate LFPs in multiple brain areas, such as the prefrontal (S. Tremblay et al., 2015) and visual (Ito et al., 2011; Ito, Maldonado and Grün, 2013; Staudigl et al., 2017) cortices. While some parallels can be drawn between saccade triggered effects in visual areas and the HPC, important considerations about the different region properties

must be first addressed. Indeed, visual areas, such as V1, are retinotopic and heavily influenced by the visual properties of the stimuli (Ito, Maldonado and Grün, 2013; McFarland et al., 2015), whereas HPC neurons use an allocentric frame of reference (Feigenbaum and Rolls, 1991) and can encode spatial information regardless of visual stimulation, such as gaze position behind an obstructed view (Rolls. 1999). Despite these differences, both saccades and fixations have been found to elicit phase resets in the classical delta/theta and alpha/beta bands (Ito et al., 2011; Ito, Maldonado and Grün, 2013). Interestingly, phase preferences for both events are inverted across regions, where HPC phase is preferentially clustered by saccade onsets in the classical theta band and by foveation onsets in the alpha/beta band (Figure 3-4), whereas the opposite is true for V1 (Ito et al., 2011; Ito, Maldonado and Grün, 2013). Regardless of spatial reference frames and encoding preferences, this inversion effect could be due to the different implications of eye movements within each area. For example, within V1, saccades trigger a bi-phasic suppression-enhancement effect on neuronal activity, hypothesized to reduce interference between pre- and post-saccadic stimuli (Burr, Morrone and Ross, 1994; McFarland et al., 2015). Conversely, LFP modulation by saccade amplitudes and direction (Figures 3-7 and 3-8) suggests spatial or motor processing within the HPC.

3.4.2 Frequency specific phase resetting

We found that saccade offset/foveation and target onset triggered PC occurred within similar frequency bands; whereas, phase resetting triggered by saccades occurred in a different frequency range. Recent work has cautioned against the a priori labelling and filtering of LFP data, while highlighting the lack of coherence in frequency selections (Einevoll et al., 2013; Herreras, 2016). Indeed, a broad range of frequencies have been arbitrarily identified as theta in the hippocampal literature, anywhere between 3 and 12 Hz (Skaggs et al., 2007; Killian, Jutras and Buffalo, 2012; Ekstrom and Watrous, 2014; Jacobs, 2014; Colgin, 2016). Moreover, comparable studies of saccade triggered PC in the primate HPC have found significant results for minimally overlapping frequency ranges: 3 - 8 Hz (Hoffman et al., 2013) and 6 - 12 Hz (Jutras, Fries and Buffalo, 2013). The narrowly spaced complex Morlet wavelets used in this study have allowed us to identify three separate behavioral correlates within the hippocampal theta range of 3 - 12 Hz.

We will thus attempt to reconcile these three phenomena within the previously described hippocampal literature and highlight the putatively different cognitive processes involved within each frequency band.

Firstly, we found that frequencies between 8 and 16 Hz, labelled as alpha/beta, were more strongly correlated with incoming sensory signals (target onset: Figure 3-3; foveation onset: Figure 3-4) than with saccadic activity, regardless of condition. Consistently, multiple studies have found significant correlations between the HPC and prefrontal cortex (PFC) LFPs following stimulus exploration, within the same frequencies. For example, Place et al. (2016) simultaneously recorded from rodents' HPC and PFC and found significant bidirectional phase coherence between 7 – 12 Hz during the first second of contextual and target sampling. Interestingly, during contextual exploration HPC phase preceded PFC phase, while this relationship was reversed during target sampling. Similarly, Brincat and Miller (2015), as well as Loonis et al. (2017), showed a strong HPC led phase coherence between 9 - 16 Hz following correct trial outcome feedback in macaque monkeys. Although these results must be interpreted cautiously due to the lack of homology between rodent and primate PFC (Kaas, 2013; Carlén, 2017), they reveal a degree of homology across mammalian brains. Human intracranial recordings, albeit limited to the neocortex, also found significant phase clustering between 6 - 13 Hz following stimulus onset, with the preferred phase varying between the encoding and retrieval epochs of the task (Rizzuto et al., 2006). Moreover, despite being defined in lower frequencies in rodents (i.e. 4 – 9 Hz), a strong parallel can be drawn between our findings and the "sensory processing" hippocampal type 2 theta oscillation (Sainsbury, Harris and Rowland, 1987; Bland and Oddie, 2001; Gangadharan et al., 2016). Future studies investigating the directionality and information content of saccade triggered alpha/beta interactions between HPC and PFC in primates are still required to validate this hypothesis.

Secondly, we found that frequencies in the "classical theta" range, based on the EEG literature between 4 – 8 Hz (Tremblay et al., 2015), presented strong PC aligned to the onset of saccades (Figure 3-4), whose power reliably correlated with saccade amplitude (Figure 3-7). Hippocampal theta band power (i.e. "type 1") has been repeatedly correlated with locomotion speed (Bland and Oddie, 2001; Ekstrom and Watrous, 2014) and has also been shown to encode

distance travelled by abrupt displacements, namely jumping or teleportation, in both rodents and humans (McNaughton et al., 2006; Vass et al., 2016). Interestingly, Vass et al. (2016) demonstrated that this distance encoding after teleportation occurred even without visual input during teleportation, suggesting an internal representation of space independent from visual, vestibular and self-motion cues. Considering that primates primarily use vision to explore their environment (Jutras and Buffalo, 2014; Meister and Buffalo, 2016), that saccade related hippocampal activity is from an extra-retinal source (Sobotka and Ringo, 1997) and that gaze location within an environment is sufficient to elicit place-like responses (Rolls and O'Mara 1995; Rolls et al. 1997; Wirth et al. 2017), it has been proposed that saccadic modulation of theta activity in primates is similar to the modulation elicited by exploratory movements in rodents (Sobotka and Ringo, 1997; Killian, Jutras and Buffalo, 2012). We therefore propose a strong relationship between the pathway for the internal representations of movements (Sommer and Wurtz, 2002), the saccade triggered event-related potentials in the medial septum (Sobotka and Ringo, 1997) and the medial septum dependent, internally driven, hippocampal firing fields and theta sequences identified by Wang et al. (2014).

As mentioned above primates have an extraordinarily developed visual processing system (Kaas, 2013) that allow rapidly and effectively identify transient signals, and assign to them behaviorally relevance (Khayat and Martinez-Trujillo, 2015). They also have an oculomotor system that allows orienting the fovea in space towards behaviorally relevant information via saccades or head movements (Crawford, Martinez-Trujillo and Klier, 2003). It is likely that the primate brain evolution has linked these important sensory and motor events that "tag" sensory signals processed in close temporal proximity as behaviorally relevant, to the mechanisms of memory formation in the Hippocampus, which have more ancient phylogenetic roots in early mammals.

Lastly, we showed that the delta band (≤ 4 Hz) phase correlated with saccade direction, independent of power (Figure 3-8). These results validate the findings of Soboka et al, (1997) which have found infrequent, yet highly significant, differences in evoked responses of right vs. left saccades. Furthermore, behaviorally correlated phase modulation within the delta band, also identified as "human theta" (Watrous et al., 2013; Jacobs, 2014), is in accordance with the

coordinating role of the HPC (Buzsáki, 2002; Colgin, 2016). Saccade direction modulation of delta phase seemed to be dominated by differences in upward versus downward saccades, where upward saccades were related to the falling edge of the low frequency oscillation, whereas downward saccades were related to rising edge (Figures 3-8 B-C). Considering the 3D projection of the virtual environment on the 2D computer screen and the quasi-linear shape of the maze, upward saccades typically shifted gaze farther in the environment, while downward saccades brought gaze closer to the subject. Analogously, place cell firing in animals has been repeatedly correlated with the phase of hippocampal theta oscillations with regards to where within a place field the animal is, a process termed phase precession. During this process, place cells' spiking correlates with late, or rising edge, phase when animals enter the place field, and correlates with early, or falling edge, phase when animals leave the place field (O'Keefe and Recce, 1993; Dragoi and Buzsáki, 2006). Studies on the functional role of phase precession have further hypothesized its involvement in attention to either proximal or distal cues (Fenton et al., 2010) or in prospective versus retrospective position encoding (Lisman and Redish, 2009; Bieri, Bobbitt and Colgin, 2014). In our data, near and distant spatial processing correlate, respectively, with late and early delta phase suggesting a relationship between these variables.

Since recent studies challenged the "local" extent of LFPs (Kajikawa and Schroeder, 2011; Herreras, 2016), the measured correlations with saccade parameters could reflect artefactual or motor signals, although we argue that this hypothesis is largely unlikely. Firstly, as saccade amplitudes and directions are encoded by different neurons within the corollary discharge pathway, and not by the rate of individual neurons (Sommer and Wurtz, 2002), it is unlikely that saccades of different amplitudes would yield different power values. Secondly, while to our knowledge no neurons encoding saccade parameters have been found in the primate HPC, neurons have been shown to encode gaze position within an environment (Rolls and O'Mara 1995; Georges-François et al. 1999) and the HPC receives direct input from the entorhinal cortex, contain gaze and saccade direction sensitive cells (Killian, Jutras and Buffalo, 2012; Killian, Potter and Buffalo, 2015).

In summary, we have confirmed that both internally and externally generated signals trigger phase resting in the primate HPC in different frequencies. Invariance of saccade triggered

phase resetting across behavioral states and correlation with saccade parameters suggest a prominent role of saccade commands in resetting primate hippocampal LFPs. This could act as a mechanism for the temporal binding of behaviorally relevant information into associative memories, where visual attention is first shifted to the saccadic target prior to movement onset (Deubel and Schneider, 1996), followed by saccade triggered event-related potentials in the medial septum (Sobotka and Ringo, 1997) and septal dependent spike-field coherence of the HPC (Wang et al., 2014). Consistently, attention (Aly and Turk-Browne, 2016), saccadic behavior (Meister and Buffalo, 2016) and medial septum integrity (Hasselmo and Stern, 2014) have been closely linked with memory formation.

3.5 Materials and Methods

3.5.1 Subjects

Two healthy adult male rhesus macaques (*Macaca mulatta*) were used for this study. Animals were obtained from, and under the care of, the McGill Comparative Medicine and Animal Resources Center. Monkey W (7 years old; 7 kg) was group housed and monkey R (14 years old; 12 kg) was single housed, and both monkeys had access to large playpen enclosures and were trained to enter a side cage prior to testing. All handling and procedures were in accordance with the Canadian Council for Animal Care Guidelines and approved by the McGill University Animal Care Committee.

3.5.2 Surgical procedures

Prior to any surgical procedures, anatomical MRI scans were taken for each animal (500 μm isotropic T1-weighted 3T). We then used a neuro-navigation suite (BrainSight, Rogue Research, Quebec, Canada) to obtain a 3D reconstruction of the animals' skull. Head-post and recording chamber positions were then planned and custom built from these reconstructions.

Two consecutive surgeries under general anesthesia, separated by a recovery period of at least 8 weeks, were performed to implant the head-post and subsequently the recording chamber. Recording chambers were positioned over the right pre-frontal cortex, to obtain electrode trajectories perpendicular to the long and transverse axis of the right hippocampus.

Recording chamber placement was validated with a post-recovery CT scan, with cannulas strategically placed within the recording chamber grid, later co-registered with the anatomical MRI scan. Electrode trajectories and terminal depths were then precisely mapped to grid holes.

3.5.3 Experimental setup

Monkeys were seated in a custom-built primate chair and head-fixed ~80 cm away from a computer monitor (1280 x 1024 resolution; 44 x 33 cm; 32 x 24 degrees of visual angle; DVA) refreshing at 75 Hz. The chair was also fitted with a customized two-axis joystick (M212, PQ Controls, Connecticut USA) to allow navigation in the virtual tasks. Eye movements were monitored by video-oculography (EyeLink 1000, SR Research, Ontario, Canada), tracking the left eye at 500 Hz.

Two separate display software were used for visual stimulation. Firstly, for the Cued Saccade task, stimuli were presented using the Psychophysics Toolbox (Brainard, 1997). Secondly, the virtual navigation tasks were presented using an open-source library (Doucet, Gulli and Martinez-Trujillo, 2016) running a freely available videogame engine (Unreal Engine, Epic Games, Inc., North Carolina, USA) on a separate computer. Subject positions in the virtual environment were timestamped and recorded at every frame before being sent to the central control computer over a network link.

The central computer ran an experimental suite programmed in Matlab (Mathworks Inc, Massachusetts, USA), tasked with temporally aligning visual stimulus, gaze and neural data, while controlling trial progression. A juice incentive was used to reward correct trials.

3.5.4 Behavioral tasks

Monkeys were trained on three separate tasks. Firstly, in the Cued Saccade (CS) task (Figure 3-1 A), monkeys were simply trained to shift and hold their gaze within 2 DVA of a small white dot (1 DVA diameter) pseudo-randomly presented at one of 9 possible locations on a 24 by 16 DVA grid. The background luminance was set to match the average luminance of the virtual tasks to minimize pupil size variations.

Secondly, we trained the monkeys to freely navigate within a virtual double-ended Y maze by using a two-axis joystick. Acceleration to top speed along the linear or angular axes was instantaneous, and top speed maintained for the entire duration of joystick movement. Visual stimulation during the two VR tasks was kept constant and no inter-trial intervals were used, except for "time-out" trials where the monkey failed to respond within 50 seconds. In this case, the monkeys were sent to a black screen for 5 seconds before being sent back to the maze to begin a new trial. During normal task flow, a new trial would begin at the exact moment the previous one ended. Two tasks were undertaken within this framework.

The Foraging (FOR) task (Figure 3-1 B), required monkeys to find, and navigate to, a semi-transparent red volume, randomly appearing at one of 84 possible locations. Considering the continuous nature of the visual stimulation, the target could either be directly visible upon trial onset or require the monkey to initiate searching behavior. To identify target onsets, we computed the animal's field of view on each recorded frame and identified the first one where the target was visible on screen.

Lastly, in the Associative Memory (AM) task (Figure 3-1 C), monkeys navigated within the same environment as the FOR task but were required to learn a context-dependent color hierarchy. Upon entering the central corridor (point 1, Figure 3-1 C), one of two possible contextual cues were displayed on the maze walls. Context information dictated the order of a three-color reward hierarchy, inverted across contexts (e.g. Red > Green > Blue in context 1; Blue > Green > Red in context 2). Two randomly selected colored targets were displayed upon departure from the central corridor (point 2; Figure 3-1 C), one in each maze arm (Red and Green circles; Figure 3-1 C). Animals then integrated both color and contextual information and navigated

toward the target with the highest reward value. Decision onset (point 3; Figure 3-1 C) was defined as the first point where heading differed by more than 10 degrees from the vertical meridian. Learning occurred through trial and error and hierarchies were pseudo-randomly selected at the start of each recording session. Again, this task did not include inter-trial intervals, meaning that monkeys were required to turn around upon trial completion and initiate a new trial in the opposite direction. Moreover, only behavioral data from tasks containing at least 20 completed trials were kept for analyses (CS task: 38 sessions; FOR task: 36 sessions; AM task 40 sessions; MLR analyses 36 sessions).

3.5.5 Saccade detection

Prior to saccade detection, gaze data was first cleaned, by removing blinks, off-screen gaze and periods of valid data lasting less than 40 ms, and smoothed with a Savitzky-Golay filter (2^{nd} order with an 11 samples window). We then proceeded to identify periods of putative saccadic activity by an iteratively defined acceleration threshold: starting at 10 000 DVA/sec^2, the sum of the mean and 6 times the standard deviation of all acceleration values below the threshold was computed and defined as the new threshold. This procedure was repeated until the net iteration change was less than 1 DVA/sec^2. Values above the threshold lasting more than 10 ms were considered saccadic epochs, from which onset and offset points were calculated. Saccadic epochs less than 40 ms apart were further grouped into a single epoch.

The aforementioned procedures were modified from a pre-existing classification algorithm tailored for humans (Larsson, Nystrom and Stridh, 2013), using a fixed threshold, defined as 6 times the standard deviation above median acceleration (Nyström and Holmqvist, 2010). To our knowledge, no such thresholds have been defined to account for the increase in saccade rate, velocity and signal stability in head-restrained macaque data (Corrigan et al., 2017). We thus used a lower and iteratively defined threshold to minimize false negatives and to maintain a robust separation between saccades and smooth pursuits.

Onset and offset point were obtained from the identification of eye movement directions deviating by either more than 60^o for a single sample or by more than 20^o for 3 consecutive samples

from the saccade's main direction, specified by the average direction at peak velocity and its immediate neighbors. Points were fine tuned by confirming that the eye velocity was lower than the greater of two measures: 30^{o} per second or one fifth of the peak velocity. Saccade parameters (i.e. amplitude and direction) were obtained from the vector linking eye positions at onset and offset. Only saccades originating and terminating on the screen were used for all analyses. More details about the eye movement classification procedure, as well as example eye traces, can be found in Corrigan et al. (2017).

3.5.6 Saccade probability

Saccade probability across trials was obtained by first creating saccade onset raster plots for each trial, matching the LFP sampling period of 1 ms. Each raster was then convolved with an asymmetric exponential function (1 ms growth; 20 ms decay), used in spike density function analyses, to increase the precision of onset time and match neural data (Thompson et al., 1996). Probabilities were later averaged over all trials.

3.5.7 Gaze processing

Gaze target identification in the virtual navigation tasks was undertaken by first matching every displayed frame and its associated player position in the 3D environment, with the concurrent on-screen gaze position in pixels. Knowing the subject location within the environment and both horizontal and vertical field of views, we projected the on-screen gaze onto the farthest plane of the viewing frustum, thus translating them into 3D coordinates. We then computed the base vector components linking the position of the subject's virtual eyes in the environment and the 3D gaze coordinates. To account for the approximate size of foveal vision, we repeated this procedure for another eight gaze positions equidistant on a 1 DVA radius circle centered on gaze coordinates.

All visible objects in the environment being traversed by these vectors were identified as foveated objects.

As multiple objects could be included within each gaze sample, we applied a behavioral relevance hierarchy (i.e. target > contextual information > environment), where the entire sample was classified as belonging to the category of the object with highest relevance. Saccade targets were then defined as the category of the gaze sample at the time of saccade offset.

3.5.8 Electrophysiological recordings and signal pre-processing

We collected data over 41 sessions, simultaneously recording with up to four single high-impedance tungsten electrodes (0.4-1.5 MΩ; lowering speed: 0.01 mm/sec; referenced to dura penetrating guide tube). Electrode trajectories were mapped to the MRI beforehand and expected distances to grey and white matter tracts were predicted along the descending paths, terminating at putative CA3 recording sites. Neural activity changes were monitored on-line to approximate transitions between white and grey matter and to validate terminal recording depths.

Neural activity was recorded at 30 kHz using a multi-channel data acquisition system (128 channels Cerebus System, BlackRock Microsystems) with analog 0.3 Hz and 7.5 kHz high-pass and low-pass filters. We then filtered the signal backwards with matching digital filters to correct for phase shifts induced by hardware filters (Zanos, Mineault and Pack, 2011; Cohen, 2014). To obtain the raw LFP signal, we further low-pass filtered the data (zero-phase using Matlab function *filtfilt*; 250 Hz cut-off, 4^{th} order Butterworth) and removed power line noise using 3^{rd} order two-pass elliptical band-stop filters at 60, 120 and 180 Hz (Zanos et al., 2012). LFP data was then down-sampled to 1 kHz and manually thresholded for artefact removal. All values exceeding the set threshold were discarded from future analyses.

In order to account for differences in baseline voltage and signal amplitude across electrodes, LFP voltage values (Figures 3-2 and 3-4 to 3-7) were first z-scored over their entire recording session. This procedure thus kept the shape of individual waveforms constant, while allowing for comparable scales across electrodes and conditions. Note that raw voltage values were used for power and phase computations.

3.5.9 Power and phase computation

To obtain the analytical signal from the pre-processed LFP data, we used complex Morlet wavelet convolution, with 7 oscillations (Tallon-Baudry et al., 1997) with 34 logarithmically spaced center frequencies ranging from 2.63 to 256 Hz (Hughes et al., 2012; Liebe et al., 2012; S. Tremblay et al., 2015). Power was obtained from the squared magnitude of the signal, while phase was derived from the angle between the real and complex parts of the signal. We avoided edge effects and allowed analyses periods to be shorter than full oscillation cycles by applying the convolution to entire recording sessions. We could therefore obtain reliable instantaneous power and phase estimations at every time point (1 ms resolution), regardless of the duration of our epochs of interest.

To account for the 1 / frequency power scaling and to allow for cross-task and cross-electrode comparisons, we z-scored the power values, individually for each center frequency, within entire recording sessions, regardless of behavior. The same procedure was also undertaken for the LFP voltage values, after wavelet convolution.

3.5.10 Phase clustering

In order to quantify the degree of PC for stimulus and saccade triggered data, we computed a phase clustering index, defined as the norm of the vectoral average of unit length 2D vectors, whose directions are specified by the phase values. In other words, angular phase values are mapped onto 2D unit vectors, which are then averaged, resulting in an index that ranges from 0, for a uniform distribution, to 1 , for identical angles. (Cohen, 2014). This calculation was completed independently within each electrode for all time-frequency points (1 ms sampling period) in a 2 second window for inter-trial PC (±1000 ms; Figure 3-2) and in a 1 second window for inter-saccade PC (±500 ms; Figures 3-3 to 3-6).

Moreover, as the index value is dependent on the number of points used for its computation, it is possible to estimate a theoretical significance threshold from a desired p-value (Figure 3-S1 AB Right):

$$PC_{Threshold} = \sqrt{\frac{-\ln(p)}{N}},$$

where N is the number of observations and p is the desired p-value (Cohen, 2014, p. 488), in our case set at 0.01 / 34 frequencies / 14 bins.

3.5.11 Phase clustering differences between conditions

To compare the magnitude of phase clustering triggered by neighboring events (Figures 3-3 and 3-4, ΔPC) and paired conditions (Figure 3-9), we took advantage of the high sensitivity of the PC metric to jitter. As previously stated, the individual phase values are mapped onto unit vectors, which are then averaged, and the magnitude of the resulting vector corresponds to the PC value. Similar to linear averaging, changes in the standard deviation of the population should not influence the resulting mean value, which, in our case, is the mean direction of the resulting vector. Conversely, a broader distribution of values would decrease the magnitude of the vector, as general coherence decreases. Assuming that any of the neighboring events is clustering the LFP phase, the added jitter in either reaction time from target onset, or in saccade duration, would be enough to negatively affect the resulting PC value. Despite these differences being of small amplitude, their reliability in direction (i.e. negative or positive) across events and electrodes can be quantified using statistical tests. Moreover, considering the significant decrease in measured PC for initial saccade to the target during the FOR task versus target onset triggered PC, and the presence of the gamma band PC only for target onsets (Figure 3-3 A), we argue that contamination from target onsets events should be minimal. This is especially true for the VR tasks, due to limited changes in visual stimulation, the added jitter in reaction times and their low number relative to the total number of saccades used in Figure 3-4: 8.8%, 2.8% and 3.5% respectively for CS, FOR and AM tasks.

We thus measured the peak PC value for each frequency within the first 200 ms following event onset, in order to remain within the previously published window of interest. Statistical significance between conditions was obtained by a Bonferroni corrected paired t-test ($p < 0.05 / 34$ frequencies).

To avoid possible confounders when the animals were not paying attention to the screen, only trials where the gaze was on the screen for all events (i.e. target, saccade and foveation onsets) were kept for analyses. Furthermore, trials where a saccade wasn't initiated within 500 ms of target onset were discarded for Figure 3-3.

3.5.12 Non-parametric permutation testing

As previously stated, PC values are dependent on the number of points used for their computation, preventing the pooling of recording sessions to run group statistics. We thus computed saccade triggered power and PC statistical significance individually for each electrode. To do so, we first created null distributions of saccade triggered LFP power and phase by randomly shifting saccade times within each trial epoch. Of note, as rewarded targets were only visible for short durations during the CS and AM tasks, as opposed to entire trials in the FOR task, null distributions for saccade to targets in Figures 3-5 (CS task), 3-6 B and 3-9 (AM Task) were computed by shifting the saccade times within the target epoch only, and not over entire trials. Correspondingly and to avoid the confounding effects of visual stimulation, null distributions for the background condition of the CS task (Figure 3-5) were obtained for the trial epochs where no target was visible. However, as the environment is constantly visible in the AM task, saccade times for the environment condition (Figure 3-6B) were shifted over entire trials.

Null distribution power averages and PC values were then calculated and only the maximal and minimal values for each wavelet center frequency were kept. This procedure was repeated 1000 times to obtain frequency specific distributions of extreme values. PC statistical threshold was defined as the 99^{th} percentile of the maximal PC values distribution (one-tailed), while power thresholds were defined as the 0.5^{th} percentile of the minimal averaged power values and the 99.5^{th} percentile of the maximal value distributions (two-tailed). This method was adapted from the non-parametric permutation "pixel based" correction method (Cohen, 2014) to account for largely different power and PC distributions across frequencies (e.g. very high power in low frequencies at target onset in the CS task).

3.5.13 Cross-electrode statistical significance and comparison

Since statistical significance was computed on a per electrode basis, we devised a way to highlight time-frequency points that were consistently significant across electrodes. To do so, we outlined the points where > 5% (thin line), > 50% (middle line) or > 75% of channels were significant (black outlines, Figures 3-3 to 3-6).

Moreover, to compare proportions of significance across non-matched conditions, namely Figures 3-5 and 3-6 where PC values can't be used for comparison, we found the peak significance probability within each frequency band and within the first 200 ms following saccade onset, and ran a chi-square test for equality of proportions across conditions. As wavelet convolution induces spectral leakage across frequency bands (i.e. they are not independent), a Bonferroni correction was applied on the p-values ($p < 0.05 / 34$ frequencies).

3.5.14 Multinomial logistic regression

To quantify the relationship between LFP and saccade parameters, we needed a regression model that could fit linear (i.e. LFP power) and circular (i.e. LFP phase) independent variables to either a linear (i.e. saccade amplitude) or a circular (i.e. saccade direction) dependent variable. To our knowledge, no regression model interchangeably accepts linear and circular data as the dependent variable. We circumvented this problem by binning saccade directions and amplitudes into respectively 16 (22.5 degrees) and 14 (2 DVA) consecutive bins and regressed bin numbers by means of multinomial logistic regression for ordinal responses (MLR; Matlab function *mnrfit*), also identified as proportional-odds model (McCullagh, 2005). This model computes how a unit change in a dependent variable affects the odds of the dependent variable being less than or equal to bins 1 to n versus bins n+1 to k, where k is the total number of bins. Calculations are made for all bin numbers n, keeping all other independent variables constant. For example, Fig 7 shows that a unit changes in gamma power at time 0 significantly predicts the probability that a saccade's amplitude belongs to bins ≤ N vs. bins > N.

Since MLR is a generalized linear model, it assumes discrete or continuous independent variables, not circular ones. However, LFP phase values are periodic over 2π and can be expressed

as a first order Fourier series expansion (Sarma and Jammalamadaka, 1993; Lund, 1999), yielding the following regression representation:

$$Bin\ Number(Y) \sim \beta_1 \times\ LFP\ Power + \beta_2 \times \sin(LFP\ Phase) +\ \beta_3 \times \cos(LFP\ Phase) +\ \beta_Y$$

Where Y is the bin number and where β_Y is the bin specific intercept. The MLR model provides a single parameter for each independent variable, with a bin specific intercept value.

Although individual p-values are obtained for each independent variable following model fitting, we set out to quantify the influence of both sine and cosine terms simultaneously. Parameter significance was thus computed by comparing nested models' deviance using a chi-square test, with degrees of freedom defined as the difference in the number of model parameters. For example, p-value for the LFP power parameter β_1 would be calculated as: 1 minus the chi-square cumulative distribution function of the deviance differences between the nested model excluding the power term and the full model. In this case, the degrees of freedom would be defined as 1 (i.e. removing β_1).

P-values for regression parameter were computed around saccade onset by taking the instantaneous power and phase values at 17 time points from 200 ms before onset, to 200 ms after onset, in 25 ms steps. Bonferroni correction was applied to the resulting p-values to determine significance ($p < 0.05 / 34$ frequencies / 17 time points). Note that we limited this analysis to times points in steps of 25 ms to maintain total computing time within a manageable range (~ 1 week).

3.5.15 Surrogate signal creation

We controlled for the effect of saccade amplitude on phase SNR by creating a surrogate signal with constant phase information and varying SNR. We first determined the real signal's SNR value (Figure S3-2 C) for each amplitude bin, by applying a spike metric defined as the peak to trough amplitude of the mean LFP deflection divided by twice the standard deviation of all deflection differences from the mean (Kelly et al., 2007; Zanos et al., 2012). We then determined our "gold standard" waveform (i.e. constant phase) as the average saccade triggered LFP from amplitude bins 4 to 9, identified as the most reliable (> 95% significant electrodes, red outline,

Figure S3-2 A right). A "clean" background LFP signal was next generated by going through each saccade and subtracting its amplitude bin averaged LFP deflection from the raw LFP signal. Surrogate signals were thus obtained by scaling the gold standard deflection and adding it to randomly selected background LFP snippets. To properly identify scale parameters and match real data SNR (Figure S3-2 C), we quantified the influence of a wide selection of arbitrarily selected scale values on obtained SNR via linear regression. Final scale parameters were computed by fitting real signal SNR values into our model. We limited this analysis to amplitude bins 1 to 9 (i.e. $\leq$ 18 DVA) as proportions of significance decreased for larger saccades due to their limited number (Figure S3-2 A-B). Lack of significant differences between the real and surrogate SNR distributions was obtained from a Wilcoxon rank sum test ($p > 0.05$).

3.5.16 Saccade matching

In order to isolate the task effects on saccade triggered LFP power and PC and to control for the different distributions of saccade amplitudes across conditions (Figure S3-2 B), we matched the saccade parameters within recording session and across the two VR tasks. To do so, we selected saccades to the target during the AM task as our gold standard, due to their multi-modal distribution of amplitudes (Figure S3-1). We then matched each AM target saccade to a single saccade from each of the three other conditions (AM environment, FOR environment and FOR target), minimizing amplitude differences (0.5 degrees threshold) within a narrow direction window (10 degrees threshold). We did not match for saccade durations and inter-saccade intervals as median values for the entire populations were highly similar and outside of our 200 ms window of interest.

3.6 Acknowledgments

We thank Matthew Leavitt and Sebastien Tremblay for critical input and discussion, and all members of the J.C.M.T. lab for support. We thank Blandine Bally, Kevin Barker, Sara Chisling, Steve Frey, Steve Nuara, and Walter Kucharski for technical assistance. This work was supported by CIHR, and NSERC grants to J.C.M.T.

3.7 Supporting results

3.7.1 Signal power and phase signal-to-noise

As averaged LFP traces (Figures 3-7 A-B) displayed a consistent and narrow peak at time 0 and a consistent trough at time 100 ms, suggesting similar phase information across amplitude bins. We further investigated this result by evaluating the relationship between saccade amplitudes and the reliability of phase information (i.e. measured PC values). To do so, we plotted the cross-electrode averaged peak PC value within the first 200 ms post-saccade onset, for each amplitude bin (Figures 3-S2 A Left). A significant increase in PC across saccade amplitudes was visible for all frequencies ($p < 10^{-20}$, ordinary least-square regression). To address the possible confounding effect of differences in the number of saccades across conditions, we also computed the probability of PC significance across electrodes at each amplitude bin (PC theoretical threshold, $p < 0.01$, Bonferroni corrected, see 3.5 - Materials and Methods). Regions of peak significance (≥ 95 % of electrodes) are highlighted in Figures S3-2 A (right, red outlines). These results indicate a clear increase in PC significance from low to high amplitude saccades that peaks between bins 4 and 9. PC significance for saccades greater than 18 degrees (i.e. bin 9) decreased as very large amplitude saccades become less numerous (Figure S3-2 B), yielding greater PC values that fail to reach statistical significance.

We next tested the hypothesis that the reliability of phase information concurrently scales with LFP deflections (i.e. power) across increasing saccade amplitude bins (Figure 3-7 D). To do so, we created a surrogate signal with constant phase information but with increasing signal to noise ratio (SNR), matching real data values (see Materials and Methods; Figure S3-2 C). Both real and surrogate signals were then processed through the MLR algorithm. Proportions of significant slope parameters across electrodes were highly similar between 4 and 16 Hz and in the gamma band (Figure S3-2 D; red outline: chi-square test, $p < 0.05$, Bonferroni corrected).

These results suggest that, as the magnitude of saccade triggered LFP deflections scale with saccade amplitudes, measured phase information becomes more and more reliable. As noise sources, such as neighboring brain activity or electrical artefacts from the recording equipment,

can't be differentiated in the recorded signal, we cannot infer physiological relevance to the relationship between measured PC and saccade amplitudes. It thus remains uncertain whether small amplitude saccades modulate hippocampal phase as efficiently as larger ones.

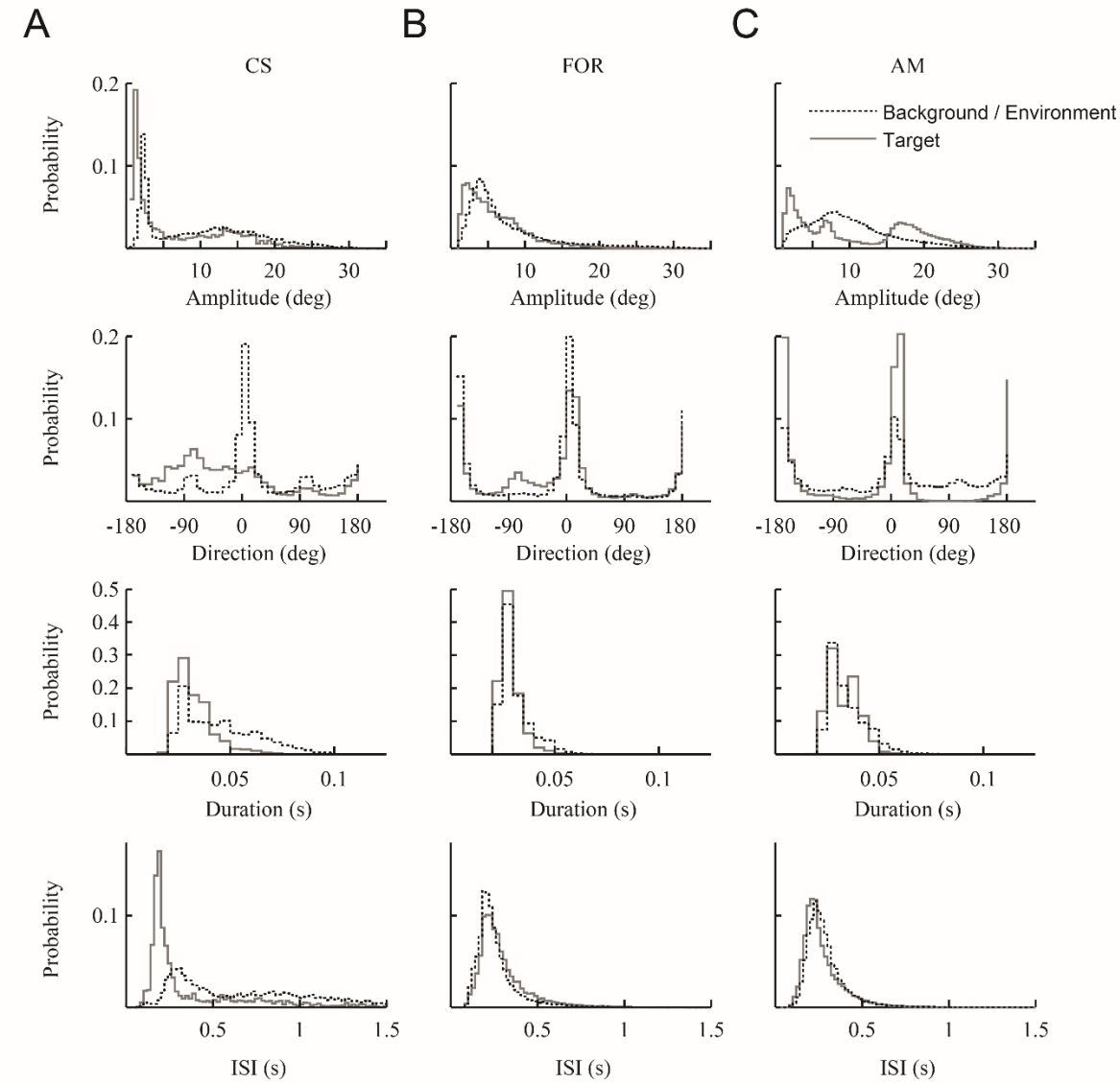

Figure S3-1. Saccade parameters distributions across tasks. Distributions of amplitudes (0.5 degrees bins), directions (10 degrees bins), durations (5 ms bins) and inter-saccade intervals (ISI; 20 ms bins) for respectively the CS (A), FOR (B) and AM (C) tasks. Dashed lines present the distributions for saccades to the background or virtual environment (CS N = 24 031; FOR N = 89 480; AM N = 365 453) and solid lines saccades to the target (CS N = 7 462; FOR N = 46 969; AM N = 108 456).

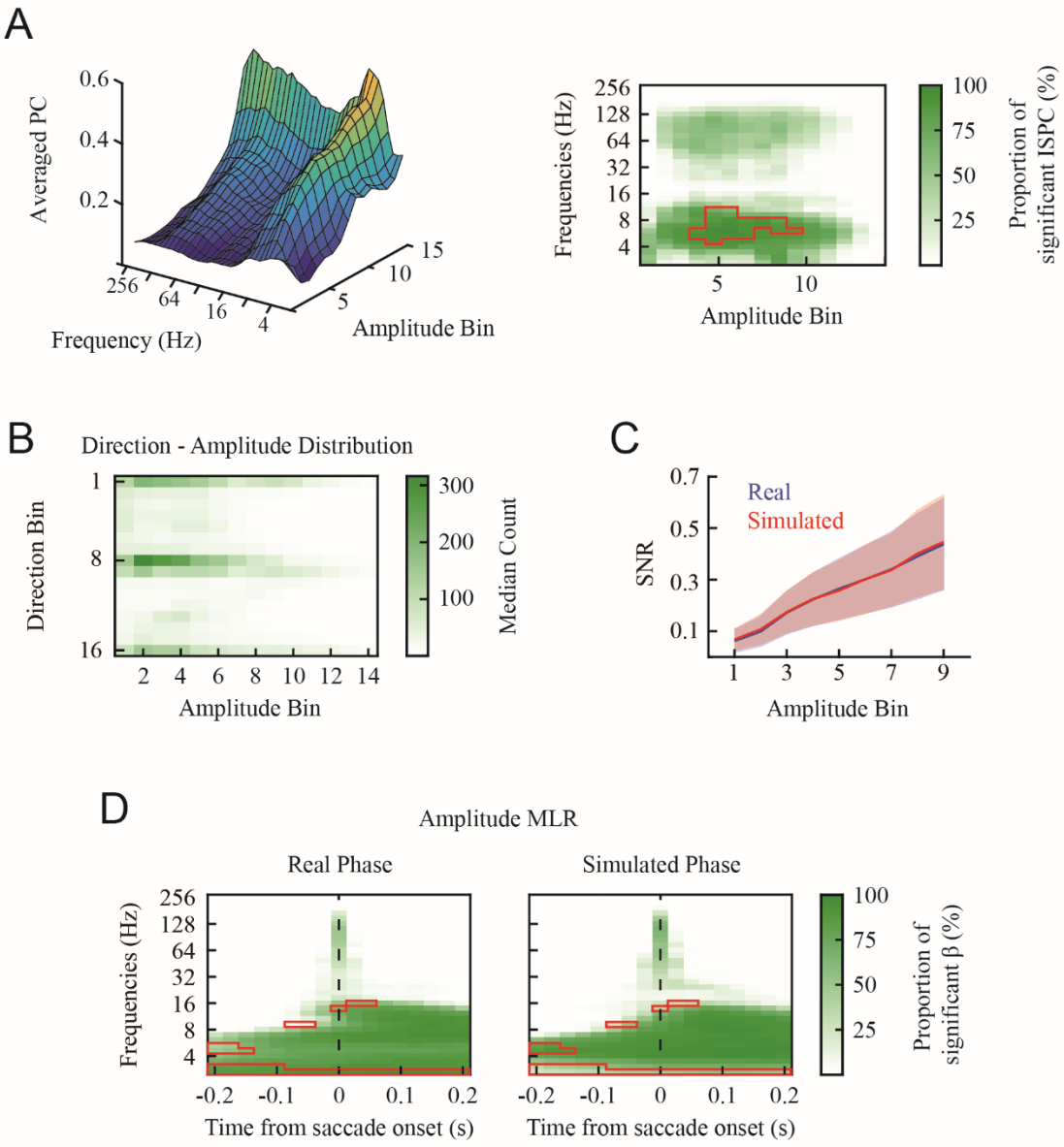

Figure S3-2. Saccade amplitude influence on phase clustering and MLR. (A) Averaged inter-saccade peak PC values by frequency and amplitude bin (left) and their proportion of significant electrodes (right) against a theoretical threshold (see Materials and Methods). Red outline indicates ≥ 95% of significance probability across all electrodes. (B) Median number of saccades within each direction – amplitude bin pairs. (C) Signal to noise values for both real (blue) and simulated (red) signals across amplitude bins used to compute the phase MLR control in panel D. (D) Proportion of significant regression parameters for the real (left) and simulated constant phase (right) signals. Red outline indicates statistical significance (Chi-Square test, Bonferroni corrected, $p < 0.05 / 34$ frequencies / 17 time points).

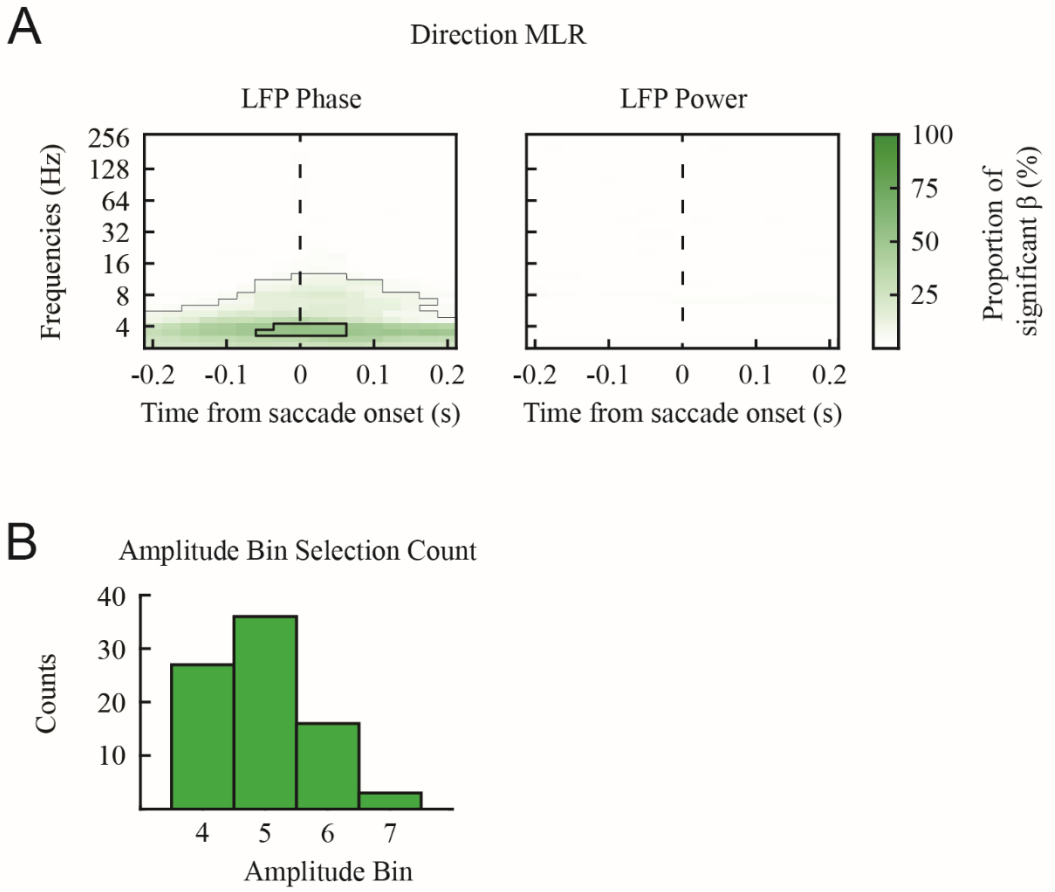

Figure S3-3. Amplitude corrected direction MLR. (A) Single amplitude bin MLR regression analysis parameter significance probability for LFP phase (left) and power (right), where the black lines represent > 5% (thin) and > 50% (thick) probabilities. (B) Distribution of amplitude bins used for all electrodes.

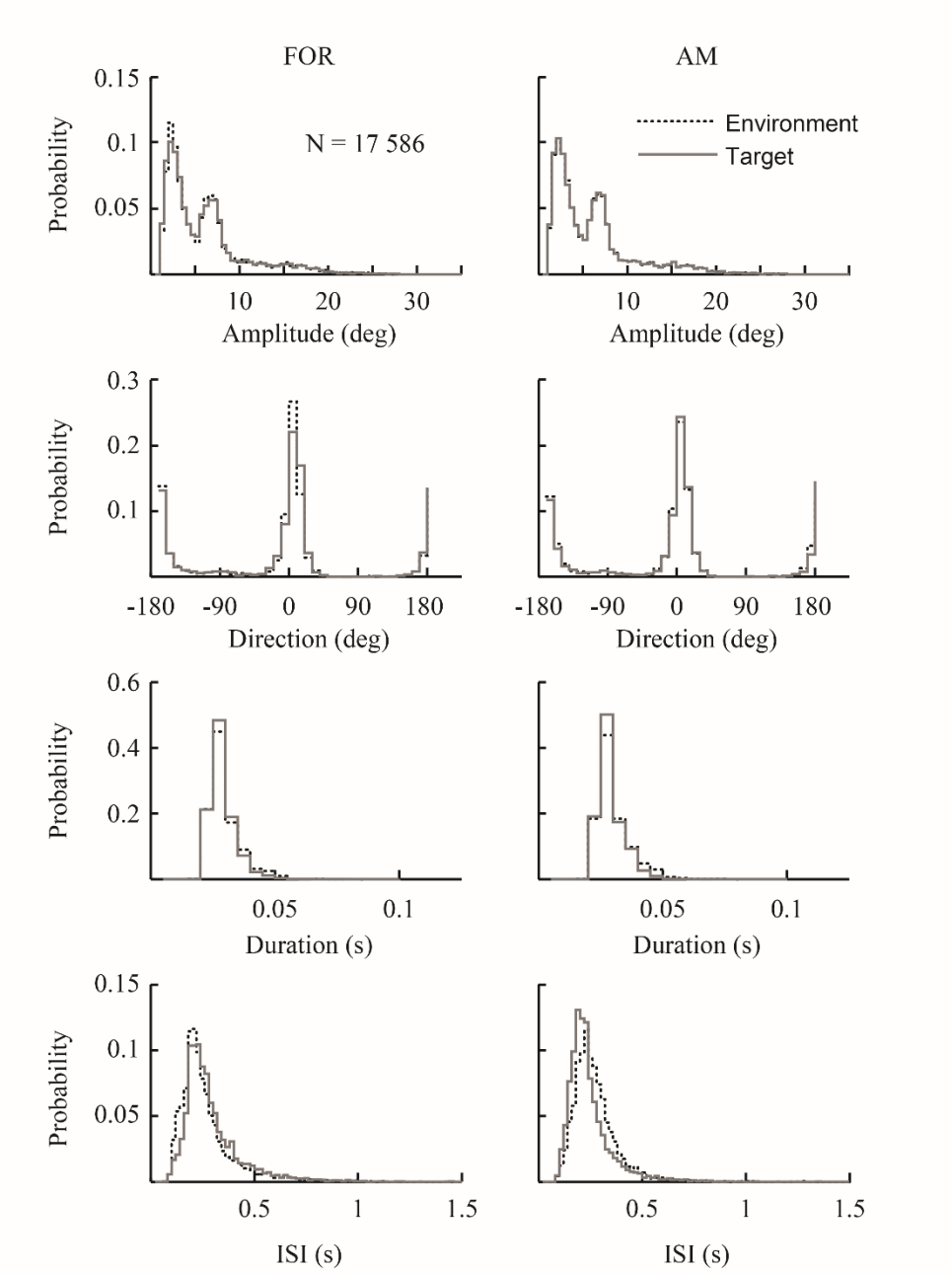

Figure S3-4. Saccade parameters distributions across matched saccades. Distributions of amplitudes (0.5 degrees bins), directions (10 degrees bins), durations (5 ms bins) and inter-saccade intervals (ISI; 20 ms bins) for respectively the FOR and AM tasks. Dashed lines present the distributions for saccades to the background or virtual environment and solid lines saccades to the target (N = 17 586 for all conditions).

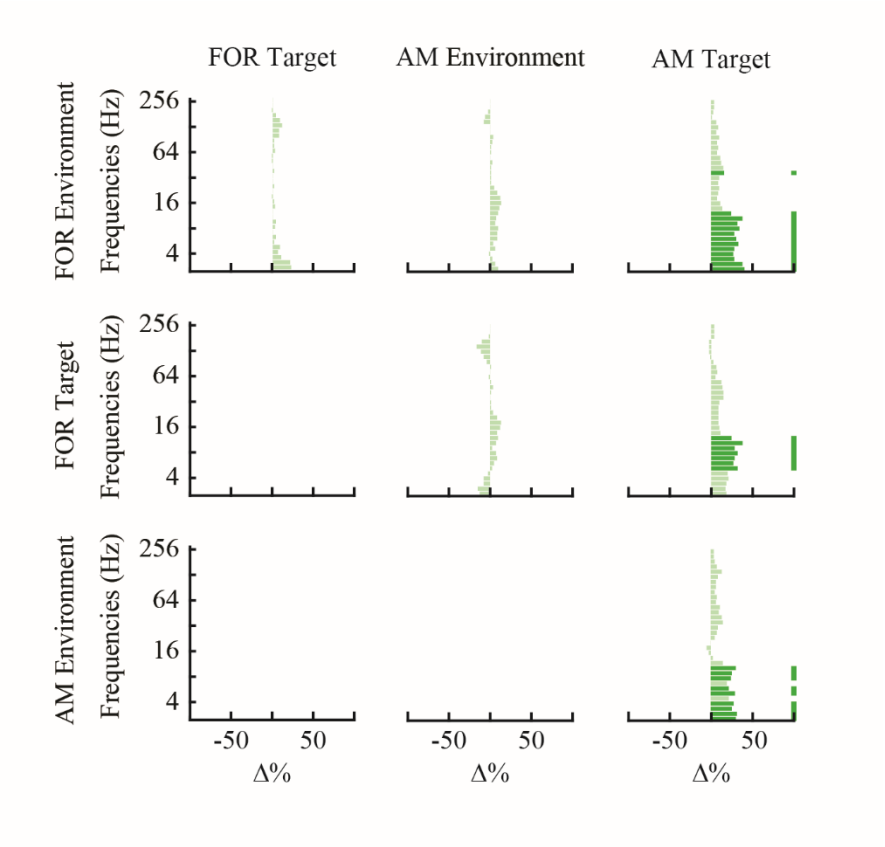

Figure S3-5. Significance probability differences for matched saccades. Difference of peak significance probability for saccade triggered power, within the first 200 ms post-saccade, between matched conditions (column – row). Dark green indicates statistical significance from a chi-square test for equality of proportions ($p < 0.05$ Bonferroni corrected).

Chapter 4

4. General Discussion

4.1 Classical experiments, virtual reality and hippocampal research

In everyday life, our senses are constantly bombarded by stimuli, to which we must allocate our limited processing resources in order to produce goal-directed behavior (Marois and Ivanoff, 2005). Attentional mechanisms are of paramount importance to this process by enhancing behaviorally relevant stimulus representations, while filtering out irrelevant representations (Desimone and Duncan, 1995). These mechanisms can be driven either externally (i.e. stimulus salience or bottom-up) or internally (i.e. self-generated or top-down). Accordingly, during the free-viewing of images or movies often used in sensory (Ito, Maldonado and Grün, 2013; Calen Walshe and Nuthmann, 2014), memory (Jutras, Fries and Buffalo, 2013) or attentional studies (Ramos Gameiro et al., 2017), the absence of a precise goal means that attentional mechanisms are mostly driven by salient sensory signals (Ingram and Wolpert, 2011). Laboratory-based tasks using simplified stimuli over uniform backgrounds, providing limited salient features, are thus viewed as insufficiently engaging (Dolins, Schweller and Milne, 2017) and are associated with a more negative subjective experience (Güçlütürk et al., 2018). These qualitative changes are accompanied by quantitative behavioral changes. For example, eye movement behaviors have been found to be affected by the quality of the visual stimulation, where minimalist stimuli were associated with a decrease in saccade amplitudes and rates (Andrews and Coppola, 1999). On the other hand, goal-directed behavior relies on top-down attention, which enhances feature (e.g. position, color) processing of stimuli matching the current goal (Desimone and Duncan, 1995). Under the current model, both attentional mechanisms rely on expectation signals computed from the current context, goals and previous experiences (i.e. memory), mostly absent in artificial tasks (Peelen and Kastner, 2014; Frank and Sabatinelli, 2017). For example, total visual search time is greatly increased by adding distracting items within an artificial search array, whereas adding realistically placed distracting items within a context (e.g. a lamp on a table and not floating in mid-air) minimally influences search time (Wolfe et al., 2011).

The HPC is believed to be involved in retrieving past information and comparing it with currently attended stimuli to form and update associative memories (Vinogradova, 2001; Ferbinteanu and Shapiro, 2003; Eichenbaum, 2004; Lisman and Grace, 2005). It is therefore unsurprising that strong interactions exist between the HPC and areas involved in attention and goal-directed behavior, such as the prefrontal cortex (PFC; Gruber et al., 2017). It has indeed been

suggested that the PFC provides the goal-directed action plan, and the HPC either provides context dependent and memory derived attentional templates (i.e. feature expectations; Peelen and Kastner, 2014) or is involved in comparing expected outcomes with received feedback (Lisman, 1999; Brincat and Miller, 2015; Numan, 2015). Additionally, attention signals from the PFC are believed to modulate HPC activity, where attended representations are better encoded within the HPC (Aly and Turk-Browne, 2016) and where place cell firing is more organized during goal-directed behavior (Mizumori and Tryon, 2015). In visual species, such as human and non-human primates, overt attentional shifts occur in the form of saccades to the attended object, a behavior dependent on the integrity of the medial temporal lobe (Buffalo, 2015; Ekstrom, 2015; Meister and Buffalo, 2016; Ramos Gameiro et al., 2017). Consequently, saccades have been shown to modulate spiking and field potential activity in both regions (Sobotka et al., 1997; Hoffman et al., 2013; Jutras et al., 2013; Tremblay et al., 2015; Tremblay et al. (1), 2015). Interestingly, as presented in Chapter 3, saccades not only modulated hippocampal LFPs, but saccades during our highly challenging and HPC dependent task (i.e. AM task) generated a more reliable PC than amplitude matched saccades during a simple navigation task (i.e. FOR task). Although the exact cause and provenance of this modulation remain unknown, it is highly plausible that the greater attentive demands of the AM task act on hippocampal LFPs to enhance neuronal organization, as is the case with place cells (Mizumori and Tryon, 2015), and increase the reliability of the phase signal.

It is obvious that further research is necessary to understand the mechanisms at play, but this won't be without difficulty. In the words of Mizumori and Tyron (2015):

> *When one considers that additional brains areas are also likely involved in our continuously dynamic real-world decisions, learning, and memory, the clear challenge for future research is to understand how such a complex network of parallel yet interconnected interactions across brain structures results in continuous and intentional goal-directed behaviors (i.e., those that change with time, space, experience, and current context).*

It is my opinion that VR will play an essential role in such research as it can replicate "real-world decisions, learning and memory", with complete experimental control over individual task variables such as "time, space, experience and context". Moreover, recent technological

advancements in eye tracking technology has allowed the integration of gaze trackers directly inside head mounted displays (e.g. tobii tracker inside the HTC Vive) and the real-time use of gaze data within the VR environment. Combining this data with body tracking enables the exact replay of every recorded experience where neuronal correlates of behavior can be obtained. Although this setup is human specific, as no head mounted displays currently fit macaques, the system described in this thesis can serve as a good approximation, assuming a few modifications.

To this end, since the time of publication of Chapter 2, a few upgrades have been made to the system. Firstly, as the Python architecture operates real-time TCP connections (Table 2-1), a TCP "tunnel" was built in Python to link the Matlab scripting language with the Unreal Engine, achieving millisecond precision on collected VR data. Secondly, the Unreal Engine and TCP tunnel were interfaced with a second recording suite, namely Monkeylogic (Asaad et al., 2012), to test the system on humans and marmosets. Lastly, I believe that combining this system with multisite recordings between PFC and HPC could reveal the flow of information during self-directed (i.e. not an explicit requirement of the task) behavior and attention. For example, a foraging task where the subject must search for cued colored objects from a limited set (e.g. red, green, blue, yellow). The color combination of the current trial (e.g. red and yellow) indicates the location of the goal in the environment (e.g. location #3 of the six possible color combinations). This task would highlight the retrieval and maintenance of attentional templates (i.e. colors and box locations), shifts in attention during search, associative learning and trial feedback. Additionally, variants of this task could be undertaken to isolate various processes, such as having the first cue constant within each trial block, to study attentional templates formation and maintenance, or having context dependent associations, to study hippocampal dependent learning.

4.2 Hippocampal local field potentials

As previously stated, LFPs provide information about the local computations and input to a brain region, where different bands highlight different processes or functions (Buzsáki, Anastassiou and Koch, 2012; Siegel, Donner and Engel, 2012). However, the common belief that the frequency of the recorded oscillations is informative about the origin, nature (i.e. inhibitory or excitatory) and local spread of the field potentials has been recently challenged (Kajikawa and

Schroeder, 2011; Herreras, 2016). Moreover, misuse of filtering and analytic methods, often taken for granted, can have a dramatic impact on the end results. In the following subsections I will first comment on the potential pitfalls of improper band separation and their influence on phase coherence analyses. Secondly, I will extend the discussion of the results from Chapter 3, regarding possible myogenic artefactual contamination, hippocampal memory function and phase clustering, as well as gamma band activity within our mid-posterior, putatively CA3, recording locations.

4.2.1 Filtering, band separation and analytic signal

The theta rhythm is the most studied rhythm of the HPC (Colgin, 2016) and is associated with a broad range of behaviors (Buzsáki, 2005). However, its definition across the literature is highly inconsistent. Indeed, when selecting frequencies of interest within the theta band, studies either provide no justification (Aru et al., 2014), are based on subjective assessments (e.g. visual inspection or intuition; Magri et al., 2012; Einevoll et al., 2013) or select the frequency band maximizing the desired effect (Gruber et al., 2017). For example, LFP signals have been band-pass filtered between the following frequencies: 3-12 Hz (Jutras, Fries and Buffalo, 2013), 4-12 Hz (Jones and Wilson, 2005; Aghajan et al., 2014; Hardcastle et al., 2017), 6-10 Hz (Wang et al., 2014) and 6-12 Hz (Gupta et al., 2012), and labelled theta. Although the edges of the band-pass filtered signals are highly similar across studies, using wide frequency bands have multiple potential pitfalls. Firstly, one cycle of the higher frequencies can contain up to 3 or 4 full cycles of the lower frequency oscillations, yielding highly unreliable phase information (Dvorak and Fenton, 2014). Secondly, there are no distinctions between hippocampal theta types 1 and 2, which are involved in different processes and dependent on different inputs (Vandecasteele et al., 2014; Gangadharan et al., 2016). Lastly, and regardless of the frequencies involved, basic filtering artefacts, such as edge effects and filter induced phase shifts, are sometimes not properly acknowledged and corrected (Dvorak and Fenton, 2014; Scheffer-Teixeira and Tort, 2016).

Filtered LFP traces are typically transformed into an analytic signal to obtain power and phase values for further analysis. While the exact method used (i.e. Hilbert, Fourier or wavelets) has no influence on the end results (Bruns, 2004), these transformations are dependent on the time-frequency resolution trade-off and are subject to the same pitfalls of improper band selection.

Firstly, mathematical theories state that power and phase are fully dissociable, however, power variations can have a strong influence on the measured signal to noise ratio of phase values (Cohen, 2014). As shown in Figure S3-2, this leads to artificially increased phase coherence measures, and despite a strong bias towards power values analyses in the literature (Magri et al., 2012; Einevoll et al., 2013), this effect is frequently overlooked (Aru et al., 2014). Consequently, a high power sub-band (e.g. 8-12 Hz), within a wide-band filtered signal (e.g. 3-12 Hz), could potentially mask a reliable phase effect of a different sub-band (e.g. 4-8 Hz) presenting significantly lower power. Lastly, some phase coherence metrics are also sensitive to the duration of the epoch of interest. Indeed, as longer durations are required to "average out" recording noise (Canolty and Knight, 2010; Tort et al., 2010), they often extend beyond the timescale at which non-linearities induced by cognitive states or stimuli occur (Aru et al., 2014; Dvorak and Fenton, 2014), preventing their correlation with undertaken behaviors.

Considering the aforementioned findings, the signal processing techniques implemented in this thesis were carefully selected to avoid most confounders and pitfalls of LFP analyses. Firstly, I used complex wavelet convolution with logarithmically spaced center frequencies, creating narrow frequency bands in the low frequencies (Cohen, 2014). This allowed for proper investigation of all frequencies, maximizing temporal resolution, without a priori assumptions about the multiple theta bands (i.e. no selection or confirmation biases). The analytic signal was further computed over entire recording sessions to avoid edge effects and to obtain the most reliable approximation of instantaneous phase and power, especially important when analyzing short durations of low frequency data. I believe that these considerations were crucial to the findings presented in Chapter 3, as I found three different behavioral correlates within the 3-12 Hz hippocampal theta band, which could have been overlooked had I used the band-pass signal. This could further explain the discrepancies found between these results and a different study with regards to the presence of PC following visually guided saccades (Jutras, Fries and Buffalo, 2013).

4.2.2 Myogenic contamination of LFP signals

The fact that the results presented in Chapter 3 are novel, and to some extent, unexpected from the literature, I think that the possibility of myogenic artefacts should be further addressed.

Indeed, the results presented in Chapter 3 display apparent similarities with previously identified myogenic contamination signals, such as saccade amplitude and direction correlation with the recorded LFPs (Keren, Yuval-Greenberg and Deouell, 2010; Kovach et al., 2011). Across both the visual cortex and medial temporal lobe literature, the myogenic effect of saccades seems to be located solely within the gamma band, and occurs mostly during the eye movements (Jerbi et al., 2009; Keren, Yuval-Greenberg and Deouell, 2010; Kovach et al., 2011; Worrell et al., 2012). Conversely, our main effects occur mostly within the lower frequencies and last well outside of saccade durations. Moreover, the previous correlations between myogenic artefacts and saccade direction were found in peak-to-trough amplitude variations (Kovach et al., 2011), whereas our data show phase differences, without concomitant power and amplitude changes. It could however be argued that the results presented in Figure 3-8 are artefactual in nature, as most points within the ± 200 ms window are significant. Although absolute artefact rejection is not possible, I hypothesize that this effect is due to the reduced temporal resolution of our low frequency wavelets, lasting at least 200 ms. Of note, single neurons responding to various saccade directions have been found within the HPC using the same electrodes used here (Guilli et al., In preparation), as well as the EC (Killian, Potter and Buffalo, 2015). While this does not disprove the possibility of an artefact, it argues in favor of a saccade direction signal within the HPC. More experiments are obviously needed to further strengthen this point.

A second possible hypothesis is that an artefactual signal could originate from the reference electrode, in our case, the guide tube used to penetrate the dura. To address this, I compared simultaneously recorded electrodes and their significance patterns. For example, of the 82 electrodes used in the amplitude MLR analyses (Figures 3-7) that were recorded during 41 session, 12 failed to create significant correlation coefficients within the classical theta range (4 - 8 Hz) in the 100 – 200 ms post-saccade onset. Interestingly, 9 out of these 12 electrodes shared a common reference with at least one other electrode associated with a significant correlation coefficient. To validate that these electrodes yielded a reliable signal, I found that 11 out of the 12 electrodes non-significant for the classical theta band generated significant correlation coefficients within the gamma band.

Lastly, considering that virtually every electrode presented significant amplitude correlations in the gamma range, that this effect was short lived and centered on eye movements,

it is highly plausible that the gamma effect is purely artefactual, as would be expected from the literature (Jerbi et al., 2009; Kovach et al., 2011). However, I will discuss in the following section how the presented results are also in accordance with the hippocampal literature. More experiments using bipolar referencing, varying references or monitoring the electrooculogram would undoubtedly be beneficial to make further claims on these results.

4.2.3 Gamma band LFPs in CA3

As previously stated, gamma band activity within hippocampal CA1 is subdivided into: slow, or CA3 mediated prospective memory signals, and fast, or EC mediated retrospective (e.g. current or recently visited locations) coding (Bieri, Bobbitt and Colgin, 2014; Colgin, 2016). Their combined strengths and phase differences are believed to drive CA1 spiking, where, for example, place cells are driven by the EC dependent fast gamma rhythm upon place field entry, triggering pattern completion in CA3, and retrieving upcoming locations upon place field exit (Lisman and Buzsáki, 2008; Schomburg et al., 2014; Fernández-Ruiz et al., 2017). Similarly, slow gamma has been shown to become progressively stronger following fixation onset in a delayed spatial alternation task, until the offset of the fixation, where it is replaced by fast gamma (Takahashi et al., 2014). Interestingly, the scale of the spatiotemporal representations encoded in CA1, or retrieved from CA3, has been found to follow a gradient along the hippocampal longitudinal axis, beginning with fast and high-resolution object-place-context conjunctions encoding in the dorsal (rodents) or posterior (primates) section, to broad multi-event and cross-context inferences in the ventral (rodents) or anterior (primates) section (Moser and Moser, 1998; Komorowski et al., 2013; Duarte et al., 2014; Strange et al., 2014; Collin, Milivojevic and Doeller, 2015; Numan, 2015; Schiller et al., 2015). The anterior HPC has further been associated with self-referenced movements, novelty and goal/reward related signals, consistent with its strong connectivity with the PFC (Poppenk et al., 2013; Strange et al., 2014; Brincat and Miller, 2015).

Considering the role of the fast gamma oscillation across the longitudinal axis of primate CA3, our data recorded from mid-posterior CA3 fulfill multiple predictions about the hypothesized anterior to posterior functional gradient. Firstly, target onsets elicited a significant power increase in the gamma range across all tasks (Figure 3-2 D), consistent with novelty and goal information

in anterior HPC, as well as robust item in place information in the posterior HPC. Secondly, saccade onsets were found to increase fast gamma power (Figures 3-4 to 3-6), where power directly correlated with saccade amplitude (Figure 3-7). The correlations between amplitude and power is in accordance with the hypothesized role of corollary discharges from the PFC in self-referenced memories (Numan, 2015), as well as a strong functional connectivity between the anterior HPC and PFC (Brincat and Miller, 2015). Consistently, the relationship between fast gamma and saccades was found to be task independent (Figures 3-9 and S3-5) and occurred directly at saccade onset, suggesting a purely motor signal (i.e. corollary discharge). On the other hand, primates rely heavily on vision to explore both individual objects and the spatial layout of their environment. This behavior fits with the proposed robust and high-resolution encoding of item-place-context of the posterior HPC, where saccade triggered changes in LFP phase and power could provide the spatial information, on which single neuron representations could be overlaid.

4.2.4 Memory and phase clustering

Although I did not test for possible memory effects of theta power and saccade triggered LFP modulations, important parallels can be drawn between the results presented here and the literature. As previously stated, hippocampal theta has been associated with the encoding of velocity and space, as well as with the quality of memory formation (Hasselmo and Stern, 2014). Moreover, the reliability of saccade triggered phase clustering (Jutras, Fries and Buffalo, 2013), pre-stimulus power (Colgin, 2013) and gamma band coupling (Tort et al., 2009) were all found to be correlated with future memory strength. Interestingly, the reliability of the theta frequency correlation with locomotor speed has also been correlated with memory strength (Richard et al., 2013), suggesting that both the sensorimotor and memory functions of the HPC might operate in a more holistic fashion than previously thought. Unfortunately, precise monitoring of sampling behaviors, such as saccade amplitudes, directions and rates, is seldomly undertaken in electrophysiological investigations of memory function, despite well established links between the two. For example, fixation patterns have been correlated with memory performance, where fixation rates predict recognition memory strength (Molitor et al., 2014) and where fixation spread can distinguish between familiarity and recollection judgements upon retrieval (Kafkas and Montaldi, 2011). Eye movement patterns are also modulated outside of awareness during

subsequent presentations of repeated or modified stimuli (Hannula et al., 2010) and can facilitate recall by making saccades to the location of previously presented stimuli, a process called re-enactment (Meister and Buffalo, 2016).

By taking these results into consideration, it is fairly obvious that a strong relationship exists between sampling behaviors, memory strength and hippocampal LFPs. However, considering the uncertainties remaining about the influence of eye movements on LFPs, I felt that proper identification of their requirements and possible functions was warranted, prior to investigating memory function. The results presented here are, in my opinion, paving the way for future and more interesting studies. For example, now knowing the relationship between saccade amplitudes and theta power, between saccade amplitude (i.e. fixation spread) and memory performance, and between theta power and memory performance, it would be interesting to explore how much of the power-memory relationship can be explained by saccade behavior. Moreover, in this dataset, amplitude and direction matched saccades during the more challenging AM task elicited stronger PC than during the simple FOR task (Figure 3-9). Investigation of the role of arousal, engagement or attention, using pupillometry could reveal a significant role of PFC in controlling delta or alpha-beta phase clustering, and therefore memory function. Lastly, further studies investigating spike-field coherence would shine light on which frequency band of saccades triggered LFPs modulates different neuronal populations. For example, place cells could be modulated according to the "reset" of the classical theta band (4 – 8 Hz) or by the phase differences of the delta band (≤ 4 Hz) during prospective vs. retrospective encoding.

In both cases I think that proper nomenclature regarding saccade triggered LFPs is paramount to extend our knowledge. Indeed, as LFP phase can be correlated with behavior, and not necessarily "reset" to a single default or "optimal" state, I propose that the term "phase reset" might not be an appropriate descriptor, hence the use of phase clustering or phase modulation in this thesis. However, the "optimal state" hypothesis can still be valid regardless, where saccades would trigger phase modulations according to the current goals, possibly controlling encoding-retrieval or acting as a gating mechanism to allow relevant information to be further processed.

4.3 General conclusions and future directions

In summary, saccadic activity allows primates to acquire a wealth of information, from broad spatio-contextual to individual object identity, whose association forms the basis of declarative memory. Consistently, by recording HPC activity around saccades, we found behavioral correlates of sensory, motor and exploratory behaviors. Firstly, a copy of the saccadic command could reach the HPC via saccade related neurons in the EC, highlighted by the increase in mid-gamma power at onset. Secondly, saccade parameters are separated into: amplitude, or distance, in the classical theta band (4 - 8 Hz) and direction, or prospective-retrospective coding, in the delta band (≤ 4 Hz). Lastly, sensory related information follows the onset of fixation (i.e. saccade offset) in the alpha-beta band, to be further processed or associated with the new gaze position. While I hypothesize that these oscillations reflect the various coordinated inputs and local computations undertaken to form associative memories, uncertainty remains about their exact origin (i.e. local vs input) and how they affect neuronal firing. Multi-site recordings across the EC, MS and HPC would provide extremely valuable field potential and spike coherence information to answer these questions.

Chapter 5

5. References

Acharya, L. et al. (2016) ‘Causal Influence of Visual Cues on Hippocampal Directional Selectivity’, *Cell*, 164(1–2), pp. 197–207. doi: 10.1016/j.cell.2015.12.015.

Adobbati, R. et al. (2001) ‘Gamebots : A 3D Virtual World Test-Bed For Multi-Agent Research’, *Proceedings of the second international workshop on Infrastructure for Agents MAS and Scalable MAS*, 45, pp. 1–6.

Adrian, E. D. (1926a) ‘The impulses produced by sensory nerve-endings: Part 4. Impulses from Pain Receptors.’, *The Journal of physiology*, 62(1), pp. 33–51.

Adrian, E. D. (1926b) ‘The impulses produced by sensory nerve endings: Part I.’, *The Journal of physiology*, 61(1), pp. 49–72.

Adrian, E. D. and Zotterman, Y. (1926a) ‘The impulses produced by sensory nerve-endings: Part II. The response of a Single End-Organ.’, *The Journal of physiology*, 61(2), pp. 151–71.

Adrian, E. D. and Zotterman, Y. (1926b) ‘The impulses produced by sensory nerve endings: Part 3. Impulses set up by Touch and Pressure.’, *The Journal of physiology*, 61(4), pp. 465–83.

Aggleton, J. P., Kyd, R. J. and Bilkey, D. K. (2004) ‘When is the perirhinal cortex necessary for the performance of spatial memory tasks?’, *Neuroscience and Biobehavioral Reviews*, 28(6), pp. 611–624. doi: 10.1016/j.neubiorev.2004.08.007.

Aghajan, Z. M. et al. (2014) ‘Impaired spatial selectivity and intact phase precession in two-dimensional virtual reality’, *Nature Neuroscience*, 18(1), pp. 121–128. doi: 10.1038/nn.3884.

Allain, P. et al. (2014) ‘Detecting Everyday Action Deficits in Alzheimer’s Disease Using a Nonimmersive Virtual Reality Kitchen’, *Journal of the International Neuropsychological Society*, 20(05), pp. 468–477. doi: 10.1017/S1355617714000344.

Aly, M. and Turk-Browne, N. B. (2016) ‘Attention promotes episodic encoding by stabilizing hippocampal representations’, *Proceedings of the National Academy of Sciences*, 113(4), pp. E420–E429. doi: 10.1073/pnas.1518931113.

Amaral, D. G. and Lavenex, P. (2006) ‘Hippocampal Neuroanatomy’, in *The Hippocampus Book*. Oxford Uni. New York, pp. 37–114. doi: 10.1093/acprof:oso/9780195100273.003.0003.

Andrews, T. J. and Coppola, D. M. (1999) ‘Idiosyncratic characteristics of saccadic eye

movements when viewing different visual environments', *Vision Research*, 39(17), pp. 2947–2953. doi: 10.1016/S0042-6989(99)00019-X.

Anguera, J. A. et al. (2013) 'Video game training enhances cognitive control in older adults', *Nature*, 501(7465), pp. 97–101. doi: 10.1038/nature12486.

Aronov, D., Nevers, R. and Tank, D. W. (2017) 'Mapping of a non-spatial dimension by the hippocampal–entorhinal circuit', *Nature*, 543(7647), pp. 719–722. doi: 10.1038/nature21692.

Aronov, D. and Tank, D. W. (2014) 'Engagement of Neural Circuits Underlying 2D Spatial Navigation in a Rodent Virtual Reality System', *Neuron*, 84(2), pp. 442–456. doi: 10.1016/j.neuron.2014.08.042.

Aru, J. et al. (2014) 'Untangling cross-frequency coupling in neuroscience.', *Current opinion in neurobiology*, 31C, pp. 51–61. doi: 10.1016/j.conb.2014.08.002.

Asaad, W. F. et al. (2012) 'High-performance execution of psychophysical tasks with complex visual stimuli in MATLAB', *Journal of Neurophysiology*, (October 2012), pp. 249–260. doi: 10.1152/jn.00527.2012.

Asaad, W. F. and Eskandar, E. N. (2008) 'Achieving behavioral control with millisecond resolution in a high level programming environment', *Journal of Neuroscience Methods*, 173(2), pp. 235–240. doi: 10.1016/j.jneumeth.2008.06.003.Achieving.

Astur, R. S. et al. (2004) 'Sex differences and correlations in a virtual Morris water task, a virtual radial arm maze, and mental rotation', *Behavioural Brain Research*, 151(1–2), pp. 103–115. doi: 10.1016/j.bbr.2003.08.024.

Augustinack, J. C. et al. (2014) 'H.M.'s contributions to neuroscience: A review and autopsy studies', *Hippocampus*, 24(11), pp. 1267–1286. doi: 10.1002/hipo.22354.

Bachevalier, J. and Nemanic, S. (2008) 'Memory for spatial location and object-place associations are differently processed by the hippocampal formation, parahippocampal areas TH/TF and perirhinal cortex', *Hippocampus*, 18(1), pp. 64–80. doi: 10.1002/hipo.20369.

Bachevalier, J., Nemanic, S. and Alvarado, M. C. (2015) 'The influence of context on recognition memory in monkeys : Effects of hippocampal , parahippocampal and perirhinal lesions',

Behavioural Brain Research, 285, pp. 89–98. doi: 10.1016/j.bbr.2014.07.010.

Baniqued, P. L. et al. (2013) 'Selling points: What cognitive abilities are tapped by casual video games?', *Acta Psychologica*, 142(1), pp. 74–86. doi: 10.1016/j.actpsy.2012.11.009.

Baniqued, P. L. et al. (2014) 'Cognitive training with casual video games: Points to consider', *Frontiers in Psychology*, 4(JAN), pp. 1–19. doi: 10.3389/fpsyg.2013.01010.

Bauer, R. M. (2008) *Textbook of clinical neuropsychology: The Three Amnesias*. Edited by J. E. Morgan and J. H. Ricker. New York.

Baus, O. and Bouchard, S. (2014) 'Moving from virtual reality exposure-based therapy to augmented reality exposure-based therapy: a review.', *Frontiers in human neuroscience*, 8(March), p. 112. doi: 10.3389/fnhum.2014.00112.

Bavelier, D. and Davidson, R. J. (2013) 'Games to do you good', *Nature*, 494, pp. 8–9.

Bayley, P. J., Frascino, J. C. and Squire, L. R. (2005) 'Robust habit learning in the absence of awareness and independent of the medial temporal lobe', *Nature*, 436(7050), pp. 550–553. doi: 10.1038/nature03857.

Belchior, H. et al. (2014) 'Increase in hippocampal theta oscillations during spatial decision making', *Hippocampus*, 24(6), pp. 693–702. doi: 10.1002/hipo.22260.

Belchior, P. et al. (2013) 'Video game training to improve selective visual attention in older adults', *Computers in Human Behavior*, 29(4), pp. 1318–1324. doi: 10.1016/j.chb.2013.01.034.

Berg, R. W., Whitmer, D. and Kleinfeld, D. (2006) 'Exploratory Whisking by Rat Is Not Phase Locked to the Hippocampal Theta Rhythm', *Journal of Neuroscience*, 26(24), pp. 6518–6522. doi: 10.1523/JNEUROSCI.0190-06.2006.

Bieri, K. W., Bobbitt, K. N. and Colgin, L. L. (2014) 'Slow and Fast Gamma Rhythms Coordinate Different Spatial Coding Modes in Hippocampal Place Cells', *Neuron*, 82(3), pp. 670–681. doi: 10.1016/j.neuron.2014.03.013.

Bittner, K. C. et al. (2015) 'Conjunctive input processing drives feature selectivity in hippocampal CA1 neurons', *Nature Neuroscience*, 18(8), pp. 1133–1142. doi: 10.1038/nn.4062.

Blacker, K. J. et al. (2014) ‘Effects of action video game training on visual working memory.’, *Journal of Experimental Psychology: Human Perception and Performance*, 40(5), pp. 1992–2004. doi: 10.1037/a0037556.

Bland, B. H. and Oddie, S. D. (2001) ‘Theta band oscillation and synchrony in the hippocampal formation and associated structures: The case for its role in sensorimotor integration’, *Behavioural Brain Research*, 127(1–2), pp. 119–136. doi: 10.1016/S0166-4328(01)00358-8.

Bohbot, V. D. et al. (2017) ‘Low-frequency theta oscillations in the human hippocampus during real-world and virtual navigation’, *Nature Communications*, 8, p. 14415. doi: 10.1038/ncomms14415.

Bohil, C. J., Alicea, B. and Biocca, F. a. (2011) ‘Virtual reality in neuroscience research and therapy’, *Nature Reviews Neuroscience*, 12(December). doi: 10.1038/nrn3122.

Bokil, H. et al. (2010) ‘Chronux: A platform for analyzing neural signals’, *Journal of Neuroscience Methods*, 192(1), pp. 146–151. doi: 10.1016/j.jneumeth.2010.06.020.

Boot, W. R. et al. (2008) ‘The effects of video game playing on attention, memory, and executive control’, *Acta Psychologica*, 129(3), pp. 387–398. doi: 10.1016/j.actpsy.2008.09.005.

Boot, W. R., Blakely, D. P. and Simons, D. J. (2011) ‘Do action video games improve perception and cognition?’, *Frontiers in Psychology*, 2(SEP), pp. 1–6. doi: 10.3389/fpsyg.2011.00226.

Brainard, D. H. (1997) ‘The Psychophysics Toolbox.’, *Spatial vision*, 10(4), pp. 433–436. doi: 10.1163/156856897X00357.

Brandon, M. P. et al. (2014) ‘New and Distinct Hippocampal Place Codes Are Generated in a New Environment during Septal Inactivation’, *Neuron*, 82(4), pp. 789–796. doi: 10.1016/j.neuron.2014.04.013.

Brincat, S. L. and Miller, E. K. (2015) ‘Frequency-specific hippocampal-prefrontal interactions during associative learning’, *Nature Neuroscience*, 18(4), pp. 1–10. doi: 10.1038/nn.3954.

Brodal, A. (1947) ‘The hippocampus and the sense of smell’, *Brain*, 70(October), pp. 179–222.

Bruns, A. (2004) ‘Fourier-, Hilbert- and wavelet-based signal analysis: Are they really different approaches?’, *Journal of Neuroscience Methods*, 137(2), pp. 321–332. doi:

10.1016/j.jneumeth.2004.03.002.

Buckley, M. J. and Gaffan, D. (1998) 'Perirhinal Cortex Ablation Impairs Visual Object Identification', *Journal of Neuroscience*, 18(6), pp. 2268–2275.

Buffalo, E. A. (2015) 'Bridging the Gap Between Spatial and Mnemonic Views of the Hippocampal Formation', *Hippocampus*, 6(March), pp. 1–6. doi: 10.1002/hipo.22444.

Burgess, N., Maguire, E. A. and O'Keefe, J. (2002) 'The human hippocampus and spatial and episodic memory', *Neuron*, 35(4), pp. 625–641. doi: 10.1016/S0896-6273(02)00830-9.

Burgess, N., Recce, M. and O'Keefe, J. (1994) 'A model of hippocampal function', *Neural Networks*, 7(94), pp. 1065–1081. doi: 10.1016/S0893-6080(05)80159-5.

Burgess, P. W. et al. (2006) 'The case for the development and use of "ecologically valid" measures of executive function in experimental and clinical neuropsychology', *Journal of the International Neuropsychological Society*, 12(02), pp. 194–209. doi: 10.1017/S1355617706060310.

Burr, D. C., Morrone, M. C. and Ross, J. (1994) 'Selective suppression of the magnocellular visual pathway during saccadic eye movements.', *Nature*, 371(6497), pp. 511–3. doi: 10.1038/371511a0.

Burwell, R. D. (2006) 'The Parahippocampal Region: Corticocortical Connectivity', *Annals of the New York Academy of Sciences*, 911(1), pp. 25–42. doi: 10.1111/j.1749-6632.2000.tb06717.x.

Buschman, T. J. and Miller, E. K. (2007) 'Top-Down Versus Bottom-Up Control of Attention in the Prefrontal and Posterior Parietal Cortices', *Science*, 315(5820), pp. 1860–1862. doi: 10.1126/science.1138071.

Buzsáki, G. (2002) 'Theta oscillations in the hippocampus', *Neuron*, 33(3), pp. 325–340. doi: 10.1016/S0896-6273(02)00586-X.

Buzsáki, G. (2005) 'Theta rhythm of navigation: Link between path integration and landmark navigation, episodic and semantic memory', *Hippocampus*, 15(7), pp. 827–840. doi: 10.1002/hipo.20113.

Buzsáki, G., Anastassiou, C. a. and Koch, C. (2012) 'The origin of extracellular fields and currents — EEG, ECoG, LFP and spikes', *Nature Reviews Neuroscience*, 13(6), pp. 407–420. doi:

10.1038/nrn3241.

Buzsáki, G. and Moser, E. I. (2013) ‘Memory, navigation and theta rhythm in the hippocampal-entorhinal system’, *Nature Neuroscience*, 16(2), pp. 130–138. doi: 10.1038/nn.3304.

Calen Walshe, R. and Nuthmann, A. (2014) ‘Asymmetrical control of fixation durations in scene viewing’, *Vision Research*, 100, pp. 38–46. doi: 10.1016/j.visres.2014.03.012.

Canolty, R. T. and Knight, R. T. (2010) ‘The functional role of cross-frequency coupling’, *Trends in Cognitive Sciences*, 14(11), pp. 506–515. doi: 10.1016/j.tics.2010.09.001.

Caplan, J. B. et al. (2003) ‘Human theta oscillations related to sensorimotor integration and spatial learning.’, *The Journal of neuroscience : the official journal of the Society for Neuroscience*, 23(11), pp. 4726–4736. doi: 23/11/4726 [pii].

Cardoso-Leite, P. and Bavelier, D. (2014) ‘Video game play, attention, and learning’, *Current Opinion in Neurology*, 27(2), pp. 185–191. doi: 10.1097/WCO.0000000000000077.

Carlén, M. (2017) ‘What constitutes the prefrontal cortex?’, *Science*, 358(6362), pp. 478–482. doi: 10.1126/science.aan8868.

Carpin, S. et al. (2007) ‘USARSim: A robot simulator for research and education’, *Proceedings - IEEE International Conference on Robotics and Automation*, pp. 1400–1405. doi: 10.1109/ROBOT.2007.363180.

Cassel, J. C. et al. (1997) ‘The fimbria-fornix/cingular bundle pathways: A review of neurochemical and behavioural approaches using lesions and transplantation techniques’, *Progress in Neurobiology*, 51(6), pp. 663–716. doi: 10.1016/S0301-0082(97)00009-9.

Cassel, J. C. and de Vasconcelos, A. P. (2015) *Importance of the ventral midline thalamus in driving hippocampal functions*. 1st edn, *Progress in Brain Research*. 1st edn. doi: 10.1016/bs.pbr.2015.03.005.

Catanese, J. et al. (2012) ‘Dynamics of decision-related activity in hippocampus’, *Hippocampus*, 22(9), pp. 1901–1911. doi: 10.1002/hipo.22025.

Chabris, C. F. (2017) ‘Six Suggestions for Research on Games in Cognitive Science’, *Topics in Cognitive Science*, 9(2), pp. 497–509. doi: 10.1111/tops.12267.

Chadwick, M. J., Bonnici, H. M. and Maguire, E. a. (2012) 'Decoding information in the human hippocampus: A user's guide', *Neuropsychologia*, 50(13), pp. 3107–3121. doi: 10.1016/j.neuropsychologia.2012.07.007.

Chen, G. et al. (2013) 'How vision and movement combine in the hippocampal place code', *Proceedings of the National Academy of Sciences*, 110(1), pp. 378–383. doi: 10.1073/pnas.1215834110.

Clark, R. E. and Squire, L. R. (2013) 'Similarity in form and function of the hippocampus in rodents, monkeys, and humans', *Proceedings of the National Academy of Sciences*, 110(Supplement_2), pp. 10365–10370. doi: 10.1073/pnas.1301225110.

Clemens, Z. et al. (2013) 'Increased mesiotemporal delta activity characterizes virtual navigation in humans', *Neuroscience Research*, 76(1–2), pp. 67–75. doi: 10.1016/j.neures.2013.03.004.

Cohen, M. X. (2014) *Analizing Neural Time Series Data*. Cambridge, USA.

Colgin, L. L. (2013) 'Mechanisms and functions of theta rhythms', *Annual review of neuroscience*, 36, pp. 295–312. doi: 10.1146/annurev-neuro-062012-170330.

Colgin, L. L. (2016) 'Rhythms of the hippocampal network', *Nature Reviews Neuroscience*, 17(4), pp. 239–249. doi: 10.1038/nrn.2016.21.

Collin, S. H. P., Milivojevic, B. and Doeller, C. F. (2015) 'Memory hierarchies map onto the hippocampal long axis in humans', *Nature Neuroscience*, 18(11), pp. 1562–1564. doi: 10.1038/nn.4138.

Corkin, S. (2002) 'What's new with the amnesic patient H.M.?', *Nature Reviews Neuroscience*, 3(2), pp. 153–160. doi: 10.1038/nrn726.

Correll, R. E. and Scoville, W. B. (1965) 'Performance on delayed match following lesions of medial temporal lobe structures.', *Journal of comparative and physiological psychology*, 60(3), pp. 360–7.

Corrigan, B. W. et al. (2017) 'Characterizing eye movement behaviors and kinematics of non-human primates during virtual navigation tasks', *Journal of Vision*, 17(12), pp. 1–22. doi: 10.1167/17.12.15.

Crawford, J. D., Martinez-Trujillo, J. C. and Klier, E. M. (2003) 'Neural control of three-dimensional eye and head movements.', *Current opinion in neurobiology*, 13(6), pp. 655–62.

D'Hooge, R. and Deyn, P. P. De (2001) *Applications of the Morris water maze in the study of learning and memory*, *Brain Res Brain Res Rev*. doi: 10.1016/S0165-0173(01)00067-4.

Desimone, R. and Duncan, J. (1995) 'Neural Mechanisms of Selective Visual Attention', *Annual Review of Neuroscience*, 18(1), pp. 193–222. doi: 10.1146/annurev.ne.18.030195.001205.

Deubel, H. and Schneider, W. X. (1996) 'Saccade target selection and object recognition: Evidence for a common attentional mechanism', *Vision Research*, 36(12), pp. 1827–1837. doi: 10.1016/0042-6989(95)00294-4.

Ding, S. L. (2013) 'Comparative anatomy of the prosubiculum, subiculum, presubiculum, postsubiculum, and parasubiculum in human, monkey, and rodent', *Journal of Comparative Neurology*, 521(18), pp. 4145–4162. doi: 10.1002/cne.23416.

Doeller, C., Barry, C. and Burgess, N. (2010) 'Evidence for grid cells in a human memory network', *Nature*, 463(7281), pp. 657–661. doi: 10.1038/nature08704.Evidence.

Dolins, F. L., Schweller, K. and Milne, S. (2017) 'Technology advancing the study of animal cognition: Using virtual reality to present virtually simulated environments to investigate nonhuman primate spatial cognition', *Current Zoology*, 63(1), pp. 97–108. doi: 10.1093/cz/zow121.

Dombeck, D. A. and Reiser, M. B. (2012) 'Real neuroscience in virtual worlds', *Current Opinion in Neurobiology*, 22(1), pp. 3–10. doi: 10.1016/j.conb.2011.10.015.

Doucet, G., Gulli, R. A. and Martinez-Trujillo, J. C. (2016) 'Cross-species 3D virtual reality toolbox for visual and cognitive experiments', *Journal of Neuroscience Methods*, 266, pp. 84–93. doi: 10.1016/j.jneumeth.2016.03.009.

Douglas, R. J. (1967) 'The hippocampus and behavior.', *Psychological bulletin*, 67(6), pp. 416–422. doi: 10.1037/h0024599.

Dragoi, G. (2013) 'Internal operations in the hippocampus: single cell and ensemble temporal coding', *Frontiers in Systems Neuroscience*, 7(August 2013). doi: 10.3389/fnsys.2013.00046.

Dragoi, G. and Buzsáki, G. (2006) 'Temporal Encoding of Place Sequences by Hippocampal Cell Assemblies', *Neuron*, 50(1), pp. 145–157. doi: 10.1016/j.neuron.2006.02.023.

Duarte, I. C. et al. (2014) 'Anterior/posterior competitive deactivation/activation dichotomy in the human hippocampus as revealed by a 3D navigation task', *PLoS ONE*, 9(1). doi: 10.1371/journal.pone.0086213.

Dvorak, D. and Fenton, A. a. (2014) 'Toward a proper estimation of phase-amplitude coupling in neural oscillations', *Journal of Neuroscience Methods*, 225, pp. 42–56. doi: 10.1016/j.jneumeth.2014.01.002.

Eichenbaum, H. et al. (1999) 'The Hippocampus, Memory, Review and Place Cells: Is It Spatial Memory or a Memory Space?', *Neuron*, 23, pp. 209–226. doi: 10.1016/S0896-6273(00)80773-4.

Eichenbaum, H. (2004) 'Hippocampus: Cognitive processes and neural representations that underlie declarative memory', *Neuron*, 44(1), pp. 109–120. doi: 10.1016/j.neuron.2004.08.028.

Eichenbaum, H. (2014) 'Time cells in the hippocampus: a new dimension for mapping memories.', *Nature reviews. Neuroscience*, 15(11), pp. 732–44. doi: 10.1038/nrn3827.

Eichenbaum, H. (2017) 'The role of the hippocampus in navigation is memory', *Journal of Neurophysiology*, 117(4), pp. 1785–1796. doi: 10.1152/jn.00005.2017.

Eichenbaum, H. and Cohen, N. J. (2014) 'Can We Reconcile the Declarative Memory and Spatial Navigation Views on Hippocampal Function?', *Neuron*, 83(4), pp. 764–770. doi: 10.1016/j.neuron.2014.07.032.

Eichenbaum, H., Yonelinas, A. P. and Ranganath, C. (2007) 'The Medial Temporal Lobe and Recognition Memory', *Annual review of neuroscience*, 30, pp. 123–152. doi: 10.1146/annurev.neuro.30.051606.094328.

Einevoll, G. T. et al. (2013) 'Modelling and analysis of local field potentials for studying the function of cortical circuits.', *Nature reviews. Neuroscience*, 14(11), pp. 770–85. doi: 10.1038/nrn3599.

Ekstrom, a D. et al. (2003) 'Cellular networks underlying human spatial navigation', *Nature*, 425(6954), pp. 184–188. doi: 10.1038/nature01955.1.

Ekstrom, A. et al. (2007) ‘Contrasting roles of neural firing rate and local field potentials in human memory’, *Hippocampus*, 17(8), pp. 606–617. doi: Doi 10.1002/Hipo.20300.

Ekstrom, A. D. et al. (2005) ‘Human hippocampal theta activity during virtual navigation.’, *Hippocampus*, 15(7), pp. 881–9. doi: 10.1002/hipo.20109.

Ekstrom, A. D. (2015) ‘Why vision is important to how we navigate’, *Hippocampus*, 25(6), pp. 731–735. doi: 10.1002/hipo.22449.

Ekstrom, A. D. and Ranganath, C. (2017) ‘Space, time, and episodic memory: The hippocampus is all over the cognitive map’, *Hippocampus*, pp. 1–16. doi: 10.1002/hipo.22750.

Ekstrom, A. D. and Watrous, A. J. (2014) ‘Multifaceted roles for low-frequency oscillations in bottom-up and top-down processing during navigation and memory’, *NeuroImage*, 85(0 2), pp. 667–677. doi: 10.1016/j.neuroimage.2013.06.049.

Feigenbaum, J. D. and Rolls, E. T. (1991) ‘Allocentric and egocentric spatial information processing in the hippocampal formation of the behaving primate’, *Psychobiology*, 19(1), pp. 21–40. doi: 10.1007/BF03337953.

Fenton, A. A. et al. (2010) ‘Attention-Like Modulation of Hippocampus Place Cell Discharge’, *Journal of Neuroscience*, 30(13), pp. 4613–4625. doi: 10.1523/JNEUROSCI.5576-09.2010.

Ferbinteanu, J. and Shapiro, M. L. (2003) ‘Prospective and retrospective memory coding in the hippocampus’, *Neuron*, 40(6), pp. 1227–1239. doi: 10.1016/S0896-6273(03)00752-9.

Fernández-Ruiz, A. et al. (2017) ‘Entorhinal-CA3 Dual-Input Control of Spike Timing in the Hippocampus by Theta-Gamma Coupling’, *Neuron*, 93(5), p. 1213–1226.e5. doi: 10.1016/j.neuron.2017.02.017.

Frank, D. W. and Sabatinelli, D. (2017) ‘Primate visual perception: Motivated attention in naturalistic scenes’, *Frontiers in Psychology*, 8(FEB), pp. 1–7. doi: 10.3389/fpsyg.2017.00226.

Furuya, Y. et al. (2014) ‘Place-related neuronal activity in the monkey parahippocampal gyrus and hippocampal formation during virtual navigation’, *Hippocampus*, 24(1), pp. 113–130. doi: 10.1002/hipo.22209.

Fyhn, M. et al. (2004) ‘Spatial representation in the entorhinal cortex.’, *Science (New York, N.Y.)*,

305(5688), pp. 1258–64. doi: 10.1126/science.1099901.

Gaffan, D. (1974) 'Recognition impaired and association intact in the memory of monkeys after transection of the fornix.', *Journal of comparative and physiological psychology*, 86(6), pp. 1100–9.

Gangadharan, G. et al. (2016) 'Medial septal GABAergic projection neurons promote object exploration behavior and type 2 theta rhythm', *Proceedings of the National Academy of Sciences*, 113(23), pp. 6550–6555. doi: 10.1073/pnas.1605019113.

Ganier, F., Hoareau, C. and Tisseau, J. (2014) 'Evaluation of procedural learning transfer from a virtual environment to a real situation: a case study on tank maintenance training.', *Ergonomics*, 57(6), pp. 828–43. doi: 10.1080/00140139.2014.899628.

Garaizar, P. et al. (2014) 'Measuring software timing errors in the presentation of visual stimuli in cognitive neuroscience experiments.', *PloS one*, 9(1), p. e85108. doi: 10.1371/journal.pone.0085108.

Georges-François, P., Rolls, E. T. and Robertson, R. G. (1999) 'Spatial view cells in the primate hippocampus: Allocentric view not head direction or eye position or place', *Cerebral Cortex*, 9(3), pp. 197–212. doi: 10.1093/cercor/9.3.197.

Girardeau, G. et al. (2009) 'Selective suppression of hippocampal ripples impairs spatial memory.', *Nature neuroscience*, 12(10), pp. 1222–1223. doi: 10.1038/nn.2384.

Girardeau, G. and Zugaro, M. (2011) 'Hippocampal ripples and memory consolidation', *Current Opinion in Neurobiology*, 21(3), pp. 452–459. doi: 10.1016/j.conb.2011.02.005.

Givens, B. (1996) 'Stimulus-evoked resetting of the dentate theta rhythm: relation to working memory.', *Neuroreport*, 8(1), pp. 159–163. doi: 10.1097/00001756-199612200-00032.

Gluth, S. et al. (2015) 'Effective Connectivity between Hippocampus and Ventromedial Prefrontal Cortex Controls Preferential Choices from Memory', *Neuron*, 86(4), pp. 1078–1090. doi: 10.1016/j.neuron.2015.04.023.

Gonçalves, R. et al. (2012) 'Efficacy of Virtual Reality Exposure Therapy in the Treatment of PTSD: A Systematic Review', *PLoS ONE*, 7(12), pp. 1–7. doi: 10.1371/journal.pone.0048469.

Goris, J., Jalink, M. B. and ten Cate Hoedemaker, H. O. (2014) 'Training basic laparoscopic skills using a custom-made video game', *Perspectives on Medical Education*, 3(4), pp. 314–318. doi: 10.1007/s40037-013-0106-8.

Gray, W. D. (2017) 'Game-XP: Action Games as Experimental Paradigms for Cognitive Science', *Topics in Cognitive Science*, 9(2), pp. 289–307. doi: 10.1111/tops.12260.

Green, C. S. and Bavelier, D. (2003) 'Action video game modifies visual selective attention', *Nature*, 423(6939), pp. 534–537. doi: 10.1038/nature01647.

Green, C. S., Strobach, T. and Schubert, T. (2013) 'On methodological standards in training and transfer experiments', *Psychological Research*, 78(6), pp. 756–772. doi: 10.1007/s00426-013-0535-3.

Grion, N. et al. (2016) 'Coherence between Rat Sensorimotor System and Hippocampus Is Enhanced during Tactile Discrimination', *PLoS Biology*, 14(2), pp. 1–26. doi: 10.1371/journal.pbio.1002384.

Gruber, M. J. et al. (2017) 'Theta phase synchronization between the human hippocampus and the prefrontal cortex supports learning of unexpected information', *bioRxiv*, pp. 1–17. doi: 10.1101/144634.

Güçlütürk, Y. et al. (2018) 'Representations of naturalistic stimulus complexity in early and associative visual and auditory cortices', *Scientific Reports*, 8(1), p. 3439. doi: 10.1038/s41598-018-21636-y.

Guo, Z. V. et al. (2014) 'Procedures for behavioral experiments in head-fixed mice', *PLoS ONE*, 9(2). doi: 10.1371/journal.pone.0088678.

Gupta, A. S. et al. (2012) 'Segmentation of spatial experience by hippocampal θ sequences.', *Nature neuroscience*, 15(7), pp. 1032–1039. doi: 10.1038/nn.3138.

Hafting, T. et al. (2005) 'Microstructure of a spatial map in the entorhinal cortex.', *Nature*, 436(7052), pp. 801–806. doi: 10.1038/nature03721.

Hannula, D. E. et al. (2010) 'Worth a glance: using eye movements to investigate the cognitive neuroscience of memory.', *Frontiers in human neuroscience*, 4(October), p. 166. doi:

10.3389/fnhum.2010.00166.

Hardcastle, K. et al. (2017) 'A Multiplexed, Heterogeneous, and Adaptive Code for Navigation in Medial Entorhinal Cortex', *Neuron*, 94(2), p. 375–387.e7. doi: 10.1016/j.neuron.2017.03.025.

Hargreaves, E. L. et al. (2012) 'Conserved fMRI and LFP Signals during New Associative Learning in the Human and Macaque Monkey Medial Temporal Lobe', *Neuron*, 74(4), pp. 743–752. doi: 10.1016/j.neuron.2012.03.029.

Harris, K. D. et al. (2016) 'Improving data quality in neuronal population recordings', *Nature Neuroscience*, 19(9), pp. 1165–1174. doi: 10.1038/nn.4365.

Hartley, T. et al. (2014) 'Space in the brain: how the hippocampal formation supports spatial cognition', *Philosophical Transactions of the Royal Society B: Biological Sciences*, 369(1635), pp. 20120510–20120510. doi: 10.1098/rstb.2012.0510.

Harvey, C. D. et al. (2009) 'Intracellular dynamics of hippocampal place cells during virtual navigation.', *Nature*, 461(7266), pp. 941–946. doi: 10.1038/nature08499.

Hasselmo, M. E. (2005) 'What is the function of hippocampal theta rhythm? - Linking bahavioral data to phasic properties of field potential and unit recording data', *Hippocampus*, 15(7), pp. 936–949. doi: 10.1002/hipo.20116.

Hasselmo, M. E. and Stern, C. E. (2014) 'Theta rhythm and the encoding and retrieval of space and time', *NeuroImage*, 85, pp. 656–666. doi: 10.1016/j.neuroimage.2013.06.022.

Hebart, M. N., Görgen, K. and Haynes, J.-D. (2014) 'The Decoding Toolbox (TDT): a versatile software package for multivariate analyses of functional imaging data.', *Frontiers in neuroinformatics*, 8, p. 88. doi: 10.3389/fninf.2014.00088.

Helmchen, C., Straube, A. and Büttner, U. (1994) 'Saccade-related activity in the fastigial oculomotor region of the macaque monkey during spontaneous eye movements in light and darkness', *Experimental Brain Research*, 98(3), pp. 474–482. doi: 10.1007/BF00233984.

Henriksen, E. J. et al. (2010) 'Spatial representation along the proximodistal axis of CA1', *Neuron*, 68(1), pp. 127–137. doi: 10.1016/j.neuron.2010.08.042.

Herreras, O. (2016) 'Local Field Potentials: Myths and Misunderstandings', *Frontiers in Neural*

Circuits, 10(December), pp. 1–16. doi: 10.3389/fncir.2016.00101.

Herreras, O., Makarova, J. and Makarov, V. A. (2015) 'New uses of LFPs: Pathway-specific threads obtained through spatial discrimination', *Neuroscience*. IBRO, 310, pp. 486–503. doi: 10.1016/j.neuroscience.2015.09.054.

Van Hoesen, G. W. (1985) 'Neural Systems of the Non-human Primate Forebrain Implicated in Memory', *Annals of the New York Academy of Sciences*, 444(1), pp. 97–112. doi: 10.1111/j.1749-6632.1985.tb37582.x.

Hoffman, K. L. et al. (2013) 'Saccades during visual exploration align hippocampal 3-8 Hz rhythms in human and non-human primates.', *Frontiers in systems neuroscience*, 7, pp. 1–10. doi: 10.3389/fnsys.2013.00043.

Hölscher, C. et al. (2005) 'Rats are able to navigate in virtual environments.', *The Journal of experimental biology*, 208(Pt 3), pp. 561–569. doi: 10.1242/jeb.01371.

Hori, E. et al. (2005) 'Place-related neural responses in the monkey hippocampal formation in a virtual space', *Hippocampus*, 15(8), pp. 991–996. doi: 10.1002/hipo.20108.

Hsieh, L. T. et al. (2014) 'Hippocampal Activity Patterns Carry Information about Objects in Temporal Context', *Neuron*, 81(5), pp. 1165–1178. doi: 10.1016/j.neuron.2014.01.015.

Huang, Z. (2016) *Signal Processing in Neuroscience*. Edited by X. Li. Singapore. doi: 10.1007/978-981-10-1822-0.

Hubel, D. H. and Wiesel, T. N. (1959) 'Receptive fields of single neurones in the cat's striate cortex.', *The Journal of physiology*, 148, pp. 574–591. doi: 10.1113/jphysiol.2009.174151.

Huerta, P. T. and Lisman, J. E. (1995) 'Bidirectional synaptic plasticity induced by a single burst during cholinergic theta oscillation in CA1 in vitro', *Neuron*, 15(5), pp. 1053–1063. doi: 10.1016/0896-6273(95)90094-2.

Hughes, A. M. et al. (2012) 'BOSC: A better oscillation detection method, extracts both sustained and transient rhythms from rat hippocampal recordings', *Hippocampus*, 22(6), pp. 1417–1428. doi: 10.1002/hipo.20979.

Huxter, J., Burgess, N. and O'Keefe, J. (2003) 'Independent rate and temporal coding in

hippocampal pyramidal cells.', *Nature*, 425(6960), pp. 828–32. doi: 10.1038/nature02058.

Hyman, J. M. et al. (2003) 'Stimulation in hippocampal region CA1 in behaving rats yields long-term potentiation when delivered to the peak of theta and long-term depression when delivered to the trough', *Journal of Neuroscience*, 23(37), pp. 11725–11731. doi: 23/37/11725 [pii].

Hyman, J. M. et al. (2005) 'Medial prefrontal cortex cells show dynamic modulation with the hippocampal theta rhythm dependent on behavior', *Hippocampus*, 15(6), pp. 739–749. doi: 10.1002/hipo.20106.

Ingram, J. N. and Wolpert, D. M. (2011) *Naturalistic approaches to sensorimotor control*. 1st edn, *Progress in Brain Research*. 1st edn. doi: 10.1016/B978-0-444-53752-2.00016-3.

Insausti, R. et al. (2002) 'Comparative aspects of the olfactory portion of the entorhinal cortex and its projection to the hippocampus in rodents, nonhuman primates, and the human brain', *Brain Research Bulletin*, 57(3–4), pp. 557–560. doi: 10.1016/S0361-9230(01)00684-0.

Ito, H. T. et al. (2015) 'A prefrontal–thalamo–hippocampal circuit for goal-directed spatial navigation', *Nature*, 522(7554), pp. 50–55. doi: 10.1038/nature14396.

Ito, J. et al. (2011) 'Saccade-related modulations of neuronal excitability support synchrony of visually elicited spikes', *Cerebral Cortex*, 21(11), pp. 2482–2497. doi: 10.1093/cercor/bhr020.

Ito, J., Maldonado, P. and Grün, S. (2013) 'Cross-frequency interaction of the eye-movement related LFP signals in V1 of freely viewing monkeys', *Frontiers in Systems Neuroscience*, 7, pp. 1–11. doi: 10.3389/fnsys.2013.00001.

Itskov, V. et al. (2008) 'Theta-mediated dynamics of spatial information in hippocampus', *Journal of Neuroscience*, 28(23), pp. 5959–5964. doi: 10.1523/JNEUROSCI.5262-07.2008.

Jacobs, J. et al. (2007) 'Brain Oscillations Control Timing of Single-Neuron Activity in Humans', *Journal of Neuroscience*, 27(14), pp. 3839–3844. doi: 10.1523/JNEUROSCI.4636-06.2007.

Jacobs, J. et al. (2013) 'Direct recordings of grid-like neuronal activity in human spatial navigation.', *Nature neuroscience*, 16(9), pp. 1188–90. doi: 10.1038/nn.3466.

Jacobs, J. (2014) 'Hippocampal theta oscillations are slower in humans than in rodents: implications for models of spatial navigation and memory.', *Philosophical transactions of the*

Royal Society of London. Series B, Biological sciences, 369(1635), pp. 1–9. doi: 10.1098/rstb.2013.0304.

Jafarpour, A. et al. (2017) 'Human hippocampal pre-activation predicts behavior', *Scientific Reports*, 7(1), pp. 1–9. doi: 10.1038/s41598-017-06477-5.

Jangraw, D. C. et al. (2014) 'NEDE : An open-source scripting suite for developing experiments in 3D virtual environments', *Journal of Neuroscience Methods*, 235, pp. 245–251. doi: 10.1016/j.jneumeth.2014.06.033.

Jeewajee, A. et al. (2013) 'Theta phase precession of grid and place cell firing in open environments', *Philosophical Transactions of the Royal Society B: Biological Sciences*, 369(1635), pp. 20120532–20120532. doi: 10.1098/rstb.2012.0532.

Jensen, O. and Lisman, J. E. (2005) 'Hippocampal sequence-encoding driven by a cortical multi-item working memory buffer', *Trends in Neurosciences*, 28(2), pp. 67–72. doi: 10.1016/j.tins.2004.12.001.

Jerbi, K. et al. (2009) 'Saccade related gamma-band activity in intracerebral EEG: Dissociating neural from ocular muscle activity', *Brain Topography*, 22(1), pp. 18–23. doi: 10.1007/s10548-009-0078-5.

Jezek, K. et al. (2011) 'Theta-paced flickering between place-cell maps in the hippocampus', *Nature*, 478(7368), pp. 246–249. doi: 10.1038/nature10439.

Johnson, A. et al. (2012) 'The hippocampus and exploration: dynamically evolving behavior and neural representations', *Frontiers in Human Neuroscience*, 6(July), pp. 1–17. doi: 10.3389/fnhum.2012.00216.

Jones, M. W. and Wilson, M. A. (2005) 'Theta rhythms coordinate hippocampal-prefrontal interactions in a spatial memory task', *PLoS Biology*, 3(12), pp. 1–13. doi: 10.1371/journal.pbio.0030402.

Jutras, M. J. and Buffalo, E. A. (2014) 'Oscillatory correlates of memory in non-human primates.', *NeuroImage*, 85 Pt 2, pp. 694–701. doi: 10.1016/j.neuroimage.2013.07.011.

Jutras, M. J., Fries, P. and Buffalo, E. A. (2013) 'Oscillatory activity in the monkey hippocampus

during visual exploration and memory formation', *Proceedings of the National Academy of Sciences*, 110(32), pp. 13144–13149. doi: 10.1073/pnas.1302351110.

Kaas, J. H. (2013) 'The evolution of brains from early mammals to humans', *Wiley Interdisciplinary Reviews: Cognitive Science*, 4(1), pp. 33–45. doi: 10.1002/wcs.1206.

Kafkas, A. and Montaldi, D. (2011) 'Recognition memory strength is predicted by pupillary responses at encoding while fixation patterns distinguish recollection from familiarity', *Quarterly Journal of Experimental Psychology*, 64(10), pp. 1971–1989. doi: 10.1080/17470218.2011.588335.

Kajikawa, Y. and Schroeder, C. E. (2011) 'How local is the local field potential?', *Neuron*, 72(5), pp. 847–858. doi: 10.1016/j.neuron.2011.09.029.

Kayser, C., Körding, K. P. and König, P. (2004) 'Processing of complex stimuli and natural scenes in the visual cortex', *Current Opinion in Neurobiology*, 14(4), pp. 468–473. doi: 10.1016/j.conb.2004.06.002.

Keene, C. S. et al. (2016) 'Complementary Functional Organization of Neuronal Activity Patterns in the Perirhinal, Lateral Entorhinal, and Medial Entorhinal Cortices', *The Journal of Neuroscience*, 36(13), pp. 3660–3675. doi: 10.1523/JNEUROSCI.4368-15.2016.

Kelemen, E. and Fenton, A. a. (2015) 'Coordinating different representations in the hippocampus', *Neurobiology of Learning and Memory*, 129, pp. 50–59. doi: 10.1016/j.nlm.2015.12.011.

Kelly, R. C. et al. (2007) 'Comparison of recordings from microelectrode arrays and single electrodes in the visual cortex.', *The Journal of neuroscience : the official journal of the Society for Neuroscience*, 27(2), pp. 261–264. doi: 10.1523/JNEUROSCI.4906-06.2007.

Keren, A. S., Yuval-Greenberg, S. and Deouell, L. Y. (2010) 'Saccadic spike potentials in gamma-band EEG: Characterization, detection and suppression', *NeuroImage*. Elsevier Inc., 49(3), pp. 2248–2263. doi: 10.1016/j.neuroimage.2009.10.057.

Khayat, P. S. and Martinez-Trujillo, J. C. (2015) 'Effects of attention and distractor contrast on the responses of middle temporal area neurons to transient motion direction changes', *European Journal of Neuroscience*, 41(12), pp. 1603–1613. doi: 10.1111/ejn.12920.

Killian, N. J., Jutras, M. J. and Buffalo, E. A. (2012) 'A map of visual space in the primate entorhinal cortex', *Nature*, 491(7426), pp. 761–764. doi: 10.1038/nature11587.

Killian, N. J., Potter, S. M. and Buffalo, E. A. (2015) 'Saccade direction encoding in the primate entorhinal cortex during visual exploration.', *Proceedings of the National Academy of Sciences of the United States of America*, pp. 1–6. doi: 10.1073/pnas.1417059112.

Kimble, D. P. (1963) 'The effects of bilateral hippocampal lesions in rats', *Journal of Comparative and Physiological Psychology*, 56(2), pp. 273–283. doi: 10.1037/h0048903.

Kimble, D. P. (1968) 'Hippocampus and internal inhibition.', *Psychological bulletin*, 70(5), pp. 285–95.

Kitamura, T. et al. (2017) 'Engrams and circuits crucial for systems consolidation of a memory', *Science*, 356(6333), pp. 73–78. doi: 10.1126/science.aam6808.

Komorowski, R. W. et al. (2013) 'Ventral Hippocampal Neurons Are Shaped by Experience to Represent Behaviorally Relevant Contexts', *Journal of Neuroscience*, 33(18), pp. 8079–8087. doi: 10.1523/JNEUROSCI.5458-12.2013.

Komorowski, R. W., Manns, J. R. and Eichenbaum, H. (2009) 'Robust Conjunctive Item–Place Coding by Hippocampal Neurons Parallels Learning What Happens Where', *The Journal of Neuroscience*, 29(31), pp. 9918–9929. doi: 10.1523/JNEUROSCI.1378-09.2009.

Kovach, C. K. et al. (2011) 'Manifestation of ocular-muscle EMG contamination in human intracranial recordings', *NeuroImage*. Elsevier Inc., 54(1), pp. 213–233. doi: 10.1016/j.neuroimage.2010.08.002.

Krakauer, J. W. et al. (2017) 'Neuroscience Needs Behavior: Correcting a Reductionist Bias', *Neuron*, 93(3), pp. 480–490. doi: 10.1016/j.neuron.2016.12.041.

Kraus, B. et al. (2013) 'Hippocampal "Time Cells": Time versus Path Integration', *Neuron*, 78(6), pp. 1090–1101. doi: 10.1016/j.neuron.2013.04.015.

Krause, M. R. and Pack, C. C. (2014) 'Contextual modulation and stimulus selectivity in extrastriate cortex', *Vision Research*, 104, pp. 36–46. doi: 10.1016/j.visres.2014.10.006.

Langston, R. F. et al. (2010) 'Development of the Spatial Representation System in the Rat',

Science, 328(5985), pp. 1576–1580. doi: 10.1126/science.1188210.

Larsson, L., Nystrom, M. and Stridh, M. (2013) 'Detection of saccades and postsaccadic oscillations in the presence of smooth pursuit', *IEEE Transactions on Biomedical Engineering*, 60(9), pp. 2484–2493. doi: 10.1109/TBME.2013.2258918.

Latham, A. J., Patston, L. L. M. and Tippett, L. J. (2013) 'Just how expert are "expert" video-game players? Assessing the experience and expertise of video-game players across "action" video-game genres', *Frontiers in Psychology*, 4(DEC), pp. 1–3. doi: 10.3389/fpsyg.2013.00941.

Latham, A. J., Patston, L. L. M. and Tippett, L. J. (2013) 'The virtual brain: 30 years of video-game play and cognitive abilities', *Frontiers in Psychology*, 4(September), pp. 1–10. doi: 10.3389/fpsyg.2013.00629.

Lavenex, P. B. and Lavenex, P. (2009) 'Spatial memory and the monkey hippocampus: Not all space is created equal', *Hippocampus*, 19(1), pp. 8–19. doi: 10.1002/hipo.20485.

Leighty, K. a. and Fragaszy, D. M. (2003) 'Joystick acquisition in tufted capuchins (Cebus apella)', *Animal Cognition*, 6(3), pp. 141–148. doi: 10.1007/s10071-003-0176-9.

Leonard, T. K. et al. (2015) 'Sharp Wave Ripples during Visual Exploration in the Primate Hippocampus.', *The Journal of neuroscience*, 35(44), pp. 14771–82. doi: 10.1523/JNEUROSCI.0864-15.2015.

Leonard, T. K. and Hoffman, K. L. (2016) 'Sharp-Wave Ripples in Primates Are Enhanced near Remembered Visual Objects', *Current Biology*, 27(2), pp. 257–262. doi: 10.1016/j.cub.2016.11.027.

Li, F. F. et al. (2002) 'Rapid natural scene categorization in the near absence of attention', *Proceedings of the National Academy of Sciences*, 99(14), pp. 9596–9601. doi: 10.1073/pnas.092277599.

Li, R. et al. (2009) 'Enhancing the contrast sensitivity function through action video game training', *Nature Neuroscience*, 12(5), pp. 549–551. doi: 10.1038/nn.2296.

Liebe, S. et al. (2012) 'Theta coupling between V4 and prefrontal cortex predicts visual short-term memory performance', *Nature Neuroscience*, 15(3), pp. 456–462. doi: 10.1038/nn.3038.

Lisman, J. E. (1999) ‘Relating Hippocampal Circuitry to Function’, *Neuron*, 22(2), pp. 233–242. doi: 10.1016/S0896-6273(00)81085-5.

Lisman, J. E. (2005) ‘The theta/gamma discrete phase code occuring during the hippocampal phase precession may be a more general brain coding scheme’, *Hippocampus*, 15(7), pp. 913–922. doi: 10.1002/hipo.20121.

Lisman, J. E. and Buzsáki, G. (2008) ‘A neural coding scheme formed by the combined function of gamma and theta oscillations’, *Schizophrenia Bulletin*, 34(5), pp. 974–980. doi: 10.1093/schbul/sbn060.

Lisman, J. E. and Grace, A. A. (2005) ‘The hippocampal-VTA loop: Controlling the entry of information into long-term memory’, *Neuron*, 46(5), pp. 703–713. doi: 10.1016/j.neuron.2005.05.002.

Lisman, J. E. and Jensen, O. (2013) ‘The Theta-Gamma Neural Code’, *Neuron*, 77(6), pp. 1002–1016. doi: 10.1016/j.neuron.2013.03.007.

Lisman, J. E. and Redish, A. D. (2009) ‘Prediction, sequences and the hippocampus’, *Philosophical Transactions of the Royal Society B: Biological Sciences*, 364(1521), pp. 1193–1201. doi: 10.1098/rstb.2008.0316.

Loomis, J. M., Blascovich, J. J. and Beall, A. C. (1999) ‘Immersive virtual environment technology as a basic research tool in psychology.’, *Behavior research methods, instruments, & computers : a journal of the Psychonomic Society, Inc*, 31(4), pp. 557–64.

Loonis, R. F. et al. (2017) ‘A Meta-Analysis Suggests Different Neural Correlates for Implicit and Explicit Learning.’, *Neuron*, 96(2), p. 521–534.e7. doi: 10.1016/j.neuron.2017.09.032.

Lund, U. (1999) ‘Least circular distance regression for directional data’, *Journal of Applied Statistics*, 26(6), pp. 723–733. doi: 10.1080/02664769922160.

Maass, A. et al. (2015) ‘Functional subregions of the human entorhinal cortex’, *eLife*, 4(JUNE), pp. 1–20. doi: 10.7554/eLife.06426.

Macrides, F., Eichenbaum, H. B. and Forbes, W. B. (1982) ‘Temporal relationship between sniffing and the limbic theta rhythm during odor discrimination reversal learning.’, *Journal of*

Neuroscience, 2(12), pp. 1705–17.

Magri, C. et al. (2012) 'Optimal band separation of extracellular field potentials', *Journal of Neuroscience Methods*, 210(1), pp. 66–78. doi: 10.1016/j.jneumeth.2011.11.005.

Malkova, L. and Mishkin, M. (2003) 'One-Trial Memory for Object-Place Associations after Separate Lesions of Hippocampus and Posterior Parahippocampal Region in the Monkey', *Journal of Neuroscience*, 23(5), pp. 1956–1965.

Manns, J. R. et al. (2007) 'Hippocampal CA1 spiking during encoding and retrieval: Relation to theta phase', *Neurobiology of Learning and Memory*, 87(1), pp. 9–20. doi: 10.1016/j.nlm.2006.05.007.

Marois, R. and Ivanoff, J. (2005) 'Capacity limits of information processing in the brain', *Trends in Cognitive Sciences*, 9(6), pp. 296–305. doi: 10.1016/j.tics.2005.04.010.

Martinez-Conde, S., Macknik, S. L. and Hubel, D. H. (2004) 'The role of fixational eye movements in visual perception', *Nature Reviews Neuroscience*, 5(3), pp. 229–240. doi: 10.1038/nrn1348.

McCullagh, P. (2005) 'Proportional-Odds Model', *Encyclopedia of Biostatistics*, pp. 2–4. doi: 10.1002/0470011815.b2a10049.

McFarland, J. M. et al. (2015) 'Saccadic modulation of stimulus processing in primary visual cortex', *Nature Communications*, 6, pp. 1–14. doi: 10.1038/ncomms9110.

McGonigal, J. (2011) *Reality is broken: Why games make us better and how they can change the world.*, *Reality is broken: Why games make us better and how they can change the world.* New York, NY, US.

McKenzie, S. et al. (2014) 'Hippocampal Representation of Related and Opposing Memories Develop within Distinct, Hierarchically Organized Neural Schemas', *Neuron*, 83(1), pp. 202–215. doi: 10.1016/j.neuron.2014.05.019.

McKenzie, S. et al. (2016) 'Representation of memories in the cortical–hippocampal system: Results from the application of population similarity analyses', *Neurobiology of Learning and Memory*. doi: 10.1016/j.nlm.2015.12.008.

McNaughton, B. L. et al. (2006) 'Path integration and the neural basis of the "cognitive map"',

Nature Reviews Neuroscience, 7(8), pp. 663–678. doi: 10.1038/nrn1932.

Meister, M. L. R. and Buffalo, E. A. (2016) 'Getting directions from the hippocampus: The neural connection between looking and memory', *Neurobiology of Learning and Memory*, 134, pp. 135–144. doi: 10.1016/j.nlm.2015.12.004.

Milivojevic, B. and Doeller, C. F. (2013) 'Mnemonic networks in the hippocampal formation: From spatial maps to temporal and conceptual codes', *Journal of Experimental Psychology: General*, 142(4), pp. 1231–1241. doi: 10.1037/a0033746.

Miller, L. J. (2017) 'Creating a common terminology for play behavior to increase cross-disciplinary research', *Learning & Behavior*. doi: 10.3758/s13420-017-0286-x.

Milner, B. (2005) 'The medial temporal-lobe amnesic syndrome', *Psychiatric Clinics of North America*, 28(3 SPEC. ISS.), pp. 599–611. doi: 10.1016/j.psc.2005.06.002.

Milner, B. and Penfield, W. (1955) 'The effect of hippocampal lesions on recent memory.', *Transactions of the American Neurological Association*, 42(80th Meeting), pp. 42–8.

Minderer, M. et al. (2016) 'Neuroscience: Virtual reality explored', *Nature*, 533(7603), pp. 324–325. doi: 10.1038/nature17899.

Mizumori, S. J. Y. and Tryon, V. L. (2015) *Integrative hippocampal and decision-making neurocircuitry during goal-relevant predictions and encoding*. 1st edn, *Progress in Brain Research*. 1st edn. doi: 10.1016/bs.pbr.2015.03.010.

Molitor, R. J. et al. (2014) 'Memory-related eye movements challenge behavioral measures of pattern completion and pattern separation', *Hippocampus*, 24(6), pp. 666–672. doi: 10.1002/hipo.22256.

Mormann, F. et al. (2005) 'Phase/amplitude reset and theta-gamma interaction in the human medial temporal lobe during a continuous word recognition memory task', *Hippocampus*, 15(7), pp. 890–900. doi: 10.1002/hipo.20117.

Morris, B. J. et al. (2013) 'Gaming science: The "Gamification" of scientific thinking', *Frontiers in Psychology*, 4(SEP), pp. 1–16. doi: 10.3389/fpsyg.2013.00607.

Morris, R. (1984) 'Developments of a water-maze procedure for studying spatial learning in the

rat', *Journal of Neuroscience Methods*, 11(1), pp. 47–60. doi: 10.1016/0165-0270(84)90007-4.

Morris, R. G. M. et al. (1982) 'Place navigation impaired in rats with hippocampal lesions', *Nature*, pp. 681–683. doi: 10.1038/297681a0.

Moser, E. I., Kropff, E. and Moser, M.-B. (2008) 'Place cells, grid cells, and the brain's spatial representation system.', *Annual review of neuroscience*, 31, pp. 69–89. doi: 10.1146/annurev.neuro.31.061307.090723.

Moser, M. B. and Moser, E. I. (1998) 'Functional differentiation in the hippocampus', *Hippocampus*, 8(6), pp. 608–619. doi: 10.1002/(SICI)1098-1063(1998)8:6<608::AID-HIPO3>3.0.CO;2-7.

Movshon, J. A. and Simoncelli, E. P. (2014) 'Representation of Naturalistic Image Structure in the Primate Visual Cortex', *Cold Spring Harbor Symposia on Quantitative Biology*, 79, pp. 115–122. doi: 10.1101/sqb.2014.79.024844.

Mueller, C. et al. (2012) 'Building virtual reality fMRI paradigms: A framework for presenting immersive virtual environments', *Journal of Neuroscience Methods*, 209(2), pp. 290–298. doi: 10.1016/j.jneumeth.2012.06.025.

Muller, E. et al. (2015) 'Python in neuroscience', *Front. Neuroinformatics*, 9(April), pp. 14–17. doi: 10.3389/fninf.2015.00011.

Murray, E. A., Bussey, T. J. and Saksida, L. M. (2007) 'Visual Perception and Memory: A New View of Medial Temporal Lobe Function in Primates and Rodents', *Annual Review of Neuroscience*, 30(1), pp. 99–122. doi: 10.1146/annurev.neuro.29.051605.113046.

Murray, E. A. and Mishkin, M. (1998) 'Object recognition and location memory in monkeys with excitotoxic lesions of the amygdala and hippocampus.', *J Neurosci*, 18(16), pp. 6568–6582.

Naya, Y. and Suzuki, W. a (2011) 'Integrating what and when across the primate medial temporal lobe.', *Science*, 333(6043), pp. 773–776. doi: 10.1126/science.1206773.

Neunuebel, J. P. et al. (2013) 'Conflicts between Local and Global Spatial Frameworks Dissociate Neural Representations of the Lateral and Medial Entorhinal Cortex', *Journal of Neuroscience*, 33(22), pp. 9246–9258. doi: 10.1523/JNEUROSCI.0946-13.2013.

Newman, E. L. et al. (2007) ‘Learning your way around town: How virtual taxicab drivers learn to use both layout and landmark information’, *Cognition*, 104(2), pp. 231–253. doi: 10.1016/j.cognition.2006.05.013.

Nishimoto, S. and Gallant, J. L. (2011) ‘A Three-Dimensional Spatiotemporal Receptive Field Model Explains Responses of Area MT Neurons to Naturalistic Movies’, *Journal of Neuroscience*, 31(41), pp. 14551–14564. doi: 10.1523/JNEUROSCI.6801-10.2011.

Nouchi, R. et al. (2013) ‘Brain Training Game Boosts Executive Functions, Working Memory and Processing Speed in the Young Adults: A Randomized Controlled Trial’, *PLoS ONE*, 8(2). doi: 10.1371/journal.pone.0055518.

Numan, R. (2015) ‘A Prefrontal-Hippocampal Comparator for Goal-Directed Behavior: The Intentional Self and Episodic Memory’, *Frontiers in Behavioral Neuroscience*, 9(November), pp. 1–19. doi: 10.3389/fnbeh.2015.00323.

Nyström, M. and Holmqvist, K. (2010) ‘An adaptive algorithm for fixation, saccade, and glissade detection in eyetracking data.’, *Behavior research methods*, 42(1), pp. 188–204. doi: 10.3758/BRM.42.1.188.

O’Keefe, J. and Dostrovsky, J. (1971) ‘The hippocampus as a spatial map. Preliminary evidence from unit activity in the freely-moving rat’, *Brain Research*, 34(1), pp. 171–175. doi: 10.1016/0006-8993(71)90358-1.

O’Keefe, J. and Recce, M. L. (1993) ‘Phase relationship between hippocampal place units and the EEG theta rhythm’, *Hippocampus*, 3(3), pp. 317–330. doi: 10.1002/hipo.450030307.

O’Mara, S. M. (1995) ‘Spatially selective firing properties of hippocampal formation neurons in rodents and primates.’, *Progress in neurobiology*, 45(3), pp. 253–74. doi: 10.1016/0301-0082(94)00050-R.

Olton, D. S. and Samuelson, R. J. (1976) ‘Remembrance of places passed: Spatial memory in rats.’, *Journal of Experimental Psychology: Animal Behavior Processes*, pp. 97–116.

Orbach, J., Milner, B. and Rasmussen, T. (1960) ‘Learning and Retention in Monkeys After Amygdala-Hippocampus Resection’, *Archives of Neurology*, 3(3), pp. 230–251. doi:

10.1001/archneur.1960.00450030008002.

Owen, A. M. et al. (2010) ‘Putting brain training to the test’, *Nature*, 465(7299), pp. 775–778. doi: 10.1038/nature09042.

Packard, M. G. and McGaugh, J. L. (1996) ‘Inactivation of Hippocampus or Caudate Nucleus with Lidocaine Differentially Affects Expression of Place and Response Learning’, *Neurobiology of Learning and Memory*, 65(1), pp. 65–72. doi: 10.1006/nlme.1996.0007.

Palombo, D. J., Keane, M. M. and Verfaellie, M. (2015) ‘How does the hippocampus shape decisions?’, *Neurobiology of Learning and Memory*, 125, pp. 93–97. doi: 10.1016/j.nlm.2015.08.005.

Parsons, T. D. (2015) ‘Virtual Reality for Enhanced Ecological Validity and Experimental Control in the Clinical, Affective and Social Neurosciences’, *Frontiers in Human Neuroscience*, 9(December), pp. 1–19. doi: 10.3389/fnhum.2015.00660.

Patel, T. P. et al. (2015) ‘Automated quantification of neuronal networks and single-cell calcium dynamics using calcium imaging’, *Journal of Neuroscience Methods*, 243, pp. 1–13. doi: 10.1016/j.jneumeth.2015.01.020.

Peelen, M. V. and Kastner, S. (2014) ‘Attention in the real world: Toward understanding its neural basis’, *Trends in Cognitive Sciences*, 18(5), pp. 242–250. doi: 10.1016/j.tics.2014.02.004.

Peirce, J. W. (2007) ‘PsychoPy-Psychophysics software in Python’, *Journal of Neuroscience Methods*, 162(1–2), pp. 8–13. doi: 10.1016/j.jneumeth.2006.11.017.

Perkel, J. M. (2015) ‘Programming: Pick up Python.’, *Nature*, 518(7537), pp. 125–6. doi: 10.1038/518125a.

Pitimon, I. and Nintanavongsa, P. (2014) ‘An IPv6 Network Congestion Measurement Based on Network Time Protocol’, *TENCON 2014 - 2014 IEEE Region 10 Conference*, pp. 4–7.

Place, R. et al. (2016) ‘Bidirectional prefrontal-hippocampal interactions support context-guided memory’, *Nature Neuroscience*, 19(8), pp. 992–994. doi: 10.1038/nn.4327.

Poppenk, J. et al. (2013) ‘Long-axis specialization of the human hippocampus’, *Trends in Cognitive Sciences*. Elsevier Ltd, 17(5), pp. 230–240. doi: 10.1016/j.tics.2013.03.005.

Quirk, G. J., Muller, R. U. and Kubie, J. L. (1990) 'The firing of hippocampal place cells in the dark depends on the rat's recent experience', *Journal of Neuroscience*, 10(6), pp. 2008–2017.

Ramos Gameiro, R. et al. (2017) 'Exploration and Exploitation in Natural Viewing Behavior', *Scientific Reports*, 7(1), p. 2311. doi: 10.1038/s41598-017-02526-1.

Rangel, L. M. et al. (2016) 'Rhythmic coordination of hippocampal neurons during associative memory processing', *eLife*, 5, pp. 1–24. doi: 10.7554/eLife.09849.

Ravassard, P. et al. (2013) 'Multisensory control of hippocampal spatiotemporal selectivity.', *Science*, 340(6138), pp. 1342–6. doi: 10.1126/science.1232655.

Reader, A. T. and Holmes, N. P. (2016) 'Examining ecological validity in social interaction: problems of visual fidelity, gaze, and social potential', *Culture and Brain*, 4(2), pp. 134–146. doi: 10.1007/s40167-016-0041-8.

Rey, H. G., Fried, I. and Quian Quiroga, R. (2014) 'Timing of single-neuron and local field potential responses in the human medial temporal lobe', *Current Biology*, 24(3), pp. 299–304. doi: 10.1016/j.cub.2013.12.004.

Richard, G. R. et al. (2013) 'Speed modulation of hippocampal theta frequency correlates with spatial memory performance', *Hippocampus*, 23(12), pp. 1269–1279. doi: 10.1002/hipo.22164.

Rieke, F., Bodnar, D. A. and Bialek, W. (1995) 'Naturalistic stimuli increase the rate and efficiency of information transmission by primary auditory afferents.', *Proceedings. Biological sciences*, 262(1365), pp. 259–65. doi: 10.1098/rspb.1995.0204.

Rigotti, M. et al. (2013) 'The importance of mixed selectivity in complex cognitive tasks', *Nature*, 497(7451), pp. 585–590. doi: 10.1038/nature12160.

Ringo, J. L. et al. (1994) 'Eye movements modulate activity in hippocampal , parahippocampal , and inferotemporal neurons', *Journal of Neurophysiology*, 71(3), pp. 1285–1288.

Ritchey, M., Libby, L. A. and Ranganath, C. (2015) *Cortico-hippocampal systems involved in memory and cognition: The PMAT framework*. 1st edn, *Progress in Brain Research*. 1st edn. doi: 10.1016/bs.pbr.2015.04.001.

Rizzuto, D. S. et al. (2006) 'Human neocortical oscillations exhibit theta phase differences between

encoding and retrieval', *NeuroImage*, 31(3), pp. 1352–1358. doi: 10.1016/j.neuroimage.2006.01.009.

Robertson, R. G. et al. (1998) 'Head direction cells in the primate hippocampal formation', *Hippocampus*, 9, pp. 206–219. doi: 10.1002/(SICI)1098-1063(1999)9:3<206::AID-HIPO2>3.0.CO;2-H.

RockStar Games (2014) *Grand Theft Auto Online Census: The world so far*.

Rolls, E. T. (1999) 'Spatial view cells and the representation of place in the primate hippocampus', *Hippocampus*, 9(4), pp. 467–480. doi: 10.1002/(SICI)1098-1063(1999)9:4<467::AID-HIPO13>3.0.CO;2-F.

Rolls, E. T. and O'Mara, S. M. (1995) 'View-Responsive Neurons in the Primate Hippocampal Complex', *Society for Neuroscience Abstracts*, 19, p. 409:424.

Rolls, E. T., Robertson, R. G. and Georges-frangois, P. (1997) 'Spatial View Cells in the Primate Hippocampus', *European Journal of Neuroscience*, 9, pp. 1789–1794.

Rolls, E. T. and Xiang, J.-Z. (2006) 'Spatial view cells in the primate hippocampus and memory recall', *Reviews in the Neurosciences*, pp. 1–26.

Roux, L. et al. (2017) 'Sharp wave ripples during learning stabilize the hippocampal spatial map', *Nature Neuroscience*, (March). doi: 10.1038/nn.4543.

Rutishauser, U. et al. (2010) 'Human memory strength is predicted by theta-frequency phase-locking of single neurons.', *Nature*, 464(7290), pp. 903–907. doi: 10.1038/nature08860.

Sainsbury, R. S., Harris, J. L. and Rowland, G. L. (1987) 'Sensitization and hippocampal type 2 theta in the rat', *Physiology and Behavior*, 41(5), pp. 489–493. doi: 10.1016/0031-9384(87)90085-0.

Sakon, J. J. et al. (2014) 'Context-dependent incremental timing cells in the primate hippocampus', *Proceedings of the National Academy of Sciences*, 111(51), pp. 18351–18356. doi: 10.1073/pnas.1417827111.

Salvucci, D. D. and Goldberg, J. H. (2000) 'Identifying Fixations and Saccades in Eye-Tracking Protocols', *Proceedings of the Eye Tracking Research and Applications Symposium*, pp. 71–78.

doi: 10.1145/355017.355028.

Sarma, Y. and Jammalamadaka, S. R. (1993) 'Circular Regression', *Statistical Sciences and Data Analysis*, pp. 109–128.

Sato, N. et al. (2004) 'Navigation in virtual environment by the macaque monkey', *Behavioural Brain Research*, 153(1), pp. 287–291. doi: 10.1016/j.bbr.2003.10.026.

Scheffer-Teixeira, R. and Tort, A. B. (2016) 'On cross-frequency phase-phase coupling between theta and gamma oscillations in the hippocampus.', *eLife*, 5(2), pp. 134–8. doi: 10.7554/eLife.20515.

Schiller, D. et al. (2015) 'Memory and Space: Towards an Understanding of the Cognitive Map', *Journal of Neuroscience*, 35(41), pp. 13904–13911. doi: 10.1523/JNEUROSCI.2618-15.2015.

Schomburg, E. W. et al. (2014) 'Theta Phase Segregation of Input-Specific Gamma Patterns in Entorhinal-Hippocampal Networks', *Neuron*, 84(2), pp. 470–485. doi: 10.1016/j.neuron.2014.08.051.

Schroeder, C. E. et al. (2010) 'Dynamics of Active Sensing and perceptual selection.', *Current opinion in neurobiology*, 20(2), pp. 172–6. doi: 10.1016/j.conb.2010.02.010.

Schultheis, M. T., Himelstein, J. and Rizzo, A. a (2002) 'Virtual reality and neuropsychology: upgrading the current tools.', *The Journal of head trauma rehabilitation*, 17(5), pp. 378–394. doi: 10.1097/00001199-200210000-00002.

Scoville, W. B. and Milner, B. (1957) 'Loss of recent memory after bilateral hippocampal lesions.', *The Journal of neuropsychiatry and clinical neurosciences*, 20(11), pp. 11–21. doi: 10.1136/jnnp.20.1.11.

Seress, L. (2007) 'Comparative anatomy of the hippocampal dentate gyrus in adult and developing rodents, non-human primates and humans', *Progress in Brain Research*, 163. doi: 10.1016/S0079-6123(07)63002-7.

Shen, H. (2014) 'Interactive notebooks: Sharing the code.', *Nature*, pp. 5–6.

Siegel, M., Donner, T. H. and Engel, A. K. (2012) 'Spectral fingerprints of large-scale neuronal interactions', *Nature Reviews Neuroscience*, 13(February), pp. 20–25. doi: 10.1038/nrn3137.

Siegle, J. H. and Wilson, M. A. (2014) ‘Enhancement of encoding and retrieval functions through theta phase-specific manipulation of hippocampus.’, *eLife*, 3, p. e03061.

Simons, D. J. et al. (2016) ‘Do “Brain-Training” Programs Work?’, *Psychological Science in the Public Interest*, 17(3), pp. 103–186. doi: 10.1177/1529100616661983.

Skaggs, W. E. et al. (1996) ‘Theta phase precession in hippocampal neuronal populations and the compression of temporal sequences.’, *Hippocampus*, 6(2), pp. 149–72. doi: 10.1002/(SICI)1098-1063(1996)6:2<149::AID-HIPO6>3.0.CO;2-K.

Skaggs, W. E. et al. (2007) ‘EEG sharp waves and sparse ensemble unit activity in the macaque hippocampus.’, *Journal of neurophysiology*, 98(2), pp. 898–910. doi: 10.1152/jn.00401.2007.

Slater, M. et al. (2006) ‘A virtual reprise of the Stanley Milgram obedience experiments’, *PLoS ONE*, 1(1). doi: 10.1371/journal.pone.0000039.

Slobounov, S. M. et al. (2014) ‘Modulation of cortical activity in 2D versus 3D virtual reality environments: An EEG study’, *International Journal of Psychophysiology*, 95(3), pp. 254–260. doi: 10.1016/j.ijpsycho.2014.11.003.

Sobotka, S., Nowicka, a and Ringo, J. L. (1997) ‘Activity linked to externally cued saccades in single units recorded from hippocampal, parahippocampal, and inferotemporal areas of macaques.’, *Journal of neurophysiology*, 78(4), pp. 2156–2163.

Sobotka, S. and Ringo, J. L. (1997) ‘Saccadic eye movements, even in darkness, generate event-related potentials recorded in medial septum and medial temporal cortex.’, *Brain research*, 756(1–2), pp. 168–173. doi: 10.1016/S0006-8993(97)00145-5.

Solstad, T. et al. (2008) ‘Representation of Geometric Borders in the Entorhinal Cortex’, *Science*, 322(5909), pp. 1865–1868. doi: 10.1126/science.1166466.

Sommer, M. A. and Wurtz, R. H. (2002) ‘A Pathway in Primate Brain for Internal Monitoring of Movements’, *Science*, 296(5572), pp. 1480–1482. doi: 10.1126/science.1069590.

Spellman, T. et al. (2015) ‘Hippocampal–prefrontal input supports spatial encoding in working memory’, *Nature*, 522(7556), pp. 309–314. doi: 10.1038/nature14445.

Spinka, M., Newberry, R. C. and Bekoff, M. (2001) ‘Mammalian play: training for the

unexpected.', *The Quarterly review of biology*, 76(2), pp. 141–68.

Squire, L. R., Wixted, J. T. and Clark, R. E. (2007) 'Recognition memory and the medial temporal lobe: a new perspective', *Nature Reviews Neuroscience*, 8(11), pp. 872–883. doi: 10.1038/nrn2154.

Stachenfeld, K. L., Botvinick, M. M. and Gershman, S. J. (2017) 'The hippocampus as a predictive map', *Nature Neuroscience*, 28(3), pp. 391–397. doi: 10.1038/nn.4650.

Staudigl, T. et al. (2017) 'Saccades are phase-locked to alpha oscillations in the occipital and medial temporal lobe during successful memory encoding', *PLOS Biology*. Edited by F. Tong, 15(12), p. e2003404. doi: 10.1371/journal.pbio.2003404.

Staudigl, T. and Hanslmayr, S. (2013) 'Theta oscillations at encoding mediate the context-dependent nature of human episodic memory.', *Current biology*, 23(12), pp. 1101–6. doi: 10.1016/j.cub.2013.04.074.

Stewart, M. and Fox, S. E. (1991) 'Hippocampal theta activity in monkeys', *Brain Research*, 538(1), pp. 59–63. doi: 10.1016/0006-8993(91)90376-7.

Strange, B. A. et al. (2014) 'Functional organization of the hippocampal longitudinal axis', *Nature Reviews Neuroscience*, 15(10), pp. 655–669. doi: 10.1038/nrn3785.

Straw, A. D. (2008) 'Vision egg: an open-source library for realtime visual stimulus generation.', *Frontiers in neuroinformatics*, 2(November), p. 4. doi: 10.3389/neuro.11.004.2008.

Suzuki, W. A. and Eichenbaum, H. (2000) 'The neurophysiology of memory.', *Annals of the New York Academy of Sciences*, 911(212), pp. 175–191. doi: 10.1111/j.1749-6632.2000.tb06726.x.

Takahashi, M. et al. (2014) 'Theta phase shift in spike timing and modulation of gamma oscillation: a dynamic code for spatial alternation during fixation in rat hippocampal area CA1.', *Journal of neurophysiology*, 111(8), pp. 1601–14. doi: 10.1152/jn.00395.2013.

Tallon-Baudry, C. et al. (1997) 'Oscillatory gamma-band (30-70 Hz) activity induced by a visual search task in humans.', *The Journal of neuroscience : the official journal of the Society for Neuroscience*, 17(2), pp. 722–734. doi: 10.1007/s11064-011-0538-7.

Tanaka, J. W. et al. (2010) 'Using computerized games to teach face recognition skills to children

with autism spectrum disorder: The Let's Face It! program', *Journal of Child Psychology and Psychiatry and Allied Disciplines*, 51(8), pp. 944–952. doi: 10.1111/j.1469-7610.2010.02258.x.

Tarr, M. J. and Warren, W. H. (2002) 'Virtual reality in behavioral neuroscience and beyond.', *Nature neuroscience*, 5 Suppl, pp. 1089–1092. doi: 10.1038/nn948.

Tesche, C. D. and Karhu, J. (2000) 'Theta oscillations index human hippocampal activation during a working memory task.', *Proceedings of the National Academy of Sciences*, 97(2), pp. 919–924. doi: 10.1073/pnas.97.2.919.

Thompson, K. G. et al. (1996) 'Perceptual and motor processing stages identified in the activity of macaque frontal eye field neurons during visual search.', *Journal of neurophysiology*, 76(6), pp. 4040–4055.

Thompson, L. T. and Best, P. J. (1990) 'Long-term stability of the place-field activity of single units recorded from the dorsal hippocampus of freely behaving rats', *Brain Research*, 509(2), pp. 299–308. doi: 10.1016/0006-8993(90)90555-P.

Topalidou, M. et al. (2015) 'A long journey into reproducible computational neuroscience.', *Frontiers in computational neuroscience*, 9, p. 30. doi: 10.3389/fncom.2015.00030.

Tort, A. B. L. et al. (2008) 'Dynamic cross-frequency couplings of local field potential oscillations in rat striatum and hippocampus during performance of a T-maze task.', *Proceedings of the National Academy of Sciences*, 105(51), pp. 20517–20522. doi: 10.1073/pnas.0810524105.

Tort, A. B. L. et al. (2009) 'Theta-gamma coupling increases during the learning of item-context associations.', *Proceedings of the National Academy of Sciences*, 106(49), pp. 20942–20947. doi: 10.1073/pnas.0911331106.

Tort, A. B. L. et al. (2010) 'Measuring phase-amplitude coupling between neuronal oscillations of different frequencies.', *Journal of neurophysiology*, 104(2), pp. 1195–210. doi: 10.1152/jn.00106.2010.

Tremblay, S. et al. (2015) 'Attentional Filtering of Visual Information by Neuronal Ensembles in the Primate Lateral Prefrontal Cortex', *Neuron*, 85(1), pp. 202–216. doi: 10.1016/j.neuron.2014.11.021.

Tremblay, S. et al. (2015) 'Single-Trial Decoding of Visual Attention from Local Field Potentials in the Primate Lateral Prefrontal Cortex Is Frequency-Dependent', *Journal of Neuroscience*, 35(24), pp. 9038–9049. doi: 10.1523/JNEUROSCI.1041-15.2015.

Tsanov, M. (2015) *Septo-hippocampal signal processing: Breaking the code*. 1st edn, *Progress in Brain Research*. 1st edn. doi: 10.1016/bs.pbr.2015.04.002.

Vandecasteele, M. et al. (2014) 'Optogenetic activation of septal cholinergic neurons suppresses sharp wave ripples and enhances theta oscillations in the hippocampus', *Proceedings of the National Academy of Sciences*, 111(37), pp. 13535–13540. doi: 10.1073/pnas.1411233111.

Vass, L. K. et al. (2016) 'Oscillations Go the Distance: Low-Frequency Human Hippocampal Oscillations Code Spatial Distance in the Absence of Sensory Cues during Teleportation', *Neuron*, 89, pp. 1–7. doi: 10.1016/j.neuron.2016.01.045.

Vertes, R. P. et al. (2007) 'Nucleus reuniens of the midline thalamus: Link between the medial prefrontal cortex and the hippocampus', *Brain Research Bulletin*, 71(6), pp. 601–609. doi: 10.1016/j.brainresbull.2006.12.002.

Vinogradova, O. S. (2001) 'Hippocampus as comparator: role of the two input and two output systems of the hippocampus in selection and registration of information.', *Hippocampus*, 11(5), pp. 578–98. doi: 10.1002/hipo.1073.

Wallisch, P. et al. (2009) *Matlab for Neuroscientists*, *Matlab for Neuroscientists*. doi: 10.1016/B978-0-12-374551-4.00028-2.

Wang, Y. et al. (2014) 'Theta sequences are essential for internally generated hippocampal firing fields', *Nature Neuroscience*, 18(2), pp. 282–288. doi: 10.1038/nn.3904.

Washburn, D. a. and Astur, R. S. (2003) 'Exploration of virtual mazes by rhesus monkeys (Macaca mulatta)', *Animal Cognition*, 6(3), pp. 161–168. doi: 10.1007/s10071-003-0173-z.

Washburn, D. A. and Gulledge, J. P. (1995) 'Game-like tasks for comparative research: leveling the playing field.', *Behavior research methods, instruments, & computers : a journal of the Psychonomic Society, Inc*, 27(2), pp. 235–8. doi: 10.3758/BF03204738.

Watrous, A. J. et al. (2013) 'A comparative study of human and rat hippocampal low-frequency

oscillations during spatial navigation.', *Hippocampus*, 23(8), pp. 656–61. doi: 10.1002/hipo.22124.

Watrous, A. J. and Ekstrom, A. D. (2014) 'The spectro-contextual encoding and retrieval theory of episodic memory.', *Frontiers in human neuroscience*, 8, pp. 1–15. doi: 10.3389/fnhum.2014.00075.

Watrous, A. J., Fried, I. and Ekstrom, A. D. (2011) 'Behavioral correlates of human hippocampal delta and theta oscillations during navigation', *Journal of Neurophysiology*, 105(4), pp. 1747–1755. doi: 10.1152/jn.00921.2010.

Weidemann, C. T., Mollison, M. V and Kahana, M. J. (2009) 'Electrophysiological correlates of high-level perception during spatial navigation.', *Psychonomic bulletin & review*, 16(2), pp. 313–319. doi: 10.3758/PBR.16.2.313.

Wikenheiser, A. M. and Redish, A. D. (2015) 'Hippocampal theta sequences reflect current goals', *Nature Neuroscience*, 18(2), pp. 1–8. doi: 10.1038/nn.3909.

Williams, J. M. and Givens, B. (2003) 'Stimulation-induced reset of hippocampal theta in the freely performing rat', *Hippocampus*, 13(1), pp. 109–116. doi: 10.1002/hipo.10082.

Wills, T. J. et al. (2010) 'Development of the Hippocampal Cognitive Map in Preweanling Rats', *Science*, 328(5985), pp. 1573–1576. doi: 10.1126/science.1188224.

Wilson, D. I. G., Langston, R. F., et al. (2013) 'Lateral entorhinal cortex is critical for novel object-context recognition', *Hippocampus*, 23(5), pp. 352–366. doi: 10.1002/hipo.22095.

Wilson, D. I. G., Watanabe, S., et al. (2013) 'Lateral entorhinal cortex is necessary for associative but not nonassociative recognition memory', *Hippocampus*, 23(12), pp. 1280–1290. doi: 10.1002/hipo.22165.

Wirth, S. et al. (2003) 'Single Neurons in the Monkey Hippocampus and Learning of New Associations', *Science*, 300(5625), pp. 1578–1581. doi: 10.1126/science.1084324.

Wirth, S. et al. (2017) 'Gaze-informed, task-situated representation of space in primate hippocampus during virtual navigation', *PLoS Biology*, 15(2), pp. 1–28. doi: 10.1371/journal.pbio.2001045.

Witter, M. P. (2007) ‘The perforant path: projections from the entorhinal cortex to the dentate gyrus’, *Progress in Brain Research*, 163, pp. 43–61. doi: 10.1016/S0079-6123(07)63003-9.

Wolfe, J. M. et al. (2011) ‘Visual search for arbitrary objects in real scenes.’, *Attention, perception & psychophysics*, 73(6), pp. 1650–71. doi: 10.3758/s13414-011-0153-3.

Worrell, G. A. et al. (2012) ‘Recording and analysis techniques for high-frequency oscillations’, *Progress in Neurobiology*. Elsevier Ltd, 98(3), pp. 265–278. doi: 10.1016/j.pneurobio.2012.02.006.

Zaki, J. and Ochsner, K. (2009) ‘The need for a cognitive neuroscience of naturalistic social cognition’, *Annals of the New York Academy of Sciences*, 1167, pp. 16–30. doi: 10.1111/j.1749-6632.2009.04601.x.

Zanos, S. et al. (2012) ‘Relationships between spike-free local field potentials and spike timing in human temporal cortex’, *Journal of Neurophysiology*, 107(7), pp. 1808–1821. doi: 10.1152/jn.00663.2011.

Zanos, T. P., Mineault, P. J. and Pack, C. C. (2011) ‘Removal of spurious correlations between spikes and local field potentials.’, *Journal of neurophysiology*, 105(1), pp. 474–486. doi: 10.1152/jn.00642.2010.

Zheng, F. et al. (2014) ‘Minimizing latency for augmented reality displays: Frames considered harmful’, in *2014 IEEE International Symposium on Mixed and Augmented Reality (ISMAR)*, pp. 195–200. doi: 10.1109/ISMAR.2014.6948427.